ABSTRACT OF THE THESIS OF

THOMAS F. LUNDEEN for the degree of DOCTOR OF PHILOSOPHY in CHEMISTRY presented on JANUARY 12, 1984

Title: Nonlinear Raman Spectroscopy of Gases

Abtract approved: Redacted for privacy
Professor J. W. Nibler

Applications of several methods of coherent nonlinear Raman Spectroscopy have been made in this thesis research. The theory and potential of one of these, Photoacoustic Raman Spectroscopy (PARS), is discussed in chapter two. Experimental results are presented which illustrate the sensitivity of this method and establish sampling conditions for maximum acoustic signals. As part of this work a new photoacoustic Raman cell was designed which is simple to use and gives improved detection capability.

Measurements of the nonresonant third order susceptibility of various gases are presented in chapter three. This quantity has been very difficult to determine in absolute terms and is needed to properly account for CARS lineshape distortions which affects frequency and intensity measurements for resonant transitions. Values were measured by first determining nonresonant susceptibilities relative to N_2. Recent linewidth and Raman cross section data were then used to calculate an absolute resonant susceptibility for H_2.

Finally, by a separate measurement of the N_2/H_2 susceptibility ratio, accurate absolute values for the nonresonant third order susceptibility of a number of common gases were deduced.

Chapter four describes a study of the rotational relaxation of para hydrogen (and various mixtures) in a supersonic free jet expansion. CARS measurements were used to determine the H_2 rotational temperature in the free jet. One goal of this work was to test several H_2 --- H_2 theoretical interaction potentials. This was done by combining models for the expansion properties of the jet and for relaxation of hydrogen with theoretical values for the cross sections. Rotational temperature profiles of the jet were calculated and the theoretical predictions of several potentials are in good accord with the actual experimental results. Using the complete fluid mechanical model for the expansion process, one can develop a light preference can be developed for the M79 potential of Schaefer and coworkers. Similar calculations were preformed for H_2 --- He mixtures.

Nonlinear Raman Spectroscopy of Gases

by

Thomas F. Lundeen

A THESIS

submitted to

Oregon State University

in partial fulfillment of
the requirements for the
degree of

Doctor of Philosphy

Completed January 12, 1984

Commencement June 1984

APPROVED:

Redacted for privacy

Professor of Chemistry in charge of major

Redacted for privacy

Head of department of Chemistry

Redacted for privacy

Dean of Graduate School

Date thesis is presented January 12, 1984

Typed by Jan Lundeen for Thomas F. Lundeen

TABLE OF CONTENTS

LIST OF FIGURES

LIST OF TABLES

Page

Tables

Nonlinear Raman Spectroscopy of Gases

CHAPTER 1

Introduction to Nonlinear Spectroscopy

1.1 Introduction

The first spontaneous Raman spectrum was obtained in 1928 by Sir C. V. Raman and since that time Raman spectroscopy has become a very important spectroscopic tool. The application of Raman spectroscopy as a general technique has been tied very closely to the development of lasers. Since lasers provide very intense and extremely monochromatic light sources they are ideally suited for conventional Raman spectroscopy, a field recently termed COORS (Common Old Ordinary Raman Spectroscopy) by a visiting seminar speaker at OSU. The use of lasers to perform Raman spectroscopy led to the development of new nonlinear Raman techniques, a few of which are RIKES (Raman Induced Kerr Effect Spectroscopy)[1], CARS (Coherent Anti-Stokes Raman Spectroscopy)[2], and SRS (Stimulated Raman Scattering)[3].

Coherent Raman techniques generally yield the same spectroscopic data as does spontaneous Raman spectroscopy. However the signal amplitudes are usually very much stronger then those from normal Raman spectroscopy under the same conditions. This large increase in signal is gained by applying two lasers of different frequency to the sample. When the frequency difference between the applied lasers ($\omega = \omega_1 - \omega_2$) is equal to the frequency of a Raman transition (ω_v), resonant coupling between the molecules and the radiation fields occurs. It is this coupling which gives rise to enhanced Raman signals and the development of new applications which will be discussed in this thesis. This research has involved three rather distinct studies and each subject will be dealt with in separate chapters. In this first chapter the objective is to give an overview of the general field of nonlinear Raman spectroscopy.

The second chapter will deal with the basic theory of the newest nonlinear Raman method, PARS (Photoacoustic Raman Spectroscopy), and will describe some of the experimental work undertaken to assess its potential as a general spectroscopic technique.

Chapter three deals with the measurement of the nonresonant third order susceptibility of various gases.

This quantity has been very difficult to measure in absolute terms and is needed to properly account for CARS lineshape distortion which effects the frequency and intensity measurements made using CARS. Values were measured by first determining nonresonant susceptibilities relative to N_2. Recent linewidth and Raman cross section data were then used to determine an absolute resonant susceptibility for H_2. Finally, by a separate measurement of the N_2/H_2 susceptibility ratio, accurate absolute values for the nonresonant third order susceptibility of a number of common gases were deduced.

The fourth and final chapter describes the use of CARS to study the cross sections for rotational relaxation of H_2 in a molecular beam. Several models for the beam expansion and the relaxation process are explored to test various theoretical potentials for the H_2 - H_2 interaction .

1.2 Polarization of Matter

When light passes through a material it tends to polarize the matter to some extent. Classically, we assume that the material is a continous dielectric with certain well-defined symmetry properties. The electric polarization induced in the medium ($\vec{P}$) can be expressed

as the tensor product of the dielectric susceptibility (χ) of the material and the applied electric field (E).

$$\vec{P} = \chi \vec{E} \tag{1.1}$$

The induced polarization arises from the displacement of the electrons and nuclei from their equilibrium positions by the applied field. The electrons tend to follow the oscillating field and their motion can be considered as harmonic. This linear response of the medium is responsible for absorption, the index of refraction and Raman scattering.

In very intense electric fields, such as those produced by a focussed laser, the electrons tend to be displaced large distances from their equilibrium positions and the harmonic approximation is no longer valid. This nonlinear response of the medium can result in oscillations of the molecules not only at the applied frequencies but also at the sums and differences of the applied frequencies. To describe this, the polarization induced in the medium is usually expressed as a power series in terms of the applied electric fields.

$$\vec{P} = \chi_1 \vec{E}_1 + \chi_2 \vec{E}_1\vec{E}_2 + \chi_3 \vec{E}_1\vec{E}_2\vec{E}_3 \tag{1.2}$$

Where χ^i is the i'th order dielectric susceptibility tensor of rank i+1.

The quadratic term (χ^2) in this expansion describes all the various processes which involve two applied fields. Some of the more important of these are frequency doubling ($\omega=2\omega_1$)[3], difference generation ($\omega=\omega_1-\omega_2$), and Hyper-Raman scattering ($\omega=2\omega_1\pm\omega_v$)[4]. For isotropic media such as gases and liquids, this term and all higher order even terms are zero, due to the symmetry restrictions of the medium[5]. In this case equation (1.2) reduces to

$$\vec{P} = \chi_1\cdot\vec{E}_1 + \chi_3\vdots\vec{E}_1\vec{E}_2\vec{E}_3 + \cdots \qquad (1.3)$$

The cubic term (χ^3), the first nonlinear term which is nonzero for all media, describes those processes which involve the application of three electric fields to a sample. Some of the processes resulting from χ^3 include third harmonic generation ($\omega=3\omega_1$), Hyper-Hyper-Raman scattering ($\omega=3\omega_1\pm\omega_v$), Coherent Anti-Stokes Raman Spectroscopy (CARS) ($\omega=\omega_1+\omega_1-\omega_2$), and Stimulated Raman Scattering (SRS) ($\omega=\omega_1-\omega_1+\omega_2$). Both of the latter tehniques were used in this thesis research.

1.3 Nonlinear Raman Spectroscopy

The field of nonlinear Raman spectroscopy was born when Woodbury and Ng first observed stimulated Raman scattering in 1962[6]. Since that time this research area has grown tremendously, as evidenced by a few of the recent reviews[7,8].

Considerable excitement has been generated by these techniques because they have many advantages over conventional Raman spectroscopy. In general they have better sensitivity and, because most generate a coherent signal beam, they can be used to probe hostile or luminescent environments[9]. Usually they don't require a spectrometer and the spectral resolution is only limited by the convolution of the input lasers.

A few of these nonlinear Raman sequences are shown in figure (1-1). These diagrams should not be taken as depicting the real time evolution of the process but are only a figurative way of showing some of the various nonlinear Raman processes.

CARS, Coherent Anti-Stokes Raman Spectroscopy (1-1A), was first observed by Terhune in 1963[2]. In CARS, two lasers ω_1 and ω_2 coherently combine in the sample to generate a new beam $\omega_3 = 2\omega_1 - \omega_2$ by means of the third order CARS susceptibility of the sample. The power of ω_3 is given by[10]

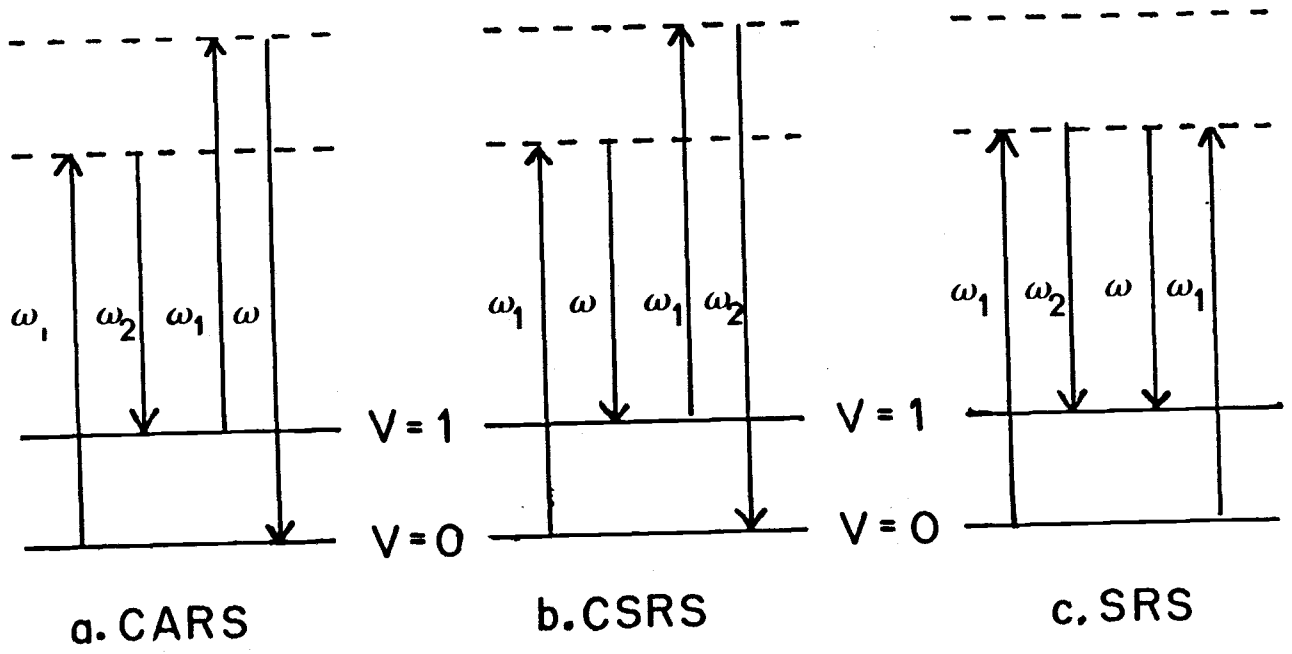

Figure 1-1 Transition schemes of a) CARS, b) CSRS and c) SRS.

$$P = C\,|\chi_{CARS}|^2\,P_1^2 P_2 \qquad (1.4)$$

$$\chi_{CARS} = \chi_{nr} + C''\left(\frac{d\sigma}{d\Omega}\right)\frac{1}{\omega_v-\omega_1-\omega_2 - i\Gamma} \qquad (1.5)$$

where ω_v is a Raman transition of the molecule, is the Raman line width (HWHM), $(d\sigma/d\Omega)$ is the Raman cross section, and χ_{nr} is the third order nonresonant susceptibility. As we can see from this expression the power of ω_3 increases dramatically when $\omega_v=\omega_1-\omega_2$. By tuning the difference between ω_1 and ω_2 and measuring the power of ω_3, we obtain a CARS spectrum for the molecule. CSRS , Coherent Stokes Raman Spectroscopy, (fig. 1-B) is similar to CARS, however the roles of the two lasers is reversed. The CARS method and its applications are considered further in chapters 3 and 4.

For SRS, Stimulated Raman Spectroscopy, two lasers with frequencies ω_1 and ω_2 are applied to the sample and when the difference between ω_1 and ω_2 equals a Raman active transition of the sample, that Raman transition is coherently driven. A decrease in the $_1$ power and a corresponding increase in the ω_2 power results as molecules are pumped from the ground state into the higher vibrational level. The change in intensity of

ω_2 is given by

$$\Delta I_2 = I_2(0)[\exp(g_s z)-1] \tag{1.6}$$

$$g_s = -\frac{16\pi^2\omega_2}{c^2 n_2 n_p}\chi'' I_1 \tag{1.7}$$

where g_s is the gain factor, z is the interaction length, n_2 is the index of refraction at ω_2, and χ'' is the real part of the third order susceptibility, which in terms of the Raman cross section is[12]

$$\chi'' = -C\left(\frac{d\sigma}{d\Omega}\right)\frac{\Gamma}{(\omega_v-\omega_1+\omega_2)^2+\Gamma^2/4} \tag{1.8}$$

The stimulated Raman effect forms the basis of several different forms of nonlinear spectroscopy. One of these is Stimulated Raman Gain (Loss) Spectroscopy (SRGS) in which the increase in ω_2 or the loss in ω_1 is monitored[13]. Another is PARS, Photoacoustic Raman Spectroscopy, in which one measures the energy input into the system as molecules are pumped into the upper state by SRS[12]. This input is detected as acoustic energy and the theory describing this process is considered in detail in chapter 2.

CHAPTER 2

Photoacoustic Raman Spectroscopy of Gases

2.1 Introduction

Since Woodbury and Ng[13] made the first observation of stimulated Raman scattering in 1962, the field of nonlinear spectroscopy has grown tremendously. Photoacoustic Raman Spectroscopy (PARS) is one of the newest versions of several nonlinear Raman techniques. Like most of these methods, it has better sensitivity and resolution then normal spontaneous Raman scattering. This chapter presents the basic theory for PARS and describes experimental work undertaken to assess its potential as a general spectroscopic technique.

Photoacoustic Raman spectroscopy was first demonstrated by Barret and Berry in 1978[14] on gaseous methane using chopped argon ion and dye laser sources. Shortly following this work, these workers demonstrated that the sensitivity of PARS could be greatly improved

using pulsed laser sources[15]. PARS has also been applied to the study of liquids by Patel and Tam[16], with a change in the acronym to OARS (Optoacoustic Raman Spectroscopy).

In photoacoustic Raman spectroscopy two spatially overlapped beams interact with a sample medium. By tuning the frequency difference between the two lasers to equal a Raman active transition of the sample molecules, vibrational and/or rotational excitation occurs by coherent Raman amplification, which is a third order nonlinear process . The excited molecules subsequently lose their vibrational-rotational energy by collisional relaxation. This causes an increase in the translational energy of the sample producing an acoustical wave which is detected by a microphone.

2.2 Theory of PARS

In this section, the basic theory of PARS will be presented and an expression for the magnitude of the PARS signal will be derived using a simple rate equation approach. A more complete discussion of the theory can be found in Barrett.[17]

In normal Raman spectroscopy (fig. 2-1a) a molecule is excited by one photon of a pump laser, at

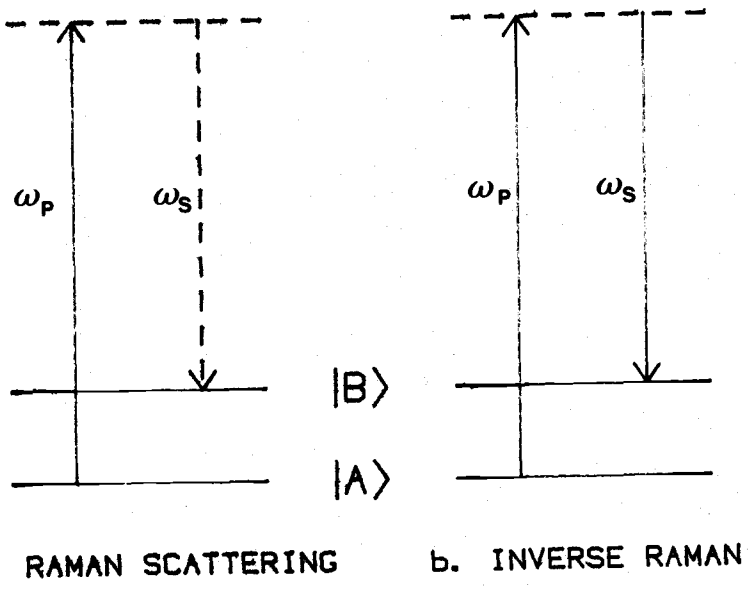

Figure 2-1 Transition schemes of (a) normal Raman scattering and (b) coherent Raman amplification. The straight arrow represents coherent radiation and the dashed arrow represents incoherent radiation.

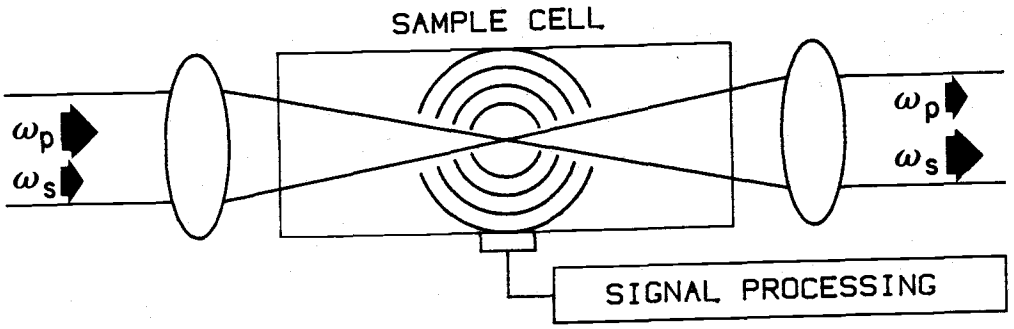

Figure 2-2 A schematic representation of the photoacoustic Raman process, showing the attenuation in ω_p, the corresponding gain in ω_s, and the generated acoustical wave.

ω_p, from an initial state $|A\rangle$ to a "virtual" state. Simultaneously, a photon ω_s, is scattered to return the molecule in the final state $|B\rangle$. This scattered photon $_s$ can be at the same frequency, a higher frequency, or a lower frequency then ω_p, corresponding to Rayleigh, Stokes, and Anti-Stokes scattering.

By applying a second beam at ω_s, the Raman transition from state $|A\rangle$ to state $|B\rangle$ can be "driven" in a coherent fashion. This nonlinear process of coherent Raman amplification is shown in figure 2-1b and results in the attenuation of the power of ω_p, a corresponding a amplification of the power of ω_s, and excitation of the molecule into state $|B\rangle$. This excited molecule can then collisionally relax to produce local heating and an acoustic wave which can be detected by a microphone (fig. 2-2).

The change in intensity of the Stokes beam (ΔI_s) is given by[12]

$$\Delta I_s = I_s(0)[\exp(g_s z)-1] \qquad (2.1)$$

where z is the interaction length of ω_p and ω_s and g_s is the gain factor. The gain factor is equal to

$$g_s = - \frac{16\pi^2\omega_s}{c^2 n_s n_p} \chi'' I_p \qquad (2.2)$$

where c is the speed of light, n_s is the refractive index at ω_s, and χ'' is the imaginary part of the third order susceptibility. By using an anharmonic approximation to describe the electron motion in an applied electric field χ'' can be expressed in terms of the differential Raman cross section $\frac{d\sigma}{d\Omega}$ as[17]

$$\chi'' = - \frac{\pi \Delta N c^4}{4h\omega_s^4} \left(\frac{d\sigma}{d\Omega}\right) \frac{\Gamma}{(\omega_v - \omega_s + \omega_p)^2 + \Gamma^2/4} \qquad (2.3)$$

where ΔN is the difference in number density between state $|A$ and State $|B$ and Γ is the half width at half maximum of the Raman transition.

Using equation (2.2) in equation (2.3) we find that g_s, expressed in terms of the differential Raman cross section is

$$g_s = \frac{4\pi^3 \Delta N c^2}{h n_p n_s \omega_s^3} \left(\frac{d\sigma}{d\Omega}\right) \frac{\Gamma}{(\omega_v - \omega_p + \omega_s)^2 + \Gamma^2/4} \qquad (2.4)$$

In most cases the gain factor $g_s z$ is small, therefore we can simplify expression (2.1) by using the approximation that $e^X = X + 1$ for small X. The error introduced by

using this approximation is relatively small even for values of X starting to approach 1[12]. Therefore equation (2.1) becomes

$$\Delta I_s = \frac{\Delta N 4\pi^3 z}{h n_p n_s \omega_s^3} \left(\frac{d\sigma}{d\Omega}\right) \frac{\Gamma}{(\omega_v - \omega_p + \omega_s)^2 + \Gamma^2/4} I_p I_s \qquad (2.5)$$

The intensity change in ω_s is directly related to the number of molecules excited from state A to state B, the important factor in determining the magnitude of the resultant pressure change in the medium. To calculate this pressure change we will use a simple two level model to determine the number of molecules that collisionally relax from state B to state A as a function of time.

The various processes for populating and depopulating the upper state in our model are shown in Fig. 2-3. The parameter S_{ij} represents the stimulated Raman transition rate. An expression for S_{01} can be determined from equation (2.5), bearing in mind that for every photon increase in ω_s we get one molecule transferred from state 0 to state 1.

$$S_{10} = \frac{16\pi^3 \Delta N z}{h n_p n_s^3 \Gamma} \left(\frac{d\sigma}{d\Omega}\right) I_p I_s \qquad (2.6)$$

The parameter R_{ij} is the radiative transition rate

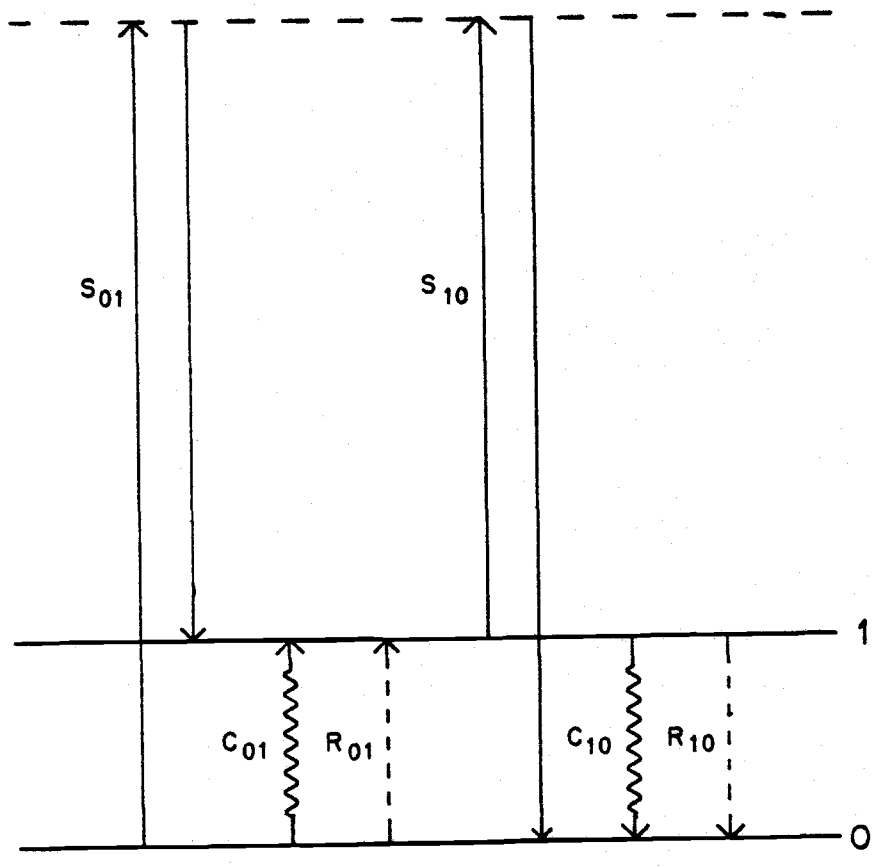

Figure 2-3 Energy level diagram showing the various processes for populating and depopulating the upper state. S, C, and R are transition probabilities for stimulated Raman, collisional, and radiative transitions respectively.

between levels i and j. R_{ij} is given by

$$R_{ij} = B_{ij}\rho(\nu) + A_{ij} \tag{2.7}$$

where $\rho(\nu)$ is the radiation density at the frequency,

$$\nu = \frac{E_j - E_i}{h} \tag{2.8}$$

E_i is energy of level i and B_{ij}, A_{ij} are the Einstein coefficients for stimulated and spontaneous emission.

The final rate constant C_{ij} represents the nonradiative collisionally induced transition rate. It is this term which gives rise to the photoacoustic signal.

During the duration of the laser pulse (~10 ns) we can assume that the only change in the population of level 1 is due to molecules being pumped into state 1 by the stimulated Raman effect. Therefore, we can write the change in the population of level one from its equilibrium value as

$$\frac{dN_1}{dt} = S(N_0 - N_1) \tag{2.9}$$

where N is the change in population of level i from its equilibrium value (N_1^e). With the definitions

$$N_1' = N_1 - N_1^e$$

$$N_0' = N_0 - N_0^e$$

$$N_1' + N_0' = 0$$

equation (2.9) becomes

$$\frac{dN_1'}{dt} = S(N_0^e - N_1^e - 2N_1') \tag{2.10}$$

$$\frac{dN_1'}{dt} = S(\ N - 2N_1') \tag{2.11}$$

where ΔN is the difference in the number density of level 0 and level 1 at equilibrium. This equation can be solved using the boundary condition that $N_1'(t=0)=0$, giving

$$N_1'(t) = \frac{1}{2}\ \Delta N[1-\exp(2St)] \tag{2.12}$$

After the laser pulse ($t=\tau$), the change in the v=1 population is therefore

$$N_1'(\tau) = \frac{1}{2}\ \Delta N[1-\exp(2S\tau)] \tag{2.13}$$

We now consider the acoustical signal generated by

the relaxation of the molecules pumped into the upper state. The relaxation rate of these molecules is

$$\frac{dN_1'}{dt} = -(R_{10}+C_{10})N_1' \tag{2.14}$$

We assume that $R_{10}=0$, since A_{10} is small for a vibrational transition and is often 0 for a Raman active mode. There is no stimulated emission at the transition frequency (in the infrared) because $\rho(\nu)=0$. Therefore

$$\frac{dN_1'}{dt} = -C_{10}N_1' \tag{2.15}$$

Integrating this expression from $t=\tau$ to ∞ and using the appropriate boundary conditions, we see that

$$N_1'(t\geq\tau) = N_1'(\tau)\exp[-C_{10}(t-\tau)] \tag{2.16}$$

The rate of heat input per unit volume at time t is therefore

$$H(t\geq\tau) = h\omega_v C_{10}N_1' \tag{2.17}$$

$$= h\omega_v C_{10}N_1'(\tau)\exp[-C_{10}(t-\tau)] \tag{2.18}$$

Using this expression we can calculate the local change in pressure at the microphone as

$$\frac{dp}{dt} = \frac{\gamma-1}{V} \int^{V_f} H(t\geq\tau)dV \qquad (2.19)$$

where V_f if the focal volume, V is the volume of the gas around the microphone, and γ is the ratio of the heat capacities (Cp/Cv). Using equation (2.18) in (2.19) we obtain

$$\frac{dp}{dt} = \frac{\gamma-1}{V} \int^{V_f} h\omega_v C_{10} N_1'(\tau)\exp[-C_{10}(t-\tau)]dV \qquad (2.20)$$

$$=(\gamma-1)\frac{V_f}{V} h\omega_o N_1'(\tau)\exp[-C_{10}(t-\tau)] \qquad (2.21)$$

Then by using equation (2.13) we find that the change in pressure at the microphone as a function of time is

$$p(t\geq\tau) = \frac{V_f}{2V} (\gamma-1)h\omega_o C_{10}\Delta N[1-\exp(-2S\tau)]$$

$$X \exp[-C_{10}(t-\tau)]\tau \qquad (2.22)$$

We can see from this equation that the pressure change is related to the rate of collisional relaxation. One way to improve the signal, therefore, would be to add a buffer gas that would allow faster relaxation of the upper state. The solution for the pressure change

from equilibrium in the presence of a buffer gas is

$$p(t \geq \tau) = \frac{V_f}{2V} (\gamma-1) h\omega_o (C_{10}+N_B C_{1B}) \Delta N$$

$$X \; [1-\exp(-2S\tau)\exp(C_{10}+N_B C_{10})(t-\tau)]\tau \quad (2.23)$$

where C_{1B} is the collisional relaxation rate of a excited sample molecule and the buffer gas and N_B is the number density of the buffer gas.

2.3 Experimental

The experimental arrangement for PARS is shown schematically in figure 2-4. The primary laser source in the photoacoustic Raman system is a Nd:YAG laser (Quanta-Ray DCR-1A) which has been modified by the addition of a second etalon and a line narrowing device (Quanta-Ray ELN 1) to increase the single mode characteristics of the laser. This laser provides between 300-600 mJ of energy at 1064 nm, with a pulse duration of approximately 8 ns and a line width of around 0.02 cm^{-1}. The output of the laser is doubled using a angle tuned KD^*P crystal to produce 50-100 mJ of 532 nm radiation. The two frequencies are then spatially separated using a dispersing prism. The

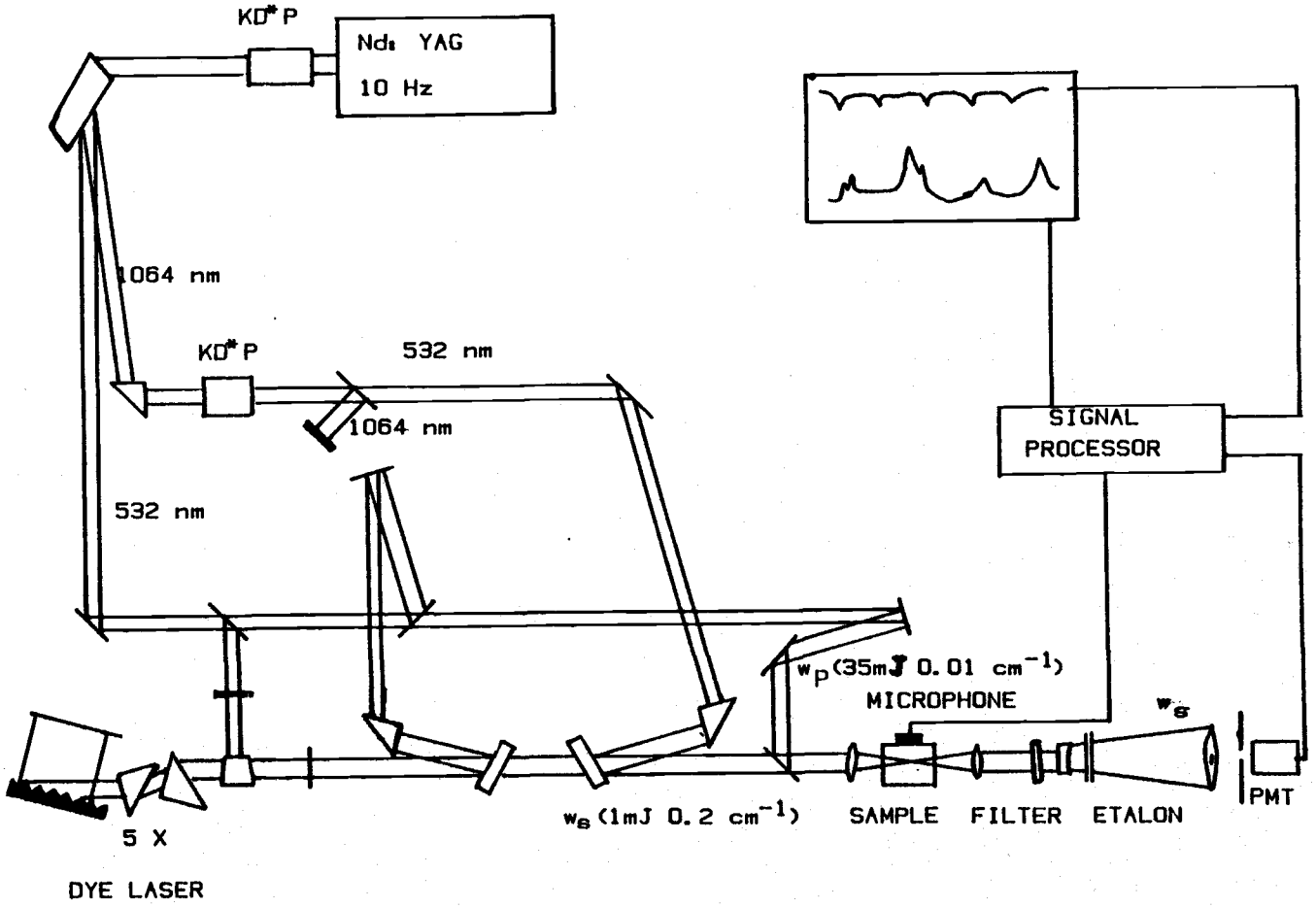

Figure 2-4 Schematic diagram of the PARS spectrometer.

remaining 1064 nm radiation is again doubled and this secondary green beam is used to longitudinally pump the second amplifier of the dye laser. The primary 532 nm green beam (ω_p) is expanded with a telescope (not shown in figure 2-4) to reduce damage to optical elements. Using dichroic mirrors part of the green beam is removed to pump the oscillator and first amplifier of the dye laser. A Littman type dye laser[18] is used consisting of a 5X beam expander and a 4 inch 2400 line/mm holographic grating in a grazing angle configuration. The tuning of the dye laser is achieved by a stepper motor attached to the back mirror. The output from the oscillator is amplified using two longitudinally pumped dye cells to give a dye laser output of 0.3 - 2 mJ and a linewidth of approximately 0.2 cm^{-1} (ω_s).

The output of the dye laser is then expanded using a telescope (not shown in figure 2-4) to match the diameter of the primary green beam and to obtain a common focus in the photoacoustic cell. The two beams are then made collinear using a dichroic mirror and are focused into the photoacoustic cell using a 300 mm focal length lens. The output from the cell is then recollimated using another 300 mm focal length lens and $_s$ is separated out using a red pass filter. The Stokes beam is then passed through an etalon to provide

frequency calibration of the dye laser.

The acoustical signal is measured using a Knowles model BT-1759 hearing aid microphone which is mounted in the photoacoustical cell. The output of the microphone is amplified and frequency filtered using an Ithaco Model 1201 low noise preamplifier. The amplified signal is then measured using either a box car integrator or is read into a PDP 11/10 computer using an A/D converter with a built in sample and hold.

2.4 Noise Sources

The most serious noise limitation in photoacoustic Raman spectroscopy is the background signal arising from the absorption of the optical beams on the cell windows and, to a lesser degree, from the absorption of scattered radiation on the cell walls.

When light passes through the entrance or exit window it can be absorbed by either the bulk material of the window or by material deposited on it. The window absorption is reduced by using high quality S-1 UV windows. The cleaning process for these consisted of successive rinsings with spectral grade hexane, acetone, and methanol. The final step in this important cleaning operation was to draw a drop of methanol across the

faces of the windows using lens paper.

The light that is absorbed by the cell walls is from back reflection off the cell exit window and from scattering of particles in the gas sample. Back reflection was minimized by placing the cell windows at Brewster's angle to the incoming plane polarized light and by keeping the cell windows cleaned. Particle scattering was reduced by the frequent refilling of the sample cell.

2.5 Photoacoustic Cell

In general all photoacoustic cells are classified as either resonant or nonresonant[19]. This designation comes from whether or not the design takes advantage of acoustical resonances of the cell to increase the photoacoustic signal measured. Because of the low repetition rate of the Quanta-Ray Nd:YAG laser (10 Hertz), we are restricted to the use of nonresonant cells.

The first attempt to achieve a photoacoustic Raman signal used a nonresonant photoacoustic cell as described by Barrett[15]. The cell (Fig. 2-5a) was made from a 1/4" Cajon Ultra-Torr T vacuum fitting modified to include a Knowles BT-1759 microphone. Brewster angle

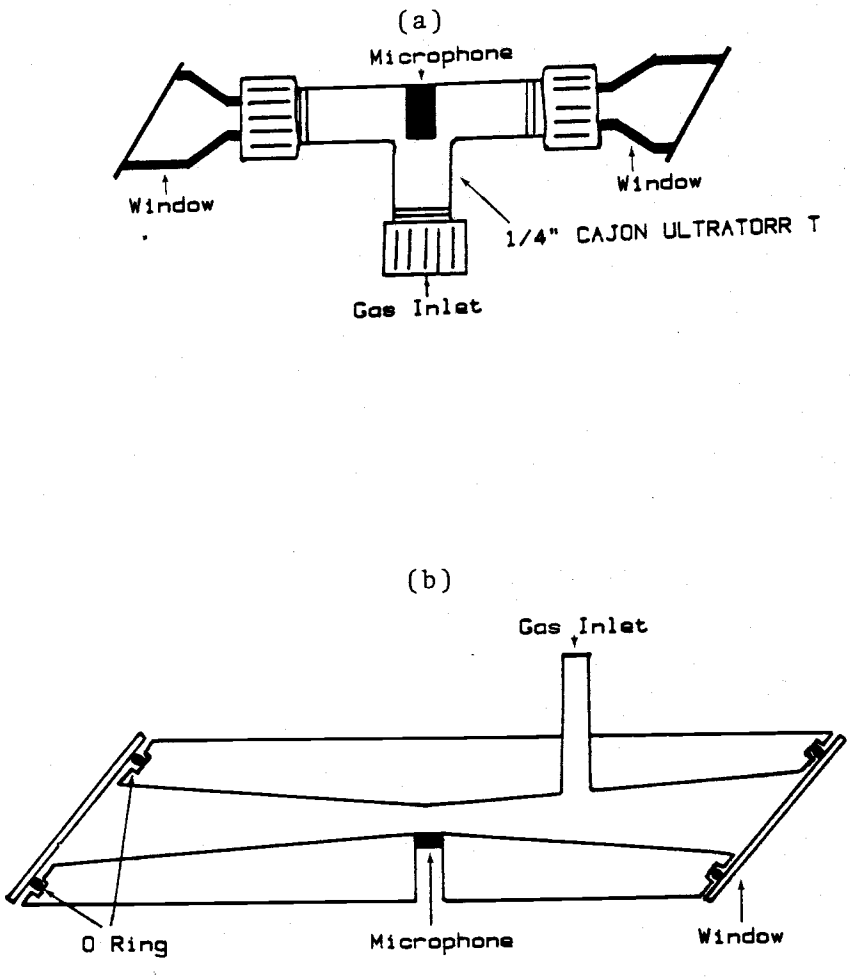

Figure 2-5 Designs of nonresonant photoacoustic Raman cells: a) early model based on Barrett's design b) Cross section of the currently used photoacoustic Raman cell.

windows attached on 1/4" glass tubing were mounted on the vacuum couplers to form the optical path. The remaining coupler was used for filling and evacuating the photoacoustic cell. This cell design had several limitations: first, it was difficult to position the cell in the optical path and second, the windows were hard to clean and replace.

These limitations led us to an improved design, the photoacoustic cell shown in fig. 2-5b. The cell was constructed of 1 1/4" aluminum round bar. Aluminum was chosen to minimize the noise caused by scattered radiation being absorbed on the cell walls[20]. The cell was made by boring out the center of the round bar with a tapered cut to form the optical path way and to minimize the volume of gas around the microphone (eq. 2.22). The ends of the cell were milled to Brewster's angle, to minimize reflection of the laser beams, and 1" circular O-ring grooves were cut for attaching the cell windows. A notch was cut in the center of the cell, for attaching the microphone. and a 1/4" tube was attached for filling and evacuating the cell. The cell was anodized black to cut down on multiple reflections of the scattered light. Finally the Knowles BT-1759 microphone was glued into place using a high vacuum cement.

This cell proved to be much better then the original design with greater sensitivity and improved improved ease of use.

2.6 Discussion

In this section we present some of the results that we have obtained in this study of the potential of photoacoustic Raman spectroscopy. The first gas examined was carbon dioxide. This gas was chosen because of it's large Raman cross section.

By scanning the dye laser, using Rhodamine 6G, we were able to obtain the photoacoustic Raman spectra shown in figure (2-6). This spectrum has not been corrected for variations of the dye laser output power, which falls off at lower frequency shift values. the two central features in the spectra, found at 1285 cm^{-1} and 1388 cm^{-1}, correspond to Q branch transitions of the Fermi resonant pair ν_1 and $2\nu_2$. The actual magnitude of the ν_1 peak, which goes well off scale in this figure, can be estimated from the corresponding ^{13}C (~1% abundance) peak found at 1370 cm^{-1}. The outer two strong Q branch transitions at 1285 cm^{-1} and 1409 cm^{-1} are corresponding hot bands of the Fermi resonant pair. Along with the Q branch transitions, we also see the O and S branch transitions of the ν_1 and

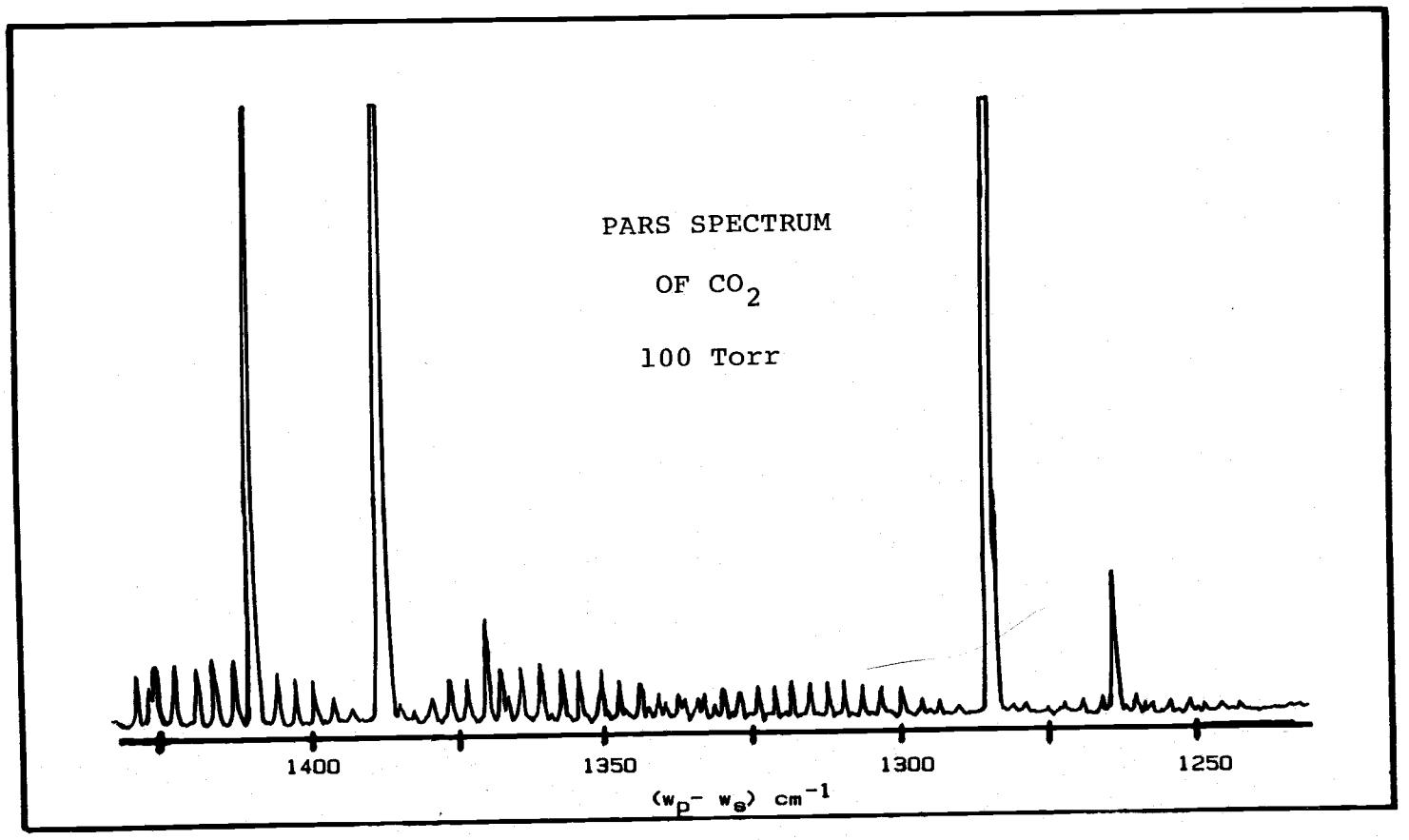

Figure 2-6 PARS spectrum of Carbon Dioxide.

$2\nu_2$ Fermi pair.

This spectrum also gives an idea of the sensitivity and the resolution which one can obtain using the PARS technique. Using PARS Siebert, West, and Berry[22] have detected samples down to 1 ppm whereas the sensitivity for CARS by comparision is about 20 ppm[21]. In PARS, since no monochromators are used, the resolution is strictly determined by the convolution of the line widths of the pump and Stokes laser. This gives a theoretical resolution limit which is ultimately governed by the Fourier transform limit of the 5 nsec pulsed laser (0.007 cm^{-1}) although our system resolution was much poorer (0.3 cm^{-1}).

Methane was another molecule studied to determine how various experimental parameters affected the photoacoustic Raman signal. To perform these tests a crystal violet dye was used in the dye laser to allow scanning over the ν_1 region of methane. A typical spectrum of the unresolved Q branch of the ν_1 transition of methane is shown in figure (2-7).

By measuring the peak signal of the ν_1 transition of methane the effect of changing the pressure of methane was examined (figure (2-8)). The excellent linearity of the plot of photoacoustic Raman signal versus the number density is consistent with the

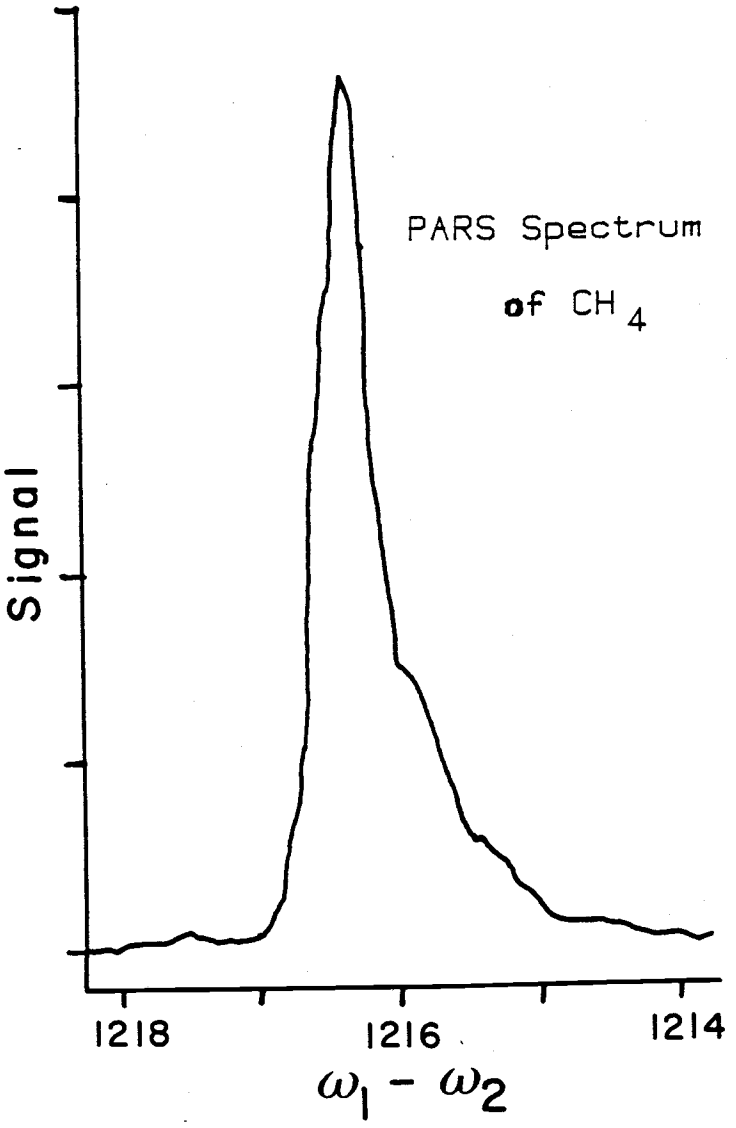

Figure 2-7 PARS spectrum of the ν_1 transition of Methane.

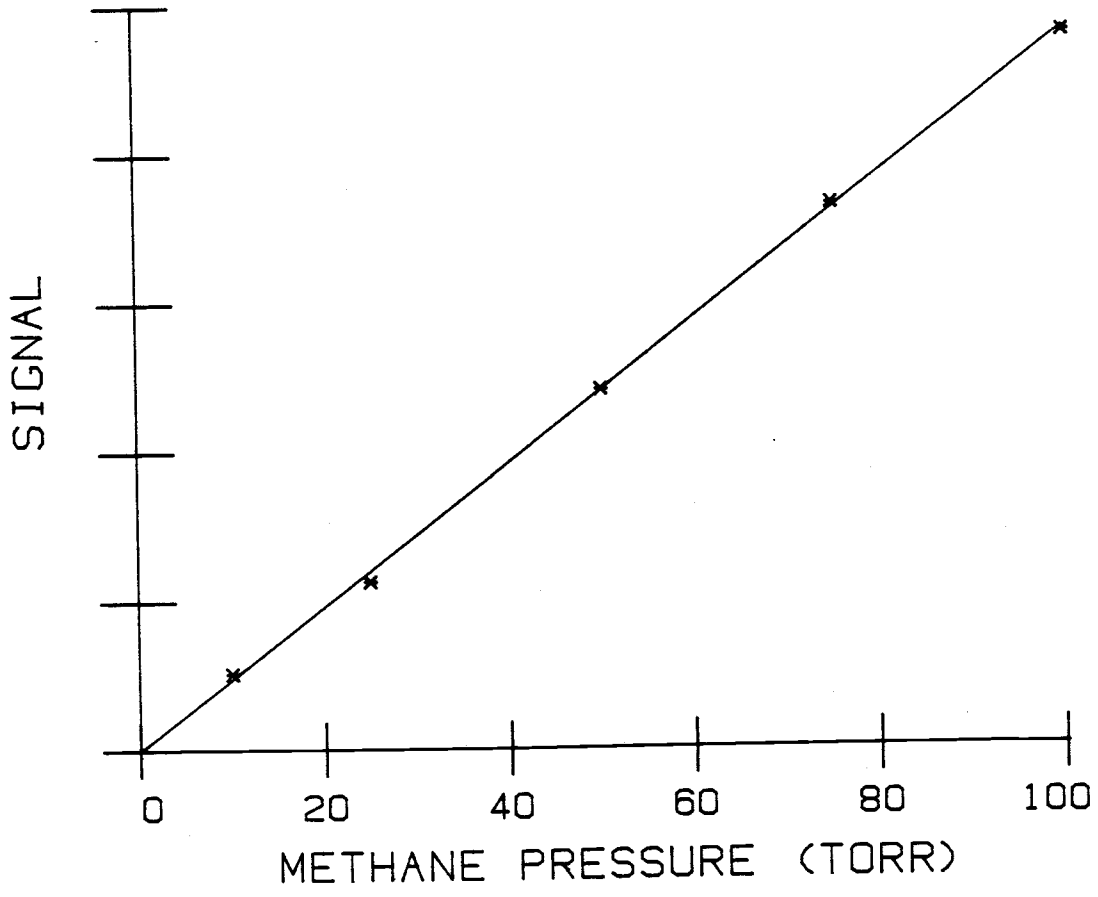

Figure 2-8 Plot of the peak PARS signal versus gas pressure.

predictions of eq. 2.23 and points to the analytical utility of this method.

By measuring the peak signal of the ν_1 transition of methane, the effects of adding a buffer gas were investigated. According to equation (2.24) the photoacoustic Raman signal should increase with the addition of a buffer due to an increase in the rate of collisional relaxation. Figure (2-9) shows the effect of addition of N_2 on the acoustical signal of a sample of methane at 10 Torr. We see that significant gains in the signal strength are achieved due to the improved coupling between the sample and the microphone. One would expect that this plot should level out at higher buffer gas pressures since the amount of energy input into the sample is fixed.

Besides N_2 we have also looked at the effects of adding $SF_6$and He. We found that for 10 Torr of methane and 90 Torr of buffer gas we achieve a gain of 5.82 for N_2, 5.78 for SF_6, and 3.06 for He. According to Rosencwaig[20] the collision relaxation rate should be proportional to the reduced mass of the collisional pair and the energy loss to translation in the collision. Therefore, He should give the smallest increase and SF_5 the greatest increase in photoacoustic signal. Our results did confirm that He gave the smallest increase

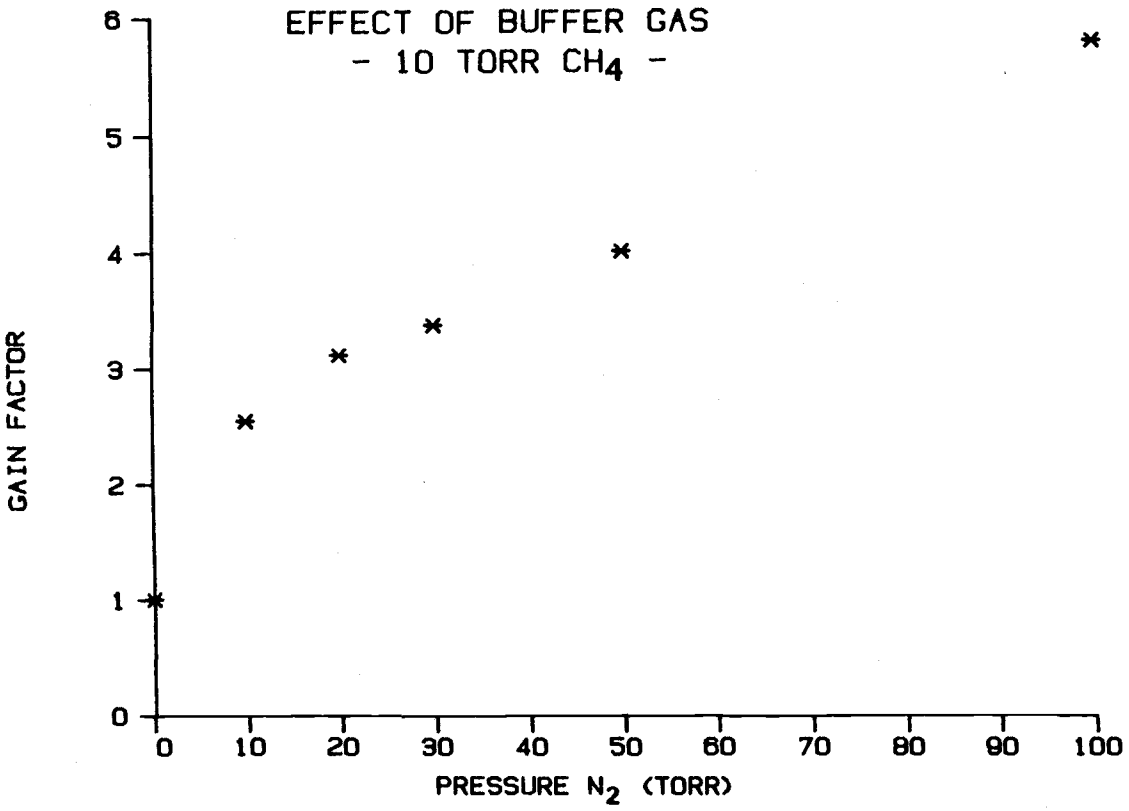

Figure 2-9 Plot of the gain in the peak PARS signal versus the buffer gas pressure.

in signal but both N_2 and SF_6 gave approximately the same increase in signal. As mentioned above, at this point, the signal is probably limited by the amount of heat input and not by the relaxation rate.

2.7 Conclusions

In this chapter we have briefly described some preliminary results using photoacoustic Raman spectroscopy. This nonlinear Raman technique is based upon the acoustical detection of the stimulated Raman effect.

Since photoacoustic Raman spectroscopy measures directly the energy input into the system and not a change in the intensity of radiation passing through the cell it is inherently more sensitive than Raman Gain (Loss) Spectroscopy. Using the PARS technique Siebert[22] has been able to achieve a detection limit of 1 ppm. Thus the method may have important applications in the measurement of atmospheric contaminates.

The second area in which PARS should prove useful is in the measurement of frequencies of Raman transitions. These are unshifted and the lineshapes undistorted by nonresonant contributions of the third order susceptibility, contributions which become quite

large for CARS spectra of trace amounts of sample. In principle the resolution of PARS is limited mainly by the convolution of the pump and probe laser line widths. By using copropagating lasers and low pressures the effects of collisional and Doppler broadening on molecular linewidths can be reduced. A limit here is that sufficient buffer gas must be kept to provide good coupling to the microphone. Assuming that it requires a total cell pressure of 10 mtorr, this limits the resolution for polar molecule to about 0.0075[23] cm^{-1} and 0.003 cm^{-1} for nonpolar molecules[24] due to pressure broadening. A second limitation is that corrosive gases will attack the microphone.

The application of PARS technique to study pure rotational Raman transitions was demonstrated by West and Barrett[22]. In the low shift region PARS has an advantage over Raman spectroscopy and other nonlinear Raman techniques in that optical discrimination against the intense input lasers is unnecessary. Therefore, PARS can be used to obtain high resolution spectra at very low shifts for the determination of rotational constants of molecules which are Raman active. Low frequency vibrations can also be examimed. For example by studying the torsional modes of various conformers of a molecule as a function of temperature one could use

PARS measurments to calculate the energy barrier between the various conformers of a molecule such as 1-2 diflurroethane. The present work has demonstrated the feasibility of PARS with sources available to us and has revealed some of the advantages and disadvantages of the method. The conclusion is that PARS is nontrivial but promising for many future applications in chemistry.

CHAPTER 3

Third Order Nonresonant Susceptibilty of Various Gases

3.1 Introduction

In recent years many new nonlinear optical techniques have been developed and applied to problems in physics and chemistry. Some of these techniques, like CARS (Coherent Anti-Stokes Raman Spectroscopy)[10,25,26], measure a bulk third order susceptibility (χ)

$$\chi = \chi_r + \chi_{nr} \tag{3.1}$$

made up of resonant (χ_r) and nonresonant (χ_{nr}) terms[7,8,27]. Usually the objective of these measurements is to determine population densities and/or resonant transition frequencies. However, the nonresonant term leads to significant frequency shifts and spectral line distortion[10]. This effect can be

compensated for if one knows the relative values of χ_{nr} and χ_{r}. Unfortunately only a few values for χ_{nr} have been reported for gases[28,29] and their absolute accuracy is uncertian[28,30]. These values of $_{nr}$ were obtain using a stimulated Raman beam produced from H_2 by a Ruby laser at 694 nm. In this chapter we will report extensive measurements using a frequency doubled Nd:YAG laser at 532 nm.

The determination of the nonresonant susceptibilities of the various gases was done in two steps. In the first step we measured the nonresonant value of each gas relative to that of nitrogen. Then, to convert to absolute values, the nonresonant susceptibility of nitrogen was measured relative to the resonant susceptibility of hydrogen, whose absolute susceptibility can be determined using recent Raman cross section and linewidth data[27,29,31].

In part, the motivation for these measurements came from our use in chapter four of nonresonant samples to obtain the power distribution of a broadband ω_2 source used in multiplexed CARS studies of molecules in free jet expansions[31,32]. The nonresonant anti-Stokes (ω_3) curve is especially useful since it represents the convolutions of the ω_2 distribution with the transmission function (for filters and spectrometer)

that affects the resonant signal of the gas of interest. Under the tight focussing conditions of these experiments, appreciable nonresonant signals could be obtained which showed the expected quadratic growth at low pressures but, surprisingly, much larger signals at higher densities, due to the onset of dielectric breakdown of the gas.

3.2 Theory

The field induced polarization of a medium for a third order process is given by[35,36]

$$\vec{P} = K\chi\ \vec{E}_1\vec{E}_2\vec{E}_3 \qquad (3.2)$$

where K is a numerical constant which depends on the particular combination of electric field frequencies involved in the nonlinear process. The virtue of using this definition of is that it allows one to directly compare χ's measured by different techniques since they all approach the same static limit. In the case of CARS $[\chi(-\omega_3;\omega_1,\omega_1,-\omega_2)]$ K = 3/4. However, K differs for other third order processes such as third harmonic generation THG $[\chi(-3\omega_1;\omega_1,\omega_1,\omega_1)]$ where K=1/4, dc field induced second harmonic generation dcSHG

$[\chi(-2\omega_1;0,\omega_1,\omega_1)]$ where K = 3/2, or the KERR effect $[\chi(-\omega_1;0,0,\omega_1)]$ where K=3.

For monochromatic ω_1 and ω_2 sources, the power of the CARS signal generated at ω_3 is given by

$$P = C\Delta N^2 P_1^2 P_2 |\chi|^2 \tag{3.3}$$

where c is a constant and ΔN is the difference in number density of the two states envolved in the process. As stated earlier χ is the sum of a resonant and a nonresonant term. In the case of CARS where ω_1, ω_2, and χ_3 all have the same polarization $\chi_{||}=\chi_r$, equation (3.3) becomes

$$P = C\Delta N^2 \ |\chi_r + \chi_{nr}|^2 \ P_1^2 P_2 \tag{3.4}$$

3.2.A Nonresonant to Nonresonant Ratio

Off resonance, when $\chi_{nr} >> \chi_r$, the power of the CARS beam is only related to the nonresonant part of χ. Therefore using equation (3.4) we can see that the power of the nonresonant signal (P_{nr}) is

$$P_{nr} = C\Delta N^2 \, |\chi_{nr}|^2 \, P_1^2 P_2 \tag{3.5}$$

By taking the ratio of the nonresonant signal of some sample gas, at a pressure p(sam), to that of a standard nonresonant signal, we find that

$$\frac{P_{nr}(sam)}{P_{nr}(std)} = \frac{p^2(sam)}{p^2(std)} \left| \frac{\chi_{nr}(sam)}{\chi_{nr}(std)} \right|^2 \tag{3.6}$$

The P_1 and P_2 power dependence cancels out as long as it is the same for both the sample and the standard gases. Equation (3.6) defines a linear relationship between the nonresonant ratio and the square of the sample pressure, with the slope being equal to

$$\text{Slope} = \frac{1}{p^2(std)} \left| \frac{\chi_{nr}(sam)}{\chi_{nr}(std)} \right|^2 \tag{3.7}$$

The ratio of any two slopes is therefore equal to the ratio of the squares of their nonresonant susceptibilities.

$$\frac{\text{Slope}(1)}{\text{Slope}(2)} = \left|\frac{\chi_{nr(1)}}{\chi_{nr}(2)}\right|^2 \tag{3.8}$$

Using the values calculated from this ratio we can then calculate the nonresonant susceptibility of one gas when the other is known.

3.2.B Nonresonant to Resonant Ratio

When using a broadband ω_2 source the integrated CARS power (P_{int}) is[37]

$$P_{int} = C\Delta N \int |\chi_r + \chi_{nr}|^2 P_1^2 P_2 d\omega \tag{3.9}$$

We assume that ω_1 is monochromatic and that ω_2 has a uniform power density in the resonance region, this is true as long as the line width of ω_2 is much greater then the Raman line width of the transition and if ω_2 is continuous. The integrated CARS power then becomes

$$P_{int} = C\Delta N^2 P_1^2 P_2^o \int |\chi_r + \chi_{nr}|^2 d\omega \tag{3.10}$$

where P^o is the power of ω_2 at the resonance frequency. In the resonance region we can assume that $\chi_{nr} << \chi_r$, so

$$P_{int} = C\Delta N^2 P_1^2 P_2^o \int |\chi_r|^2 \, d\omega \tag{3.11}$$

However, χ_r can be written as

$$|\chi_r|^2 = |\chi_r^o|^2 \frac{\Gamma^2}{\delta + \Gamma^2} \tag{3.12}$$

where χ_r^o is the peak susceptibility, $\delta = \omega_v - \omega_1 + \omega_2$, and Γ is the half width of the Raman transition. Using this expression in equation (3.11) we get

$$P_{int} = C\Delta N^2 P_1^2 P_2^o \int |\chi_r|^2 \frac{\Gamma}{\delta + \Gamma^2} \, d\omega \tag{3.13}$$

$$P_{int} = C\Delta N^2 P_1^2 P_2^o |\chi_r|^2 \pi\Gamma \tag{3.14}$$

By replacing the resonant sample with a nonresonant sample in equation (3.10) and integrating the resulting

expression over the frequency interval Z, corresponding to one channel on our detector the power generated at the resonant channel is

$$P_{nr} = C\Delta N^2 Z P_1^2 P_2^o |\chi_{nr}|^2 \qquad (3.15)$$

By dividing equation (3-14) into equation (3-15), we find that the ratio of the nonresonant susceptibility of one gas to the resonant susceptibility of another at the resonant frequency is

$$\frac{P_{nr}}{P_{int}} = \left|\frac{\chi_{nr}}{\chi_r^o}\right| \frac{Z}{\pi\Gamma} \qquad (3.16)$$

This measurement therefore allows one to calculate the nonresonant susceptibility of one gas if the resonant susceptibility of the other gas is known or vice versa.

3.3 Calculation of $\chi_{||}$ for Hydrogen

The value of $\chi_{||}$ for a gas can be calculated from the Raman cross section and line width data. The expression relating the third order resonance

susceptibility (χ_{11}) for CARS and the parallel component of the Raman polarizability (α_{11}^2) has been derived by both classical[30,31] and quantum mechanical methods[25,27]

$$\chi_{11} = \frac{\alpha_{11}^2}{3h(\delta - i\Gamma)} \tag{3.17}$$

The parellel component of the Raman cross section is related to the total Raman polarizability element (α^2) by the relationship[31,38]

$$\alpha_{11}^2 = \frac{\alpha^2}{1+\rho_L} \tag{3.18}$$

where ρ_L is the depolarization ratio for linearly polarized light. In terms of the total Raman scattering cross section

$$\alpha^2 = \left(\frac{c}{\omega_3}\right)^4 \left(\frac{d\sigma}{d\Omega}\right)(1 + \rho_L)^{-1} \tag{3.19}$$

Schrotter[39] recently reviewed existing Raman cross section data and referenced all the values to the polarizability of the Q branch of N_2

$$\alpha^2_{N_2} = 3.26 \pm 0.06 \times 10^{-51} \text{ cm}^6/\text{sr} \qquad (3.20)$$

This table of $S = (\alpha_i/\alpha_{N_2})^2$ cites values for H_2 of 3.45, 3.64, 4.15, and 4.2 for this ratio at wavelengths of 515, 488, 436, and 377 nm respectively. The increase in cross sections towards shorter wavelengths is consistent with theory[40]. However, all the values are within the uncertainties given by Schrotter, 10% in the visible and 15% in the UV. For the purpose of these calculations we have taken the average of values at 515 and 488 nm, since they represent the most recent laser excitation data and are closest in wavelength to 532 nm. We use them to calculate a value of 3.54 at 532 nm with an assumed uncertainty of 10%. Since this value represents the total Q branch intensity and not just the Q_1 line we have to multiply this value by the fraction of the total Q branch which Q_1 comprises. At 20 C this is 0.664[40]. Using the experimental value of $\rho_L = 1/2\,\rho_N = 0.036$[42,43] we obtain $\alpha^2_{\perp} = (7.36 \pm 0.75) \times 10^{-51}$ cm^6/sr for the Q_1 branch of H_2.

From the line width measurements of Owyoung[42] we can calculate for our experimental conditions (7000 Torr and 20 C) that the Q_1 branch of H_2 has a line width of

$\Delta\nu$= 473.1 ± 6.1 MHz. Using equation (3.17) and the values of Γ and α^2 just calculated, we find finally that the peak CARS susceptibilty (Γ=0) for Q_1 branch of H_2 is χ_{II} = (1.57 ± 0.16) X 10^{-33} cm^6/sr molecule.

3.4 Experimental

The experimental apparatus used for these measurements is shown in figure (3-1). The apparatus is based upon a Nd:Yag laser (Quanta Ray DCR-1A) which has been modified by the addition of a second etalon. The output from the Nd:Yag laser is doubled to produce 532 nm radiation pulses of 10 nsec duration at 10 Hz. This 532 nm source is used as the ω_1 beam and to pump the oscillator and the amplifier cells of the dye laser. The dye laser oscillator consisted of a transversely pumped flowing dye cell, a 35% reflective front mirror, a optical polarizer, a low dispersion prism, and a totally reflective back mirror. Using experimental red dye (Exciton) the oscillator, when combined with two transversely pumped dye cell amplifiers, gives ω_2 powers of 1 to 3 mJ/pulse with a line width (FWHM) of 75 to 125 cm^{-1}. The ω_1 and ω_2 beams are combined using a dichroic mirror and focused into the sample cell using either a 100 or 300 mm focal length lens. The

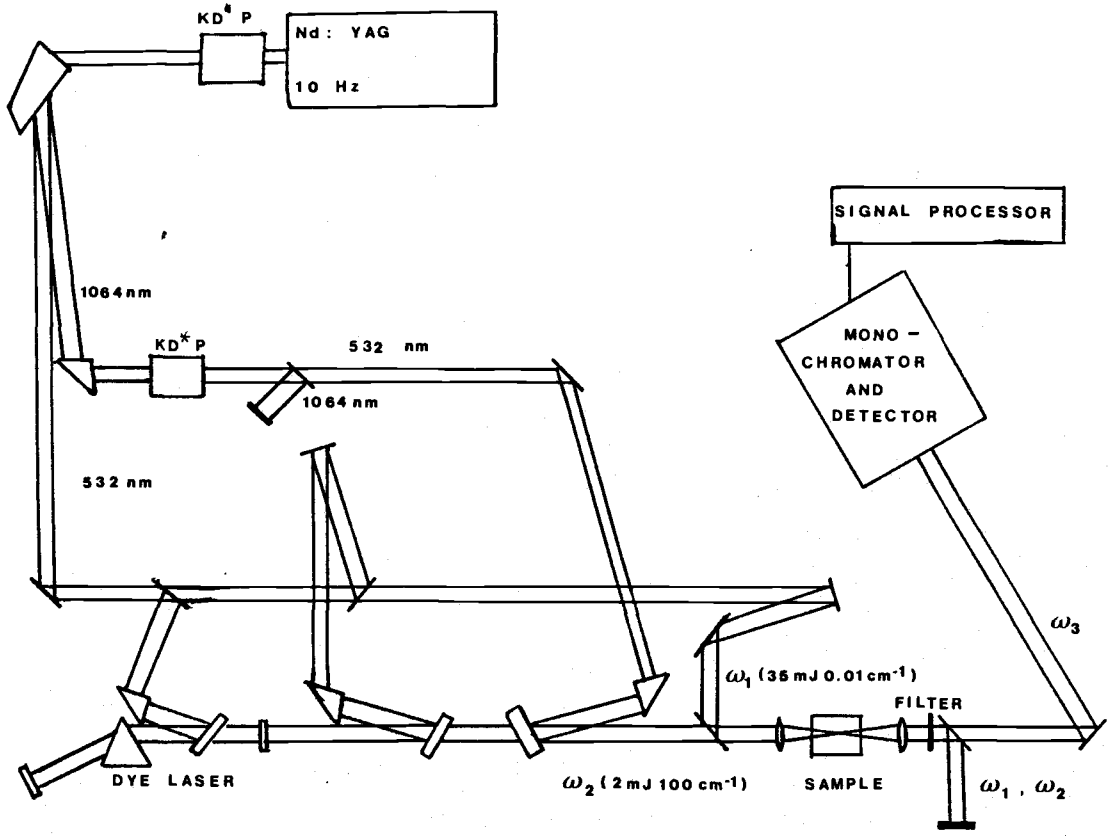

Figure 3-1 Schematic diagram of the broadband CARS apparatus.

collimated ω_3 beam is then separated from ω_1 and ω_2 using a Corning 5-60 filter and a dichroic mirror.

For the measurement of the relative nonresonant values, ω_3 was spectrally filtered further using a monochromator (McPherson 218) with a band pass of 100 cm^{-1}. The intensity of the CARS beam (ω_3) was monitored using a photomultiplier (RCA 31034A). The output of the photomultiplier was then amplified and read into a PDP 11/10 using an A/D converter with a built in sample and hold. For each sample pressure 1000 measurements were averaged, corrected for background and ratioed against the nonresonant signal of 30 torr of nitrogen. The sample and reference measurements were taken using the same cell in an interleaved fashion to minimize the effects of long term power fluctuations. The programs used for the data collection, calculations, and plotting of the nonresonant ratios are given in Appendix A.

For the measurement of the nonresonant to resonant ratio, ω_3 was dispersed by a double monochromator (SPEX 1402) onto the vidicon of an optical multichannel analyzer (PAR OMA-2) with a dispersion of 0.3563 cm^{-1}/channel. These measurements were made using a stainless steel sample cell to allow for the high pressure of hydrogen (7000 Torr) required to ensure the

validity of the pressure broadened line width expressions of Owyoung. The high pressure of H_2 required that OD 2 filters be used in both the ω_1 and ω_2 beams. This removed any stimulated Raman effects and the possibility of saturating the detector. These filters were calibrated under experimental conditions by measuring ω_3 signals with and without the filters in different combinations. In this manner the effects of thermal lensing, filter bleaching, and beam steering were minimized. Each measurement of this ratio consisted of the average of 1000 scans for N_2 and H_2.

For all of the measurements, the gases were taken directly from a gas cylinder and introduced into the sample cell. The pressure in the sample cell was monitored using either a 100, 1000, or 10000 Torr Validyne pressure transducer.

3.5 Results and Discussion

Due to the high power densities of the lasers employed in this work, we had to be careful that breakdown was not occuring in the sample cell. Breakdown could be avoided by keeping the cell pressure low and it could be detected from either florescence at the focal point or a large increase in the standard

deviation of the signal.

Figure (3-2) shows the relationship between the sample gas pressure and the nonresonant signal of argon. As predicted by equation (3.6), the signal shows a quadratic growth with pressure. The slope of the signal versus the square of the pressure was determined by performing least squares fit of the the data to a straight line (program NRLINE: Appendix A). The error determined is equal to the standard deviation of the slope.

As shown in figure 3-3 the nonresonant signal of a gas goes through two quadratic regions with sample pressure. The first one occurs at low pressures for the molecule in its natural state; the second quadratic region is attributed to excited species formed in a dielectric breakdown at higher pressures. The breakdown species clearly have a much larger nonresonant susceptibility than the ground state molecules. This effect proved to be very useful when using the weak nonresonant signals to obtain the power distribution of the broadband ω_2 source.

A value for $\chi_{nr}(N_2)/\chi_r(H_2)$ of $(6.88 \pm 0.46) \times 10^{-5}$ was obtained by taking the average of seven sets of measurements. Each set consisted of the accumulation of 1000 laser shots for N_2 and H_2. This value can be

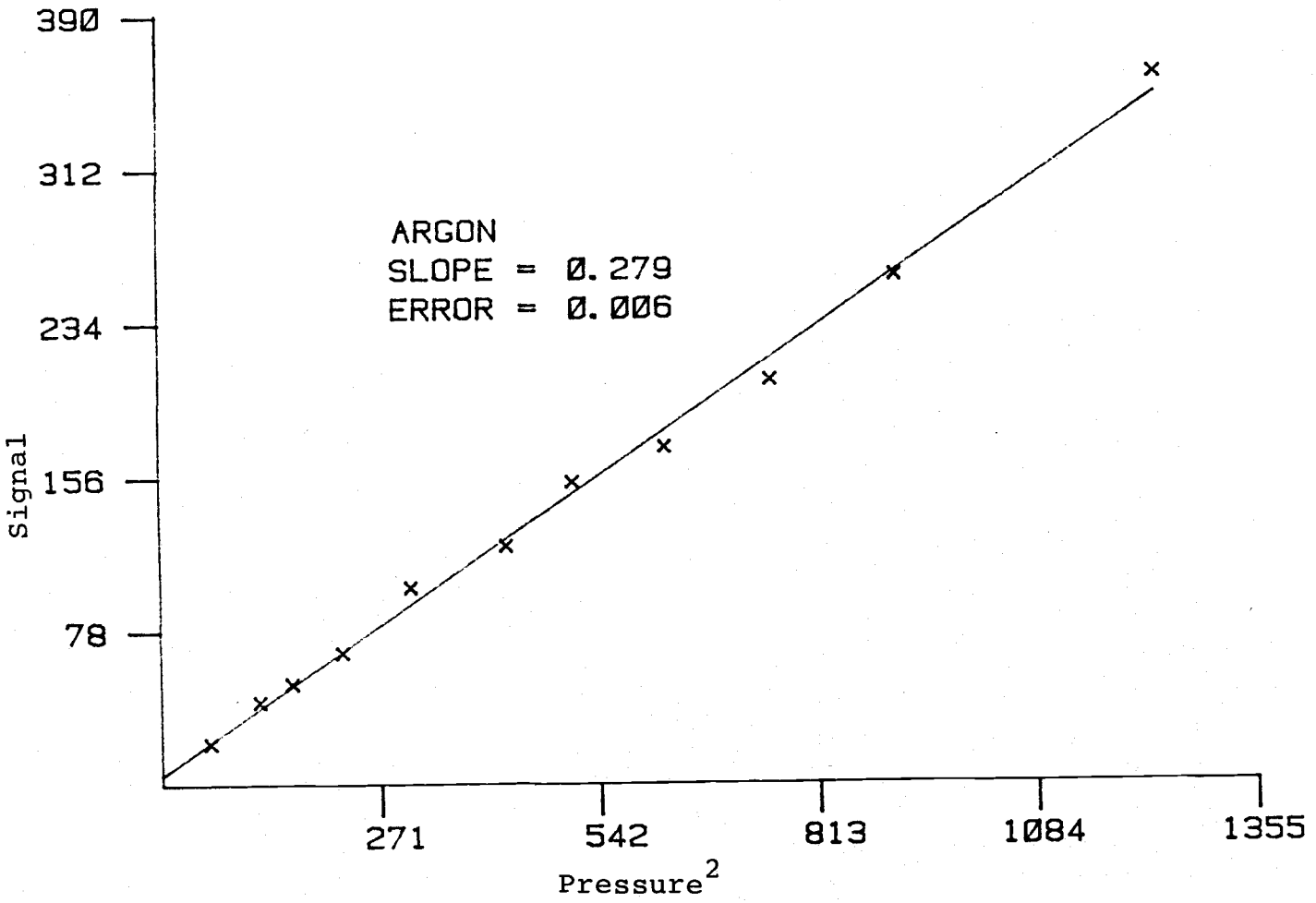

Figure 3-2 Plot of the signal dependence on the square of the sample pressure. The signal = (P_{Ar}/P_{N_2}) X 100

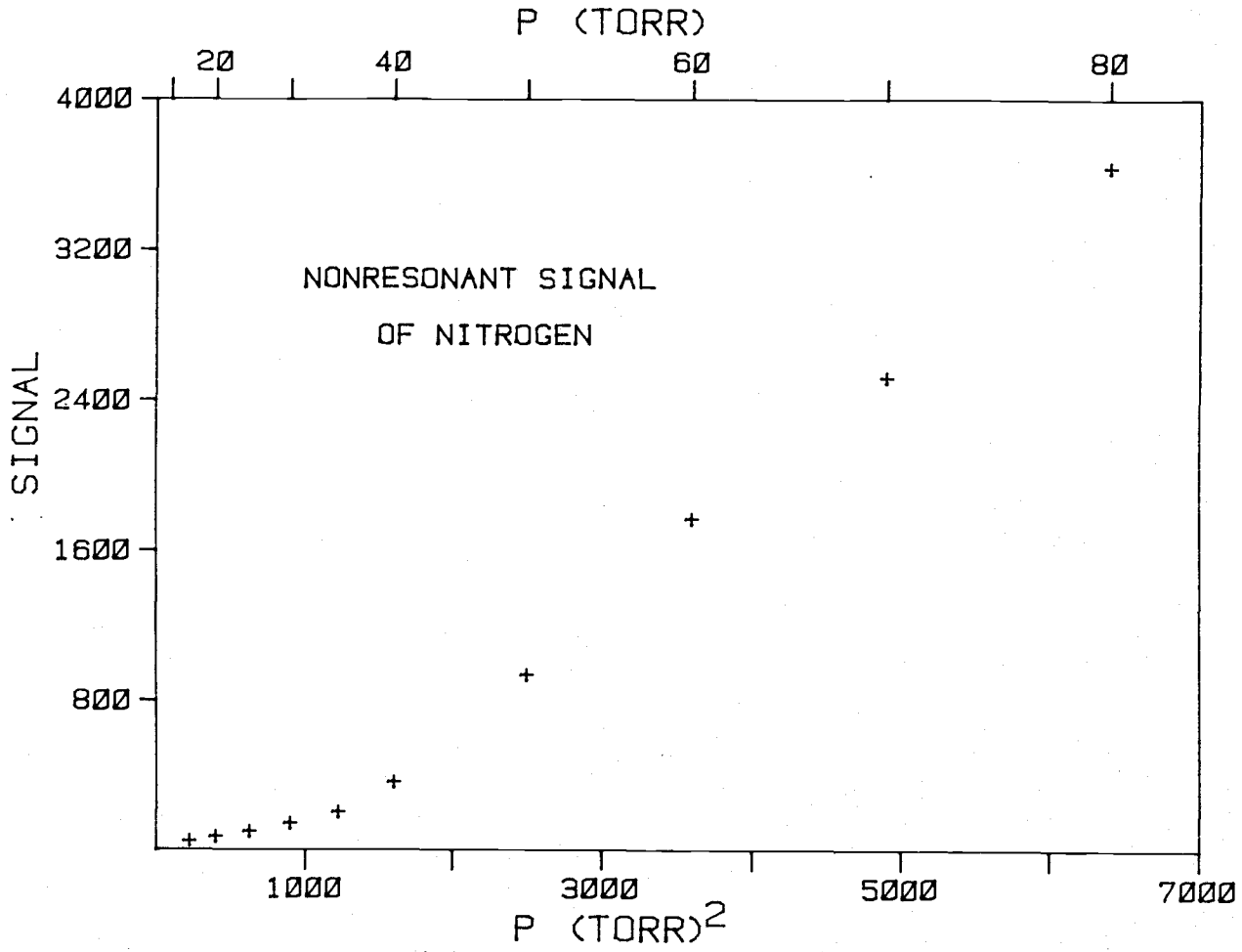

Figure 3-3 Plot of the signal dependence on pressure before and after breakdown.

compared with a value of $(6.26 \pm 0.6) \times 10^{-5}$ computed from Rado's results at 17.0 atms of H_2 by scaling his result by the ratio of line widths (473.1/823.8) due to the difference in pressure. These values agree within experimental error and since we expected the ratio to be independent of ω_1, we have taken the average of these values in calculating an absolute value for the susceptibility of N_2 at $\omega_1 - \omega_2 = 4155\ cm^{-1}$ of $(102.9 \pm 14) \times 10^{-39}\ cm^6/erg$ molecule.

The susceptibilities we measure contain some small contributions from the resonant part of χ_r. We can correct for this by calculating χ_r for each gas at 4155 nm and subtracting the results from the measured susceptibilities. The vibrational part can be calculated using equation (3.17) and the cross section data given in Ref. 38. The pure rotational part for a linear molecule is calculated by summing over all the rotational lines using the cross section data given in Ref. 38 and the polarizability anisotropy tabulated in Ref. 42. For nitrogen the vibrational contribution is $-2.9 \times 10^{-39}\ cm^6/erg$ molecule, and the rotational contribution is $0.8 \times 10^{-39}\ cm^6/erg$ molecule giving a value for the electronic nonresonant susceptibility of $(105 \pm 14) \times 10^{-39}\ cm^6/erg$ molecule. This value has been used in combination with the nonresonant ratios

measured to obtain the values of χ_{nr} given in Table I and II. We have also included in these tables all other gas phase nonresonant values known to us. These include four wave mixing (FWM) measurements at 694nm, second and third harmonic values (dcSHG and THG) and the KERR effect results.

The third order susceptibility not only contains resonant terms from vibrational and rotational but also, as the frequency combination in χ approaches an electronic resonance, increased values can result. For example, the results for Ar and Kr are in reasonable accord with the expected ordering of

$$\chi_{KERR} < \chi_{dcSHG} < \chi_{FWM}(694) < \chi_{FWM}(532) < \chi_{THG}$$

This electronic resonance effect may also accounts for the high values obtained for molecules with low lying electronic states, such as NO, CS_2, and the conjugated systems listed in Table II. This does not however explain the high values measured for CO_2 by the KERR effect and Rado's value for D_2 and probably these values should be remeasured. In the case of D_2 it is not unlikely that this result came from H_2 impurity in his D_2 sample.

Table 3-1. Nonresonant Third Order Susceptibilities for Inert Gases and Simple Diatomic and Polyatomic Molecules (a)

	FWM Vib. Cont. (b)	FWM Rot. Cont. (b)	FWM 532 + 683 nm (c)	FWM 694 + 975 nm (d)	FWM 694 + 975 nm (e)	dcSHG 694 nm (f)	KERR 633 nm (g)	THG 694 nm (h)
He (i)								
exp.	0	0	3.2	6.6	---	1.3 - 11.4	4.5+0.33	---
theory	0	0	---	---	---	(3.79)	3.66	(4.00)
Ne	0	0	---	---	---	10.5+0.34	8.5+0.7	---
Ar	0	0	131	118	(118)	119+3.8	98+7	126+20
Kr	0	0	334	---	---	291+14	230+17	386+75
Xe	0	0	---	---	---	805+57	650+50	979+190
H2	15	-4	---	---	107	65.2+0.8	47+5	80+12
D2	-11	-1	69	111	---	---	40+8	---
N2	-3	1	(105+14)	(105+14)	---	86.6+1.0	120+10	107+17
O2	-2	0	141	101	---	95.3+1.6	---	---
CO	-2	0	155	139	---	144+4	---	---
NO	-1	1	---	320	---	235+7	---	---
CO2	-4	4	153	153	---	111.9+1.3	750+160	156+23
CS2	-21	21	---	---	1350	---	---	---
H2O	-3	---	---	---	---	194+10	---	---
H2S	-22	---	---	---	---	865+22	---	---
NH3	-40	---	---	---	---	511+9	---	---
CH4	-50	0	330	275	380	263+3	242+12	---
SiF4	-2	0	---	173	---	---	---	---
SF6	-6	0	176	197	195	130+2	200+20	---

a. Units are (cm6/erg-molecule) x 10+39.
b. Calculated as described in the text using Raman and polarizability data from refs. 38, 40, 42.
c. This work. Relative uncertainties estimated at less than 5%.
d. From ref. 27 using N2 as a reference. Reproducibility of 10% is cited.
e. From ref. 28 using N2 (via Ar) as a reference. Original data given to only one or two significant figures. The H2 value was determined at w1-w2=2917 cm-1.
f. Refs. 43-45 using the theoretical value for He as a reference. Uncertainties are relative values.
g. Ref. 46-48 Uncertainties are absolute values.
h. Ref. 35 using the theoretical value for He as a reference. Uncertainties are relative values.
i. Theoretical values from ref. 49.

Table 3-2. Nonresonant Third Order Susceptibilities for Various Hydrocarbons and Halocarbons.(a)

	TWM Vib. Cont. (b)	TWM 532 + 683 nm	TWM 694 + 975 nm (c)	dcSHG 694 nm (e)	KERR 633 nm (f)
CH4	-50	330	275(d) 380	263+3	242+12
CH3F	---	---	---	239+30	---
CH3Cl	-45	510	---	570+30	---
CH3Br	-47	---	720	---	---
CH3I	(-47)	---	1850	---	---
CH3OH	-53	---	760	385	---
CH2F2	-22	---	---	154+11	---
CH2Cl2	-29	---	---	920+30	---
CHF3	-16	---	200	136+6	---
CHF2Cl	-16	480	---	---	---
CHCl3	-17	---	1200	1120+30	---
CF4	-4	---	---	91+3	125+7
CF3Cl	-6	---	---	306+13	---
CF3Br	-8	---	---	625+43	---
CF2Cl2	-9	700	---	610+10	---
CFCl3	-12	---	---	960+30	---
CCl4	-17	1140	1650	1370+20	1660+50
C2H6	-59	---	530(d)	---	320+70
C2H5Cl	-43	---	830	---	---
C2H5Br	-41	---	1350	---	---
C2H5I	(-42)	---	2600	---	---
CH3CCl2F	-31	---	820	---	---
CF3CCl2F	-9	770	---	---	---
CH3OCH3	---	---	---	529+11	---
Cyclopropane	---	---	---	---	650+130
C2H2	-29	---	---	---	1750+400
C2H4	-40	---	---	758+17	---
CH3CN	-39	---	390	---	---
CH2CHCN	-39	---	830	---	---
CH3COCH3	(-60)	---	1250	---	---
Benzene	---	---	---	2060+50	---
Butadiene	-134	---	---	2300+130	---
Hexatriene	---	---	---	7530+700	---

a. Units are (cm6/erg-molecule) x 10+39.
b. Values in parentheses are estimates.
c. From ref. 29 using N2 (via Ar) as a reference.
d. From ref. 28 using N2 as a reference.
e. From ref. 43, 45, 50, 51 using the theoretical value for He as a reference.
f. From ref. 52, 53.

3.6 Summary

In this chapter we have reported the values of the third order nonresonant susceptibility of various gases measured by CARS. For many of these gases it was the first time this quantity was determined. It is also the first time nonresonant values have been measured using a Nd:YAG laser, a popular laser in nonlinear spectroscopy.

Values for the nonresonant susceptibilities are important when doing any form of nonlinear spectroscopy which measures a bulk third order susceptibility, such as CARS. The reason is that the nonresonant susceptibility causes significant frequency shifts and line distortion which can be compensated for by knowing the value of the nonresonant susceptibility of the sample.

The absolute value of our measurements was determined by using current Raman cross section and line width data to calculate χ_r^o of H_2 which was then used with the measured ratio of $\chi_{nr}(N_2)/\chi_r(H_2)$ to determine the absolute value of $\chi_{nr}(N_2)$. In principle this process could be reversed to determine new values of the Raman cross section for other molecules using the nonresonant data given here. Also, a similar ratio could be used to determine two photon cross absorption sections.

We will also see in chapter 4 that the nonresonant signal of a gas provides an excellent way for correcting for the power distribution in ω_2 when doing broadband CARS. This is because its represents the convolution of the ω_2 distribution with the same transmission function as the resonant signal.

CHAPTER 4

CARS Study of the Rotational Relaxation of Para H_2 in a Supersonic Free Jet

4.1 Introduction

Over the last several years, supersonic expansions have been used quite extensively to study energy relaxation processes in gases.[34,54-56] In these free jet expansions a gas flows from a region of high pressure through a small hole into a region of low pressure, leading to isentropic cooling of the species in the molecular beam. The expansion thus produces a system where energy is transferred from the internal (vibrational and rotational) modes of the molecule into a rapidly cooling translational energy bath. The efficiency of this transfer for the various internal modes is measured by the cross section, a physical parameter of much theoretical and experimental interest.

The various relaxation processes are usually

categorized as rotational to translational (R->T), vibrational to rotational (V->R), vibrational to vibrational (V->V), and vibrational to translational (V->T) energy transfer. The cross section for each is governed by the anisotropic portion of the interaction potential, while a larger isotropic part simply determines elastic scattering.

Of particular interest is the H_2 --- H_2 interaction potential because it describes the simplest molecule - molecule collision.[57-66] Very detailed potential energy surfaces have been calculated for this interaction[67,68] and these can be used to calculate collisional cross sections for the various relaxation processes.[69,64,65] These cross sections have been used to reproduce results from a wide variety of different experiments.[69,58,60,66]

In this chapter we have tested several interaction potentials for H_2 using our CARS measurements of rotational cooling in free jets. This was done by combining various models for the relaxation of hydrogen with the theoretical values for the cross sections to calculate rotational temperature profiles of a supersonic jet expansion . By comparing the theoretical predictions to the actual experimental results, we obtained a measure of the accuracy of the various potentials and relaxation models.

We have also extended this study to include mixtures of H_2 with He and other gases in the jet. By combining the results from the pure H_2 modeling with cross sections for the H_2 --- He relaxation we have tested several H_2 --- He potentials.

Since hydrogen has such a small reduced mass the internal energy spacing is very large. Therefore at room temperature and below, only four rotational states are significantly populated and the population of the first vibrational state can be considered zero. Further simplification into a system effectively containing only two states was achieved by catalytic production of pure para H_2 at low temperatures. In this way the calculations were greatly simplified and a better test of the remaining cross sections was possible.

4.2 Theoretical Background

4.2.A CARS Temperature Measurements

The rotational populations (or temperature) of nonpolar molecules like H_2 are difficult to measure by normal spectroscopic techniques but they can be accessed by the CARS method. In this optical mixing process, two incident lasers ω_1 and ω_2 generate a coherent

Anti-Stokes beam at $\omega_3 = 2\omega_1 - \omega_2$ because of the third order nonlinear CARS susceptibility (χ_{CARS}) of the sample. The power generated at ω_3 (P_3) is[10]

$$P_3 = C|\chi_{CARS}|^2 P_1^2 P_2 \tag{4.1}$$

where C is a constant which is independent of frequency. χ_{CARS} contains a nonresonant term (χ_{nr}) plus the sum of resonant terms (χ_r) for every Raman active transition of the molecule.

$$\chi_{CARS} = \chi_{nr} + \sum_{ij} \chi_r \tag{4.2}$$

As seen in chapter three, χ_{nr} is small and will be neglected in the following. If we assume that we have clearly resolved transitions, as in the case of H_2, then the integrated ω_3 power (P_{int}) for a single line is

$$P_{int} = C\Delta N_{ij}^2 P_1^o P_2 |\chi_r^o|_{ij}^2 \pi\Gamma \tag{4.3}$$

where $\bar{\chi}_r^o$ is the peak resonant susceptibilty, ΔN is the difference in number density between states i and j, and

is the Raman line width (HWHM). χ_r^o in terms of the Raman cross section is

$$\chi_r^o = C' \left(\frac{d\sigma}{d\Omega}\right) \tag{4.4}$$

For H_2, where the vibration spacing is very large, ΔN can be replaced by just the ground state population. Combining equations (4.3) and (4.4) we find that

$$P_{int} = C'' P_1^2 P_2 N_i^2 \left(\frac{d\sigma}{d\Omega}\right)^2 \tag{4.5}$$

For a diatomic molecule, the Raman cross section of a Q branch transition (V=1, J=0) is[74]

$$\frac{d\sigma}{d\Omega} = \left(a_o + \frac{J(J+1)}{(2J-1)(3J+1)} \right) (V + 1/2)^2 \tag{4.6}$$

where a_o is the trace scattering coefficient for the molecule, (for H_2 a_o=6[34]). Therefore, the integrated P_{int} power for the Jth Q branch transition is

$$P_{int} = C'' P_1^2 P_2 N_J^2 \Gamma \left[a_0 + \frac{J(J+1)}{(2J-1)(3J+1)} \right] \times (V + 1/2)^2 \qquad (4.7)$$

Using the ratio of the integrated Q_2 to Q_0 CARS peaks we can measure a "Boltzmann" rotational temperature for para hydrogen via the usual thermodynamic relation. The rotational temperature for para hydrogen is

$$\left(\frac{N_2}{N_0}\right)^2 = \left(\frac{g_2}{g_0}\right)^2 \exp\left(\frac{2\varepsilon_2}{KT_{rot}}\right) = \frac{P_{Int}(2)}{P_{Int}(0)} \left(\frac{6.0}{6.258}\right)^2 \qquad (4.8)$$

$$T_{rot} = \frac{-2\varepsilon_2}{K \ln\left[\left(\frac{P_{Int}(2)}{P_{Int}(0)}\right)\left(\frac{6.0}{6.258}\right)^2 \left(\frac{1}{5}\right)^2\right]} \qquad (4.9)$$

in these experiments. ε_2 is the energy of the J=2 level and the degeneracy ratio g_2/g_0 is 5. Expressions (4.8) and (4.9) then provide the connection between the measured transition intensities (or powers) and the

population ratios or temperatures to be compared with theoretical relaxation calculations.

4.2.B Rotational Relaxation Models

We will consider three basic models for rotational relaxation. These are

I) Classical Model

$$M(Er) + A \rightarrow M(Er') + A + Et$$

II) Partial State-to-State Model

$$M(i) + A \rightarrow M(j) + A + Et$$

III) Complete State-to-State Model

$$M(i) + M(j) \rightarrow M(l) + M(m) + Et$$

4.2.B.1 Classical Model

This simple model assumes that the rotational energy levels form a continuum. Therefore each collision

$$M(Er) + A \rightarrow M(Er') + A + Et$$

of the molecule (M) with an acceptor (A) converts some of the excess rotational energy (Er) into translational

energy (Et) of the colliding molecules.

The amount of rotational energy lost on each collision is assumed to be proportional to the difference in rotational and translation energies (temperatures). The rate of change in rotational temperature is given by

$$\frac{dT_{rot}}{dt} = \frac{\nu}{Z_{rot}} (T_{tr} - T_{rot}) \qquad (4.10)$$

where is the collisional frequency and Z_{rot} is the rotational collision number. The collisional frequency for a pure gas is

$$\nu = \rho\pi\sigma_h^2\langle v\rangle \qquad (4.11)$$

where is the number density, σ_h is the hard sphere radius and <v> is the average thermal velocity

$$\langle v\rangle = \left(\frac{8KT}{\pi M}\right)^{1/2} \qquad (4.12)$$

with M being the mass of the molecule.

Z_{rot}, the rotational collision number, gives a measure of the effectiveness of each collision. The larger Z_{rot} the smaller the amount of rotational energy converted into translational energy. Equivalently, Z_{rot} may be viewed as the number of collisions that must occur before some rotational energy is transferred.

The temperature dependence of Z_{rot} is often assumed to be

$$Z_{rot} = Z^{o}_{rot} \left[\frac{T_{tr}}{T_o}\right] \qquad (4.13)$$

where Z^{o}_{rot} is the value of Z_{rot} for the initial temperature T_o. From this one can see that the greater the energy of the collision (higher T_{tr}) the less likely that rotational energy will be lost.

4.2.B.2 Partial State-to-State Model

With this model we can define the collision relaxation process as

$$M(i) + A \qquad M(j) + A + Et$$

Here a molecule in a rotational state i collides with an

acceptor and losses or gains rotational energy to produce the final state (j). Thus only one of the two colliding species changes internal energy on a given collision.

The rate of relaxation is taken as[64]

$$\frac{dN_i}{dt} = P_{j\to i}N_j - P_{i\to j}N_i \tag{4.14}$$

where N_i is the number density in state i and $P_{i\to j}$ is the probability of transition from state i to j. $P_{i\to j}$ is defined by

$$P_{i\to j} = \rho_A \langle\sigma_{i\to j,A}\rangle\langle v\rangle \tag{4.15}$$

where $\langle\sigma_{i,j,A}\rangle$ is the thermally averaged rotational cross section for the i -> j transition with A. For a pure gas

$$P_{i\to j} = \rho\langle\sigma_{i\to j}\rangle\langle v\rangle \tag{4.16}$$

Using the equilibrium condition

$$\frac{dN_i}{dt} = P_{j\to i} N_j^o - P_{i\to j} N_i^o = 0 \qquad (4.17)$$

where N_i is the equilibrium number density in state i, along with conservation of particles, equation (4.14) can be rewritten as

$$\frac{dN_i}{dt} = (P_{i\to j} + P_{j\to i})(N_i^o - N_i) \qquad (4.18)$$

Using equation (4.16) we find that

$$\frac{dN_i}{dt} = \rho\langle v\rangle(\sigma_{i\to j}+\sigma_{j\to i})(N_i^o - N_i) \qquad (4.19)$$

$$\frac{dN_i}{dt} = \rho\left(\frac{8KT_{tr}}{\pi M}\right)^{1/2} \sigma_{rot}(N_i^o - N_i) \qquad (4.20)$$

where σ_{rot} is the rotational cross section.

σ_{rot} is related to the collision number by the relation

$$Z_{rot} = \frac{\pi\sigma_h^2}{\sigma_{rot}} \tag{4.21}$$

Using (4.11), we can reexpress the relaxation rate as

$$\frac{dN_i}{dt} = \frac{\nu}{Z_{rot}} (N_i^o - N_i) \tag{4.22}$$

It is interesting to note that the classical model can be derived from this expression. If we multiply both sides of this equation by ϵ_i, the rotational energy of state i, and sum over all states i

$$\sum_i \frac{dN_i\epsilon_i}{dt} = \frac{\nu}{Z_{rot}} \sum_i (N_i^o\epsilon_i - N_i\epsilon_i) \tag{4.23}$$

this can be written as

$$\frac{dE_{rot}}{dt} = \frac{\nu}{Z_{rot}} (E_{rot}^0 - E_{rot}) \tag{4.24}$$

where E_{rot} is the total rotational energy of the sample at T_{rot} and E_{rot}^o is the rotational energy of the sample

at thermal equilibrium. If we assume a continuum of states and that $E_{rot} \propto \langle E_{rot} \rangle \propto kT_{rot}$, then

$$\frac{dT_{rot}}{dt} = \frac{\nu}{Z_{rot}} (T^{o}_{rot} - T_{rot}) \qquad (4.25)$$

At thermal equilbrium $T^{o}_{rot} = T_{tr}$ so

$$\frac{dT_{rot}}{dt} = \frac{\nu}{Z_{rot}} (T_{tr} - T_{rot}) \qquad (4.26)$$

and the classical rate equation (4.10) is obtained.

4.2.B.3 Complete State-to-State Model

We have seen so far that the classical model assumes no quantized states and the partial state-to-state model allows the levels of one of the particles to be quantized. In reality both colliding particles have quantized levels so, for a pure gas, we have the following collision process

$$M(i) + M(j) \qquad M(l) + M(m) + Et$$

The rate equation in this case can be written as[69]

$$\frac{dN_i}{dt} = \sum_j \sum_l \sum_{m>l} (N_l N_m K_{lm\to ij} - N_i N_j K_{ij\to lm}) \times G_{ijlm} \qquad (4.27)$$

where $K_{ij\to lm}$ is the rate of transition ij -> lm, and G_{ijlm} is a symmetry factor to account for the indistinguishability of identical particles

$$G_{ijlm} = [1 + \delta_{ij}(1 - \delta_{li})(1 - \delta_{mi})] \times [1 - \delta_{li}(1 - \delta_{ij})][1 - \delta_{mi}(1 - \delta_{ij})] \qquad (4.28)$$

where δ_{ij} is a delta function equal to 1 if i=j or 0 if i=j. In the case of para H_2 where we have just two levels, J=0 and J=2, we can rewrite equation (4.28) explicitly as

$$\frac{dN_2}{dt} = [(N_0 N_0 K_{00\to 02} - N_0 N_2 K_{02\to 00}) + 2(N_0 N_0 K_{00\to 22} - N_2 N_2 K_{22\to 00}) + (N_0 N_2 K_{02\to 22} - N_2 N_2 K_{22\to 02})] \qquad (4.29)$$

The rate constant $k_{ij\rightarrow lm}$ is given by

$$K_{ij\rightarrow lm} = \langle \sigma_{ij\rightarrow lm} v \rangle \tag{4.30}$$

where $\langle \sigma_{ij\ lm} V \rangle$ is the thermal average of the product of the rotational cross section for the ij->lm transition at the total energy E times the collisional velocity, i.e.

$$K_{ij\rightarrow lm} = \left(\frac{\mu}{2\pi KT}\right)^{3/2} \int_0^\infty 4\ {}^2v^3 \exp\left(-\frac{\mu v^2}{2KT}\right) \times \sigma_{ij\rightarrow lm}(E = \varepsilon_{ij} + \frac{1}{2}\mu v^2) \tag{4.31}$$

At equilibrium we have the condition that

$$N_i N_j K_{ij\rightarrow lm} = N_l N_m K_{lm\rightarrow ij} \tag{4.32}$$

Therefore using the Boltzmann equation we can solve for $k_{lm\rightarrow ij}$ in terms of $k_{ij\rightarrow lm}$

$$K_{lm\ ij} = \frac{(2i+1)(2j+1)}{(2l+1)(2m+1)} \exp\left\{\frac{(\varepsilon_{lm}-\varepsilon_{ij})}{KT}\right\} \times K_{ij\rightarrow lm} \tag{4.33}$$

where 2i+1 is the degeneracy of of state i and $_{ij}$ is the sum of the rotational energies of states i and j. Using this expression in equation (4.29) we finally obtain

$$\frac{dN_2}{dt} = (N_0N_0 - N_0N_2 \frac{1}{5} \exp\{\varepsilon_2/KT_{tr}\})K_{00\to22}$$
$$+ 2(N_0N_0 - N_2N_2 \frac{1}{25} \exp\{2\varepsilon_2/KT_{tr}\})K_{00\to22}$$
$$+ (N_0N_2 - N_2N_2 \frac{1}{5} \exp\{\varepsilon_2/KT_{tr}\})K_{02\to22} \qquad (4.34)$$

the rate equation for the complete state-to-state model

4.2.C Expansion Models

The rate equations discussed above are given in units of time. In the expansion experiments we measure the rotational temperature as a function of distance from the nozzle tip. Thus the rate expressions given above must be divided by the beam velocity (U). For example, eq. (4.20) becomes

$$\frac{dN_2}{d\bar{x}} = \frac{\rho D}{U} (8KT/\pi M)^{1/2} \sigma_{rot} (N_2^o - N_2) \qquad (4.35)$$

where X is the distance from the nozzle tip in units of X/D and D is the nozzle diameter.

It is important to remember that there are two different velocities with which we are concerned, the beam velocity (U) which measures the bulk velocity relative to the nozzle, and the collisional velocity (V) which is the relative velocity of the particles, characteristic of a certain translational temperature.

We can see from equation (4.33) that population in the N_2 state is related to the number density (ρ), the translational temperature (T_{tr}), and the beam velocity (U). Therefore, the solution of this equation requires that we know how ρ, T_{tr}, and U vary along the expansion axis. For this pupose, two models are considered.

4.2.C.1 Andersons Model

Anderson79 has proposed a set of empirical formulas for the variation of ρ, T_{tr}, and U as a function of distance from the nozzle. These are based on the experimental Mach number expressions of Ashkenas and Sherman[80]

$$Ma(\bar{x}) = A(\bar{x} - \bar{x}_o)^{\gamma-1} - \frac{1}{2A}\frac{\gamma+1}{\gamma-1}(\bar{x} - \bar{x}_o)^{1-\gamma} + C(\bar{x} - \bar{X}_o)^{-3(\gamma-1)} \quad ;\text{for } \bar{x} > \bar{x}_c \tag{4.36}$$

$$Ma(\bar{x}) = Ma(\bar{x}_c)\ \exp\left[\frac{dMa(\bar{x}_c)}{dx}\ \frac{(\bar{x} - \bar{x}_c)}{Ma(\bar{x}_c)}\right] \quad ;\text{for } \bar{x} < \bar{x}_c \tag{4.37}$$

where A, C, $\bar{x}_o$ are expansion coefficients tabulated by Ashkenas and Sherman and depend only on γ, the ratio of specific heat capacities (Cp/Cv). For all of these calculations we have used the monoatomic value for γ (1.67) since the rotational heat capacity for H_2 is small in the cooling process. $\bar{x}_c$ is the connection distance (taken to be 1.0 in this work) and is the point of changeover from eq. (4.36) to (4.37), a simpler exponential form which describes the expansion very near the nozzle. It should be pointed out that the choice of $\bar{x}_c$ is not critical; varying $\bar{x}_c$ by 20% only caused about a 1 K variation in the rotational temperature calculated at large X/D.

Using these empirical expressions, Anderson derived the following equations for the beam properties

$$\rho(\bar{x}) = \rho_o[1 + 1/2\ (\gamma-1)Ma(\bar{x})^2]^{1/(\gamma-1)} \qquad (4.38)$$

$$T_i(\bar{x}) = T_o/[1 + 1/2\ (\gamma-1)Ma(\bar{x})^2] \qquad (4.39)$$

$$U(\bar{x}) = Ma(\bar{x})\left[\frac{KT_{tr}}{M}\right]^{1/2} \qquad (4.40)$$

where the subscripted o implies initial conditions and it is assumed that the translation temperature is equal to the isentropic temperature (T_i). This set of equations (eqs. 4.36-4.40) can be used along with the numerical integration of the various relaxation models to simulate the expansion process in the free jet.

4.2.C.2 Fluid Mechanical Model

Recently Rabitz and Lam[69] have proposed a fluid mechanical model for the expansion properties of a supersonic jet. This model couples the relaxation expression directly to fluid mechanical expressions for one dimensional flow using conservation of energy, particle number and momentum. As in the Anderson model, it is assumed that the sample density can be described

by equations (4.36-4.38). However differential expressions for the translational temperature and the beam velocity are used. For a two level system, these are

$$\frac{dT_{tr}}{d\bar{x}} = \frac{2}{3} T_{tr} \left[\frac{1}{\rho} \frac{d\rho}{d\bar{x}} - \frac{2}{KT_{tr}} \frac{dP_2}{d\bar{x}} \right] \tag{4.41}$$

$$\frac{dU}{d\bar{x}} = - \frac{1}{MU} \left[\frac{5}{2} K \frac{dT_{tr}}{d\bar{x}} + \varepsilon_2 \frac{dP_2}{d\bar{x}} \right] \tag{4.42}$$

where ε_2 is the energy of the J=2 rotational level and $dP_2/d\bar{X}$ is the change in probability of being in the second level. For example, for the partial state-to-state model, this is given by

$$\frac{dP_2}{d\bar{x}} = \frac{\rho D}{U} \sigma_{rot} \left[\frac{8KT_{tr}}{\pi M} \right]^{1/2} (P_2^o - P_2) \tag{4.43}$$

since $P_2 = N_2/\rho$.

The principle difference in these two methods is that the Anderson model assumes an infinite translational heat bath whereas the fluid mechanical treatment allows for translational heating as internal

energy is transferred in the expansion process. The effect of these two assumptions on the predicted rotational temperatures has not been examined previously and is one of the questions addressed in this thesis.

4.3 Experimental

The broadband CARS apparatus is shown in figure (3-1). The primary source was a doubled Nd:Yag laser at 532 nm with pulse duration of 10 ns and line width of 0.01 cm^{-1}. Part of the 532 nm output was used to pump the dye laser which consisted of an oscillator and two transversely pumped amplifiers. The oscillator contained a transversely pumped dye cell, a 35% reflective front mirror, an optical polarizer, a dispersing prism, and a totally reflective back mirror. Using experimental red dye (Exciton) in dimethyl sulfoxide, the dye laser power at was between 2 to 3 mJ per pulse with a continuous bandwidth of 100 cm^{-1} centered at the Q_2 branch of hydrogen at 683 nm. This Stokes output and the pump beam (ω_1) were then colinearly combined using a dichroic mirror. The pump beam was optically delayed to achieve temporal overlap and both beams were focused into the supersonic jet cell using a 100 mm focal length lens. The collimated

ω_3 output was then isolated from ω_1 and ω_2 using a filter (Corning 5-60) and a dichroic mirror. ω_3 was dispersed using a double monochromator (Spex 1402) and detected using a multichannel analyzer (PAR OMA 2) with a net system dispersion of 0.3567 cm^{-1}/channel at the H_2 wavelength.

The supersonic jet cell (figure 4-1) consisted of a 10 cm cube with 3 windows (two for the light path and one on top for visual alignment of the nozzle), a nozzle port, and a vacuum port directly opposite the nozzle. The cell pressure was monitored using a Pirani gauge (Granville Phillips) or a 100 Torr pressure transducer (Validyne). The cell was evacuated using two rotary pumps (Cenco Hyvacs) with a net pumping speed of 500 liters/minute, which maintained a cell pressure of 40 mtorr during the expansions.

The whole cell was mounted on a translational stage which allowed precise positioning of the nozzle tip with respect to the laser beams. The absolute distance between the nozzle and the focal point of the beams was measured by using the lasers to burn a spot on a razor blade. This was positioned such that the edge of the blade was against the nozzle and orthogonal to the laser beams. The micrometer setting for the cell was then calibrated by measuring the distance from the burn to

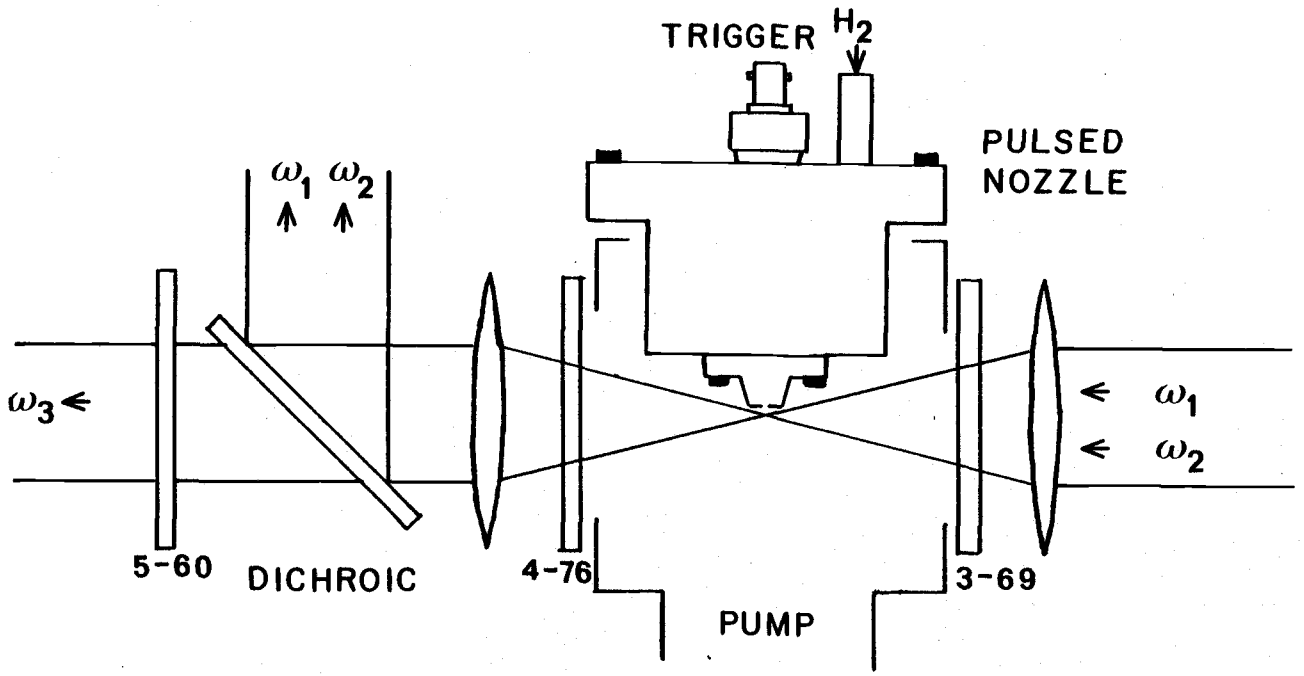

Figure 4-1 Schematic diagram of the supersonic jet cell.

the edge of the blade using a microscope with a calibrated ocular. The uncertainty of the distance calibration is estimated at 50 μm, however, relative positions made using the micrometer are believed to have an accuracy of 10 μm.

Each measurement consisted of an average of 1000 laser shots for both the background (ω_2 blocked) and the signal. The CARS spectrum was obtained as the difference. In a similar fashion the power distribution of the broadband ω_2 source was determined by recording the static spectrum of air at 75 torr which was introduced into the cell. This nonresonant anti-Stokes (ω_3) spectrum contains the convolution of the ω_2 distribution with the same transmission function (for filters and spectrometer) that affects the resonant spectra. The final corrected CARS spectrum was then obtained by ratioing the resonant and nonresonant traces.

All experiments reported here were done using para hydrogen which was produced by passing normal H_2 through a Fe_2O_3 catalyst cooled to 23 K using a Displex cryogenic refrigerator. In the studies of the H_2 --- H_2 relaxation, hydrogen was sent directly from the gas cylinder through the low temperature catalyst and into the pulsed nozzle. For studies with helium (and other

gases) the para hydrogen was collected in glass bulbs and then helium was added to form a mixture of 2 parts helium to one part hydrogen. The para H_2 would last in the glass bulbs for several hours without appreciable conversion to the ortho form.

Our initial molecular beam studies involved the use of continuously operating nozzles (also termed cw nozzles). These were used primarily because they are simple to make and are very reliable. However, because of the large flow of gas through the nozzle, they require very large amounts of sample gas and high speed pumping systems or, alternatively, very small nozzle diameters with resultant low sample densities.

The disadvantages of a cw nozzle were overcome by going to a pulsed nozzle arrangement. Here the gas flow is only on during sampling, thus reducing the average flow through the nozzle while maintaining the high number density of a large nozzle diameter. This type of nozzle is well suited for our work because of the short pulse length and low repetition rate of our Nd:YAG laser.

Several different types of pulsed nozzles are currently in use.[70-72] Our pulsed nozzle (figure 4-2) is based on the design of Cross and Valentini[72] which uses a piezoelectric crystal to open and shut the

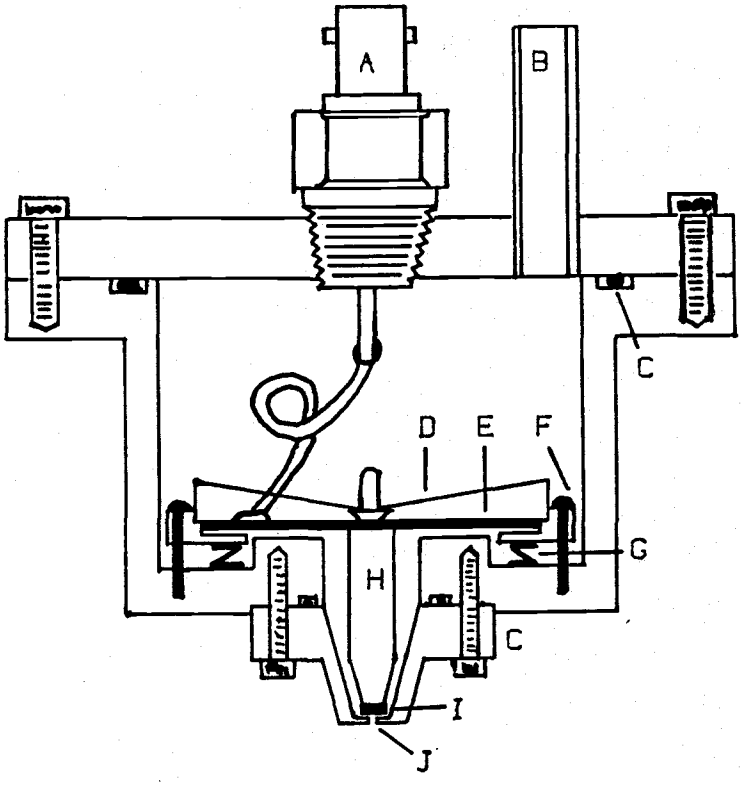

A. Electrical Feedthrough
B. Gas Inlet
C. O-Ring
D. Spring
D. Piezoelectric Crystal
F. Tension Adjustment Screw
G. Tension Spring
H. Plunger
I. Viton Seal
J. Nozzle Orifice

Figure 4-2 Drawing of the piezoelectric pulsed nozzle.

nozzle. This device has the advantage that it can operate both at high repetition rates and with short pulse duration. Valentini characterized his nozzle and found that it could operate at up to 750 Hertz and produce a minimum pulse duration of 100 μs.

For these measurements a 250 μm nozzle was used with a pulse width of 200 μs and sampling of the jet was delayed 50 μs after the start of the pulse to ensure that the gas had time to establish the properties of a cw nozzle.[73]

4.4 Results

For these experiments it was necessary to produce pure para hydrogen by catalytic conversion. Figure 4-3 shows the effect of catalyst temperature on the CARS spectrum of H_2 after heating to room temperature. We see that at 23 K we have produced essentially 100 % pure para H_2, thus reducing the number of populated states to two (J=0,2). We expect only about 1.4% population in the J = 4 state at room temperature, an amount considered negligible in the subsequent analysis.

Figure 4-4 shows the effect of the normalization procedure used in obtaining an accurate Q_2/Q_0 ratio. Dividing the upper resonant curve by the nonresonant

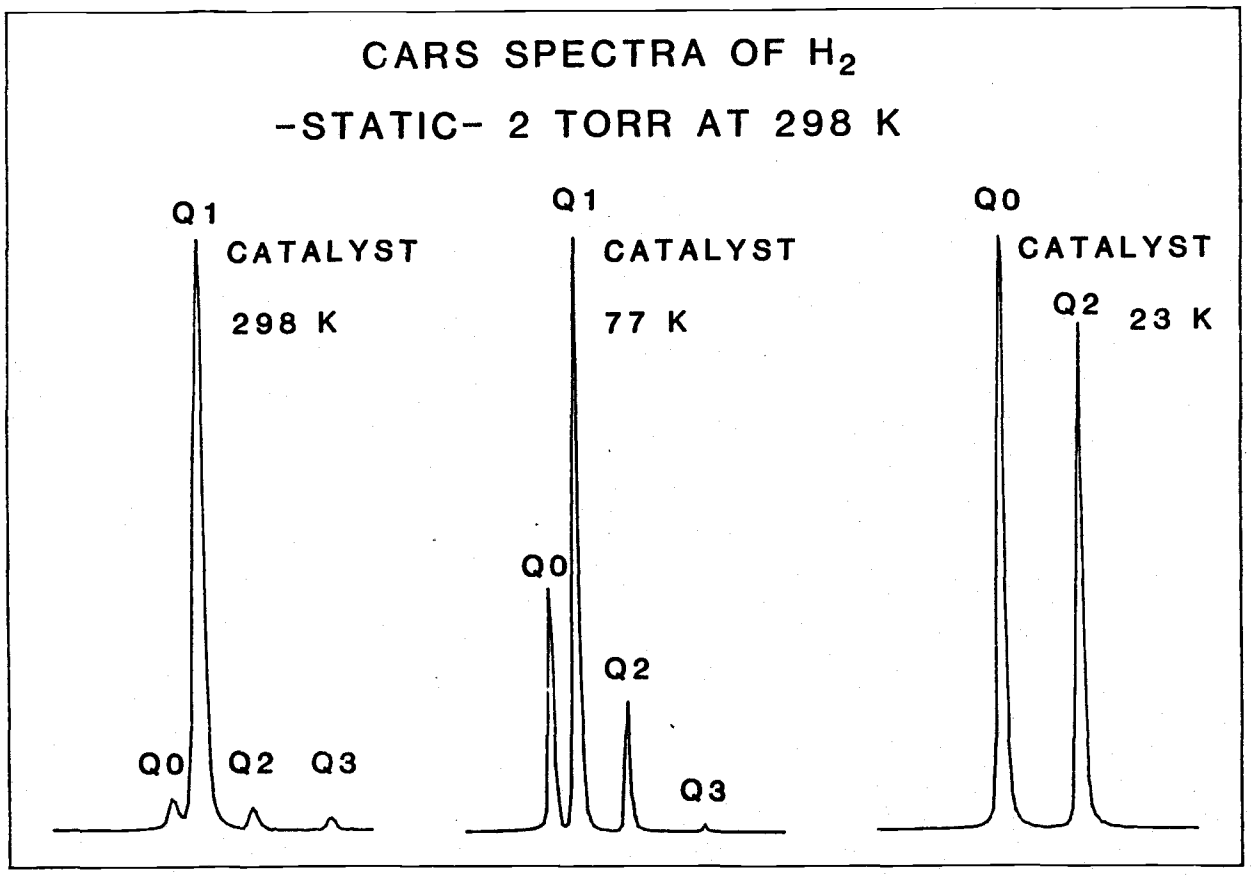

Figure 4-3 Effect of catalyst temperature on the ortho-para distribution of H_2.

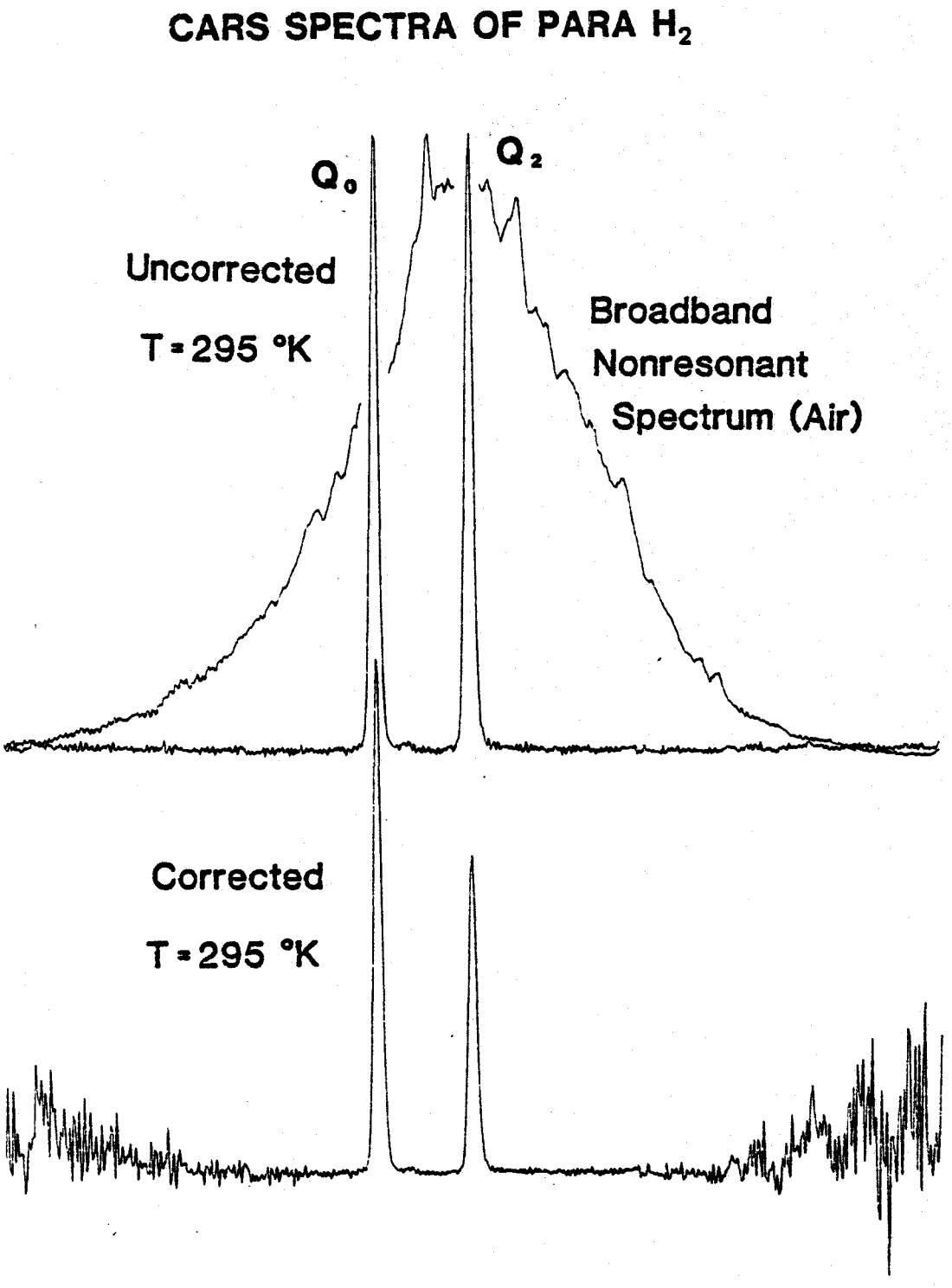

Figure 4-4 Effect of nonresonant normalization on the relative intensities of the Q_0 and Q_2 peaks of H_2.

background produced a 40% change in the relative intensities, a crucial correction for the determination of accurate rotational temperatures. The measured ratios were corrected for the variation in detector sensitivity across the multichannel analyzer by multiplying them by the ratio of the measured Q_2/Q_0 ratio of room temperature H_2 to the theoretically predicted ratio. The corrected ratios of Q_2/Q_0 were then used in eq. (4.9) to deduce the rotational temperature. By looking at the variation in the Q_2/Q_0 ratio of room temperature H_2, we determined that the uncertainty in our temperature measurements was about 3%.

Figure 4-5 shows typical spectra obtained in the pulsed jet experiments for pure para H_2 and for an Ar + H_2 mixture. The driving pressure is indicated and the X value was 1.2. The rotational cooling is obvious from the dramatic reduction of the Q_2 intensity and the calculated rotational temperatures indicated. Table 4-1 summarizes all of the data measured in these experiments. Figure 4-6 shows the effect of changing the driving pressure at a fixed point (X/D=1.2) in the expansion.

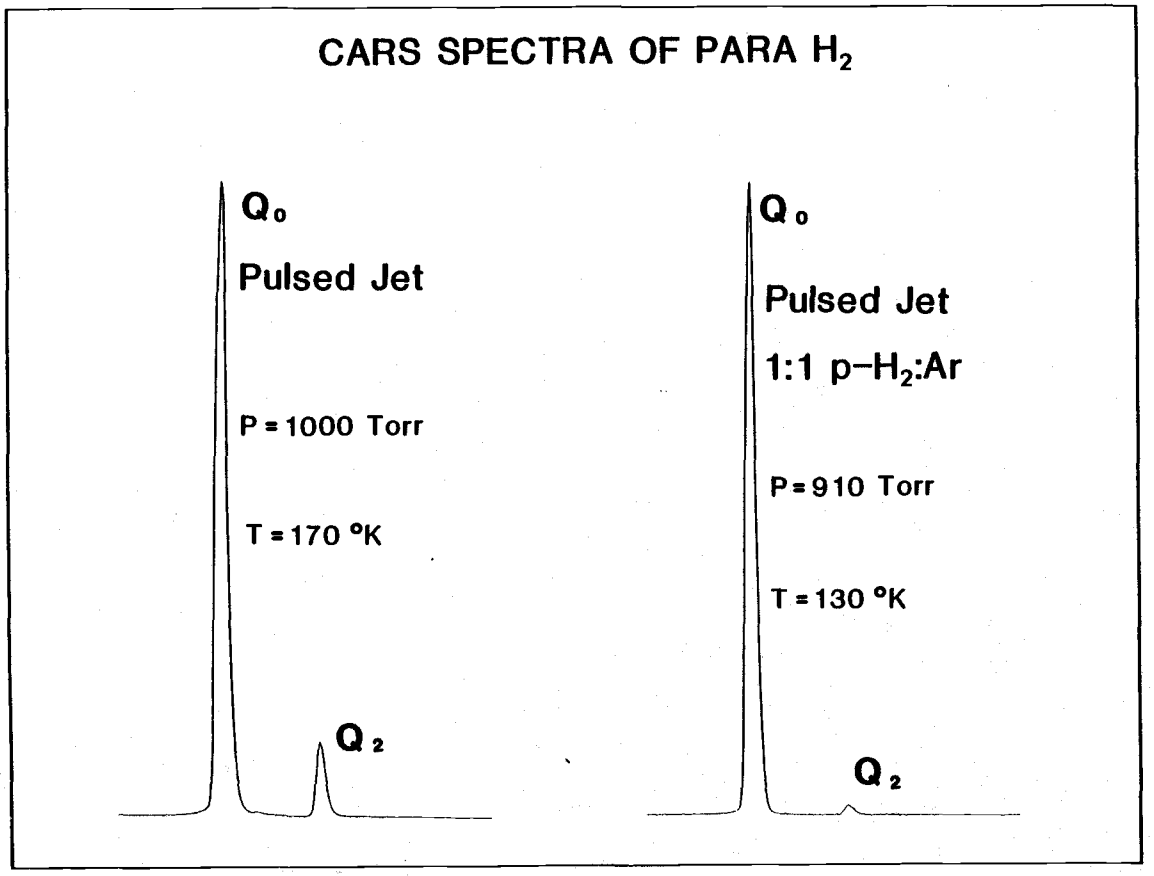

Figure 4-5 CARS spectra of para H_2 expansions using a pulsed nozzle. X/D = 1.2, nozzle diameter = 250 μm.

Table 4-1 Summary of expansion data for various mixtures with para hydrogen.

Buffer	Distance (X/D)	Pressure (Torr)	Rot. Temp. (K)	Buffer	Distance (X/D)	Pressure (Torr)	Rot. Temp. (K)
------	1.20	950	170	He	1.20	596	142
------	1.20	950	168	He	1.20	594	145
------	1.20	950	169	He	1.20	591	141
------	1.80	950	166	He	1.20	890	133
------	1.80	950	164	He	1.20	889	132
------	2.40	950	159	He	1.20	885	131
------	2.40	950	159	He	1.20	1196	128
------	2.40	950	161	He	1.20	1190	128
------	3.00	950	156	He	1.20	1184	129
------	3.00	950	157	He	1.20	1492	121
------	3.00	950	156	He	1.20	1483	121
------	3.60	950	153	He	1.20	1476	120
------	3.60	950	151	He	1.20	1748	118
------	3.60	950	156	He	1.20	1739	120
------	1.20	1570	156	He	1.20	1728	121
------	1.80	1570	152				
------	2.40	1570	148				
------	3.00	1570	143				
------	3.60	1570	143				
------	1.20	1890	148				
------	1.80	1890	142				
------	2.40	1890	139				
------	3.00	1890	136				
------	3.60	1890	136				

Table 4-1 Continued

Buffer	Distance (X/D)	Pressure (Torr)	Rot. Temp. (K)	Buffer	Distance (X/D)	Pressure (Torr)	Rot. Temp. (K)
Ne	1.20	1380	116	Ar	1.28	1725	105
Ne	1.20	1373	113	Ar	1.28	1720	105
Ne	1.20	1367	114	Ar	1.28	1717	102
Ne	1.20	1357	116	Ar	1.28	1716	101
Ne	1.20	1200	116	Ar	1.28	1509	106
Ne	1.20	1187	116	Ar	1.28	1489	105
Ne	1.20	1183	118	Ar	1.28	1497	104
Ne	1.20	1178	121	Ar	1.28	1300	107
Ne	1.20	997	123	Ar	1.28	1297	106
Ne	1.20	990	124	Ar	1.28	1297	104
Ne	1.20	986	124	Ar	1.28	1295	105
Ne	1.20	987	126	Ar	1.28	1103	108
Ne	1.20	780	127	Ar	1.28	1100	108
Ne	1.20	772	128	Ar	1.28	1098	106
Ne	1.20	772	128	Ar	1.28	1096	108
Ne	1.20	600	136	Ar	1.28	898	111
Ne	1.20	599	135	Ar	1.28	895	111
Ne	1.20	595	138	Ar	1.28	894	110
Ne	1.20	593	138	Ar	1.28	889	110
Ne	1.20	400	149				
Ne	1.20	397	149				
Ne	1.20	397	149				

Table 4-1 Continued

Buffer	Distance (X/D)	Pressure (Torr)	Rot. Temp. (K)	Buffer	Distance (X/D)	Pressure (Torr)	Rot. Temp. (K)
N_2	1.20	1610	137	D_2	1.20	1494	136
N_2	1.20	1606	136	D_2	1.20	1489	137
N_2	1.20	1600	136	D_2	1.20	1195	144
N_2	1.20	1300	135	D_2	1.20	1186	144
N_2	1.20	1295	134	D_2	1.20	1181	145
N_2	1.20	1292	132	D_2	1.20	991	150
N_2	1.20	995	141	D_2	1.20	987	149
N_2	1.20	993	142	D_2	1.20	980	147
N_2	1.20	990	143	D_2	1.20	786	157
N_2	1.20	798	141	D_2	1.20	781	158
N_2	1.20	796	142	D_2	1.20	778	158
N_2	1.20	792	141	D_2	1.20	598	165
N_2	1.20	600	148	D_2	1.20	589	165
N_2	1.20	597	148	D_2	1.20	584	165
N_2	1.20	594	149				

Figure 4-1 Continued

Buffer	Distance (X/D)	Pressure (Torr)	Rot. Temp. (K)	Buffer	Distance (X/D)	Pressure (Torr)	Rot. Temp. (K)
CO_2	1.20	1259	123	CO_2	1.20	1256	126
CO_2	1.20	1255	129	CO_2	1.20	1001	131
CO_2	1.20	999	133	CO_2	1.20	999	129
CO_2	1.20	850	134	CO_2	1.20	846	136
CO_2	1.20	845	138	CO_2	1.20	695	138
CO_2	1.20	694	140	CO_2	1.20	693	139
CO_2	1.20	549	140	CO_2	1.20	545	141
CO_2	1.20	545	141				

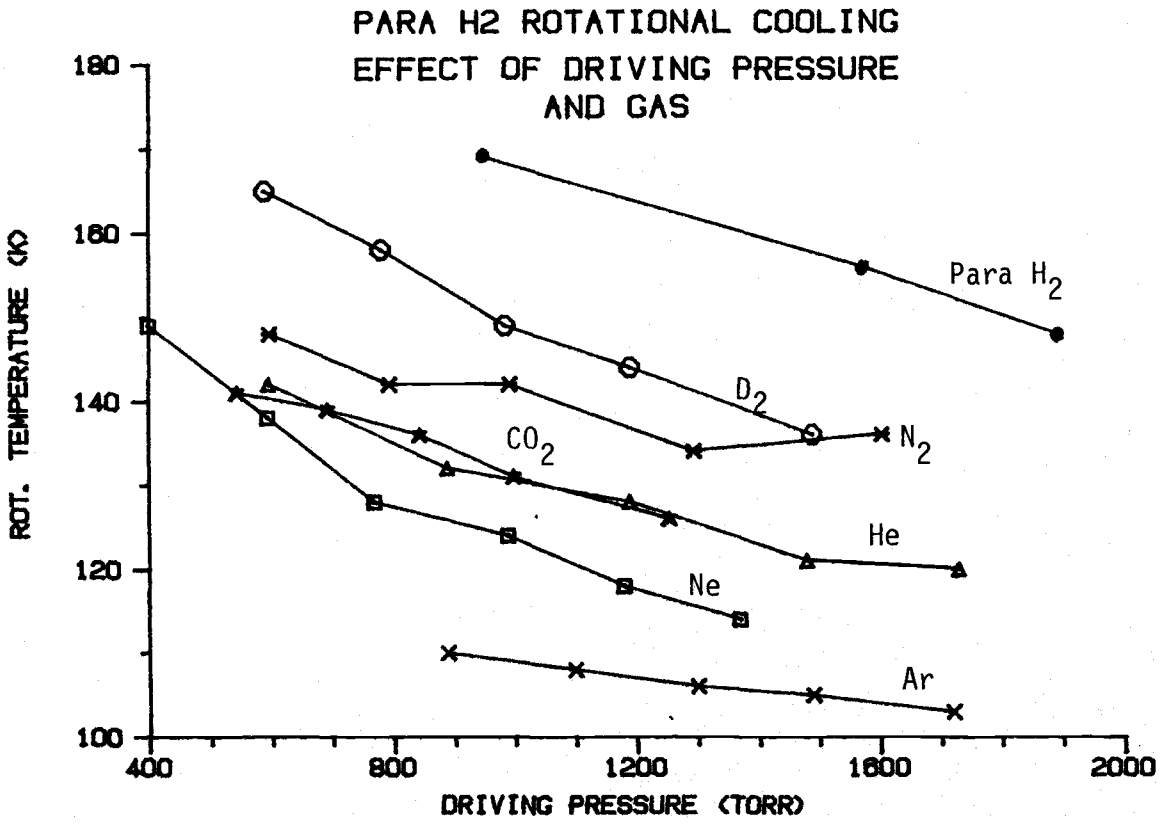

Figure 4-6 Effect of driving pressure and gas on the rotational cooling of para H_2. (X/D = 1.2, D = 250 μm, H_2:X = 1.2)

4.5 Discussion

4.5.A General Observations

From the results displayed in table 4-1 and figure 4-6, it is clear that para H_2 is cooled appreciably in these expansions. However, there is still a marked difference between the the observed rotational temperatures (~150 K) and the corresponding isentropic translational temperatures (~60 K) at the same point in the expansion. This discrepancy is reduced by the addition of various driving gases and a qualitative measure of the relative collision cross sections can be obtained from the data in figure 4-6. It is seen that cooling efficiency increases in the order He<Ne<Ar, a trend that would be expected since both the polarizability and collision diameter increase in this order. The addition of molecular buffer gases also gives greater cooling. In this case however, the net effect is reduced because the internal energy of these molecules must also be carried away. For this reason, relative values for the cross sections are not easily deduced. In the following, we consider various approaches to this task for the simplest case of pure para H_2.

4.5.B Classical Mechanical Description of Rotational Relaxation

Earlier work[34] has shown that jets of N_2 and O_2 reach rotational temperatures (10 - 20 K) which are very near the corresponding translational temperature. In these cases, the classical model has been coupled with Andersons' treatment of the expansion to give a good general description of the rotational temperature variation in the jet.[34,75,76]

In contrast, our early attempts to use this approach for H_2 showed that the relaxation could not be characterized by a single Z^o_{rot} value for different driving pressures. This poor characterization was not improved by attempts to fit the data using a more flexible description of the temperature dependence of Z_{rot},

$$Z_{rot} = Z^o_{rot} \left(\frac{T_{tr}}{T_o} \right)^n \qquad (4.44)$$

where n was treated as a fitting parameter. A rough value of $Z^o_{rot} = 300$ was deduced but no values of n and Z^o_{rot} could be found that fit all the data.

The poor result using this simple relaxation model for H_2 is perhaps not surprising since it assumes that a

continuum of rotational states is available for the relaxation process. For para H_2 there is a large energy gap between J=0 and J=2 (300 cm^{-1}) so that this is a poor approximation. However, for molecules like N_2 and O_2 where the rotational constant is much smaller than H_2 one finds that this model gives a better fit to the experimental data. In general the larger the ratio of KT/B, where T is the temperature and B is the rotational constant, the better the classical approach should be in modeling the experimental results. This may also explain why Gallagher and Fenn[57] found fairly good results for H_2 using the classical model at higher temperatures (~1000 K).

4.5.C Partial State-to-State Model

The partial state-to-state model, unlike the classical model, allows for quantum changes in one of the two collision partners and averages out any quantum effects of the other. Ab initio calculations of rotational cross sections (σ_{rot}) have been made and these can be related to Z_{rot} using eq. (4.21). Figure 4-7 shows values of σ_{rot} calculated by Kohler and Schafer[65] for two interaction potentials. It is clear from the general form of this function why the simple

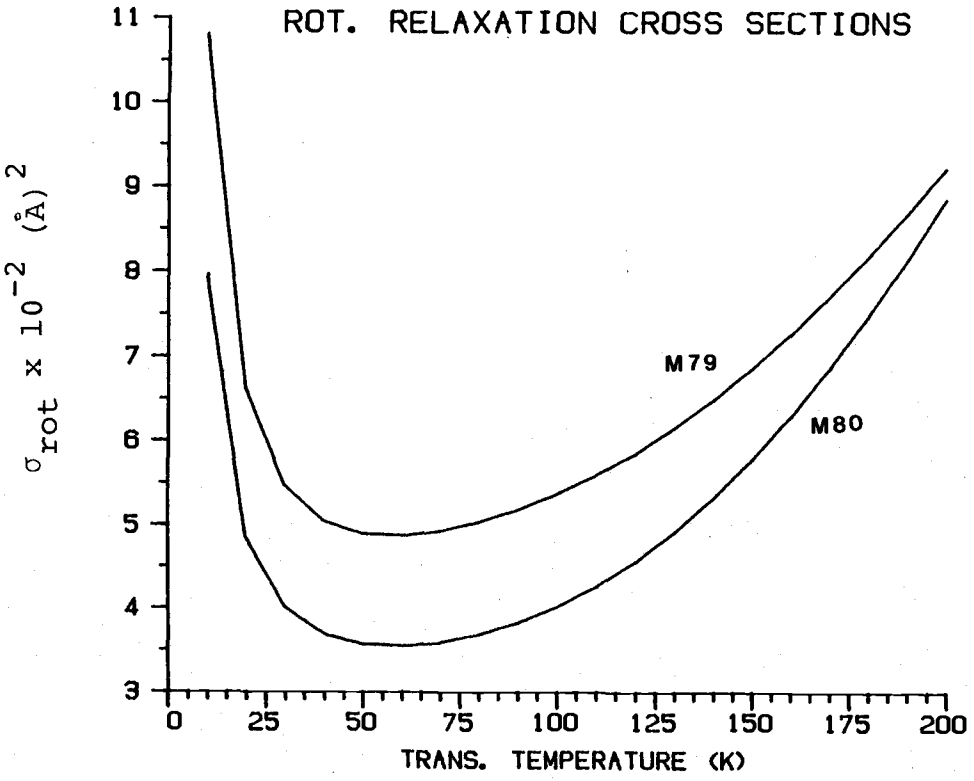

Figure 4-7 Effect of translational temperature on the para H_2 - H_2 rotational cross section. (values obtained from Kohler and Schaefer ref. 65)

monotonic function used for Z_{rot} in the classical model was not successful (note $Z_{rot}=\pi\sigma_h^2/\sigma_{rot}$). In particular, the classical expression does not reproduce the minimum in $_{rot}$ at about 60 K.

It is apparent from figure 4-7 that the σ_{rot} values are dependent upon the form of the interaction potential used. One of our goals was to see if our expansion results could aid in judging the relative merits of these cross sections. To this end, the σ_{rot} values of figure 4-7 were fitted to a polynomial form by least squares analysis. Two different functions were required,

$$\sigma_{rot} = A + BT_{tr} + CT_{tr}^2 + DT_{tr}^3 \quad ;\text{for } T_{tr}>60 \quad (4.45)$$

$$\sigma_{rot} = A + B(T_{tr})^{-C} + DT_{tr} \quad ;\text{for } T_{tr}<60 \quad (4.46)$$

where A, B, C, and D are fitting parameters in the least squares fit. Both functions were needed because of the increase in σ_{rot} below 60 K.

Using these expression for σ_{rot}, a Runge-Kutta[82,83] numerical integration of equation (4.35) was done for the M79 potential using the two different expansion models. Theoretical curves were

calculated for three different driving pressures, 1870, 1560, and 950 torr, using a nozzle diameter of 250 μm, a starting temperature of 293 K, and $\gamma = 1.67$. The results of these numerical integrations are shown in figure 4-8. It is quite apparent from these plots that the curves calculated using Anderson's model (solid traces) are well below our experimental values (x's). This excess cooling is attributed to the fact that this model doesn't take into account rotational to translation heating. This heating will decrease $T_{tr} - T_{rot}$ and hence $N_2^0 - N_2$ in eq. (4.35) so that the rate of rotational cooling is not as great.

The effect of the expansion model was examined by repeating the calculations with the fluid mechanical model of Rabitz and Lam. Equations (4.38,41,42) were integrated using a Runge-Kutta routine and the M79 cross sections. The starting values for the translational temperature and beam velocity were calculated using eqs. (4.39) and (4.40). The results for these integrations are shown as the dashed curves in figure 4-8.

As expected the results using the fluid mechanical model show a significant increase in the rotational temperatures compared to those predicted using Anderson's model and a much better simulation of our experimental data are obtained.

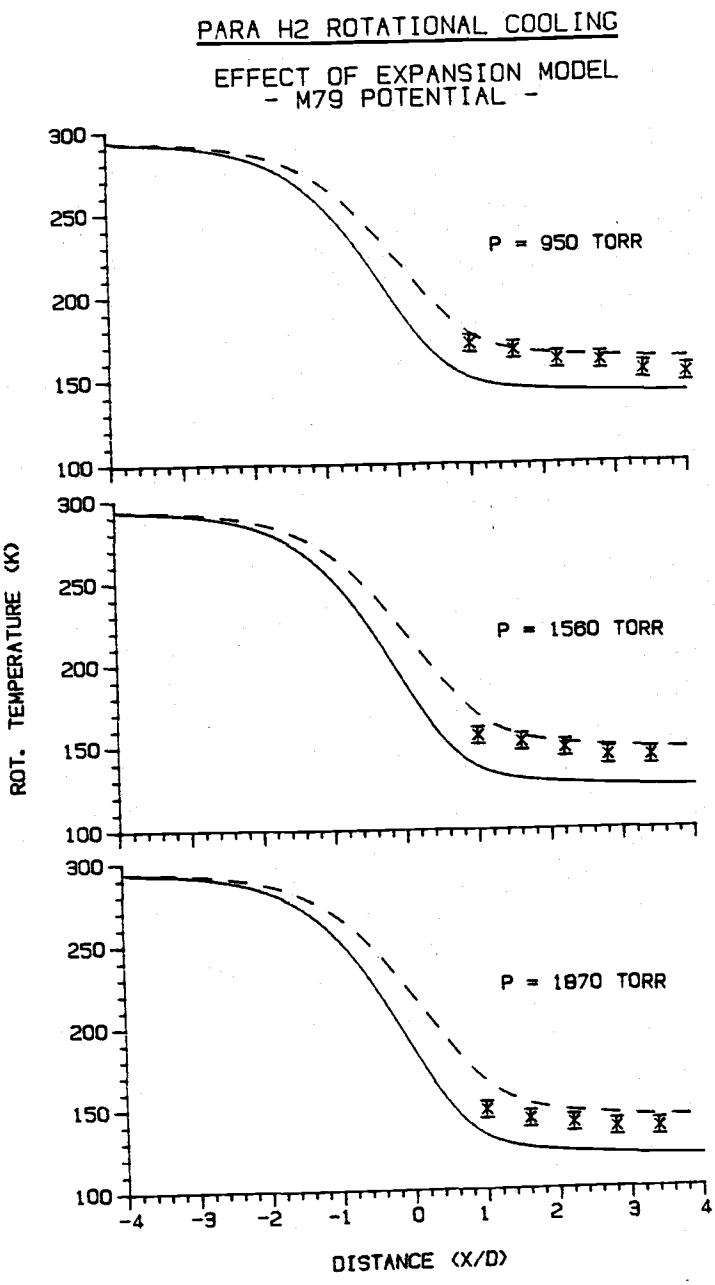

Figure 4-8 Comparison of expansion model on the theoretical rot. temperature profile of a para H_2 jet. (---- Fluid mechanical model, —— Anderson's model, the experimental data with their uncertainties are also indicated)

Figure 4-9 shows the effect of the expansion model on the translation temperature of H_2. We can see from this plot that the expansion model has a dramatic effect on the translation temperature curves. Gallagher and Fenn (figure 5 of ref. 75) have measured the translation energy of a H_2 expansion under similar conditions and their results are also in better accord with the fluid mechanical model than the Anderson Model.

Since both our results and the results of Gallagher and Fenn tend to favor the fluid mechanical model and since the fluid mechanical model seems inherently more reasonable, we have chosen to employ this model of the beam expansion in all our subsequent computations.

Using the fluid mechanical model, we next calculated theoretical curves derived by Kohler and Schaefer for the M80 potential.[65,84] Three different driving pressures were examined and figure 4-10 shows a comparison of the results for the M79 and the M80 potentials for the highest and lowest pressures. Both of the potentials seem to model the general characteristics of our data to a fair degree but both yield rotational temperatures slightly higher than we have observed experimentally. The M79 potential is better in this regard, a conclusion which is the opposite of that reached by Kohler and Schaefer.[63] Thes

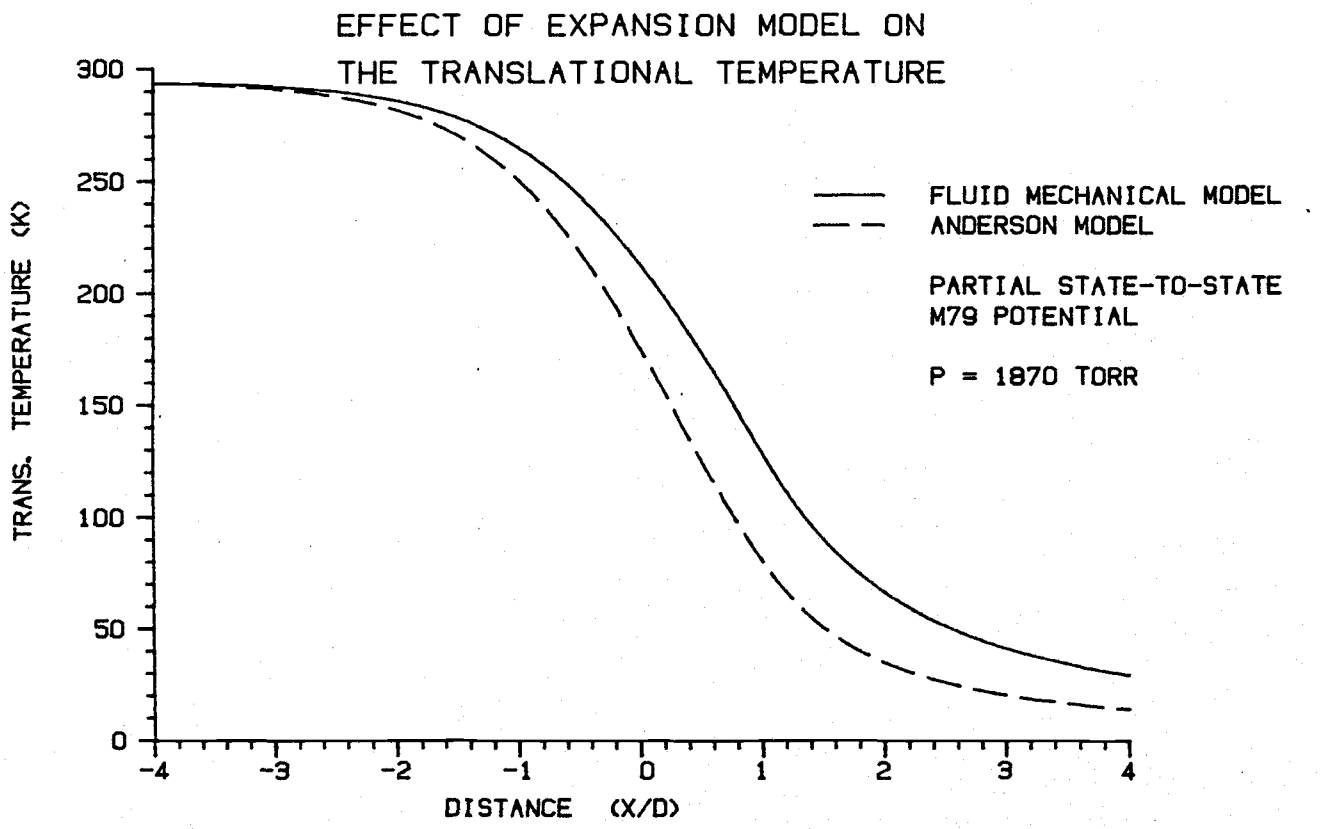

Figure 4-9 Effect of the expansion model on the translational temperature of H_2.

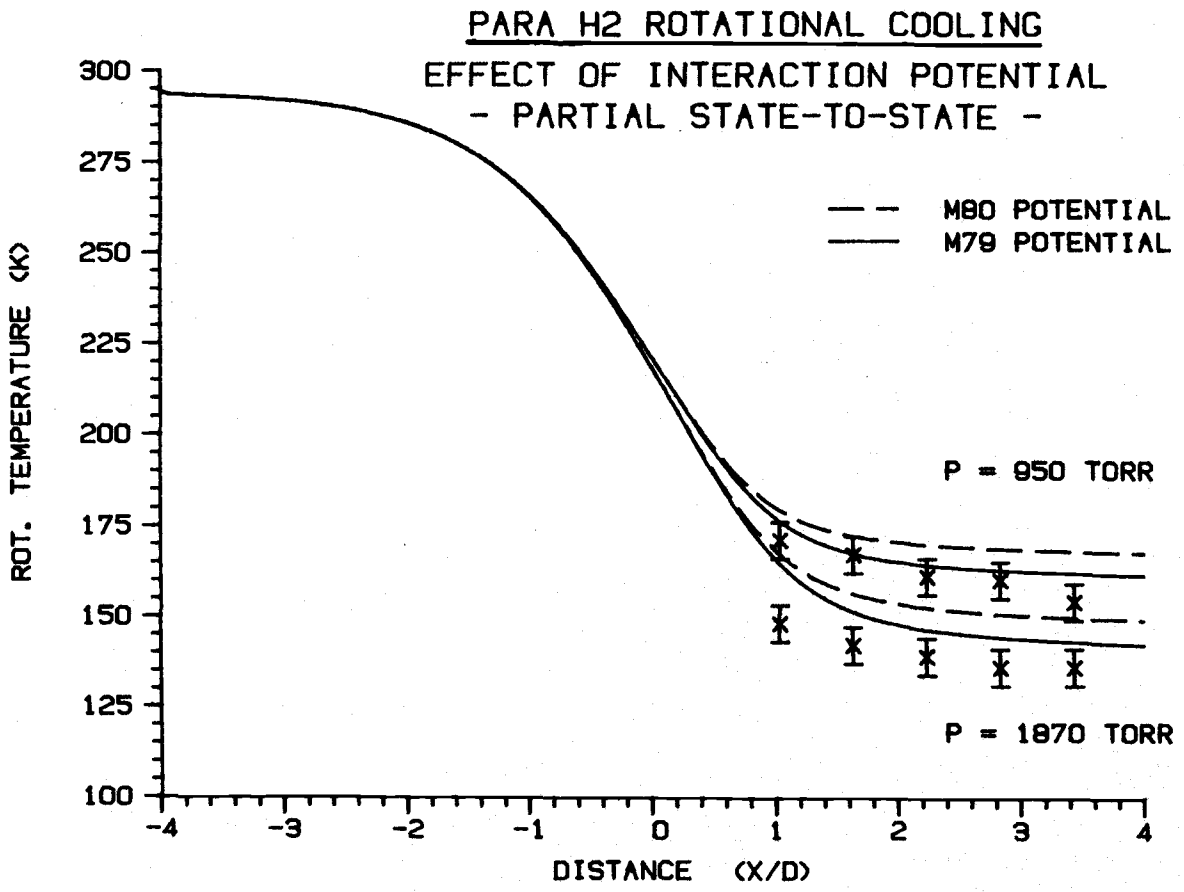

Figure 4-10 Comparison of the M79 and M80 interaction potentials using the partial state-to-state model of H_2 relaxation.

authors reached their conclusion after comparing theoretical cross sections from the M79 and M80 potentials with those measured experimentally by Jonkman[60] in static sound velocity experiments. They concluded that the M79 potential gave cross sections which were 30% too large. While our data would indicate, if anything, the cross sections are too small. The reason for this disagreement is not clear but one possibility is that the partial state-to-state model may not be adequate in describing the relaxation process. Hence, a complete state-to-state calculation was done as described in the next section.

4.5.D Complete State-to-State

Monchick and Schaefer[66] have used the M79 potential to calculate rate constants ($k_{ij \to lm}$) which can be used in the complete state-to-state model. This permits a direct comparison of the partial and complete state-to-state models. Their tabulated values of the rate constants used in eq. (4.34) were fitted to a polynomial function using a linear least squares fit. These fitted functions were then used in the numerical integration of eqs. (4.38,41,42).

Figure 4-11 compares the M79 results for the

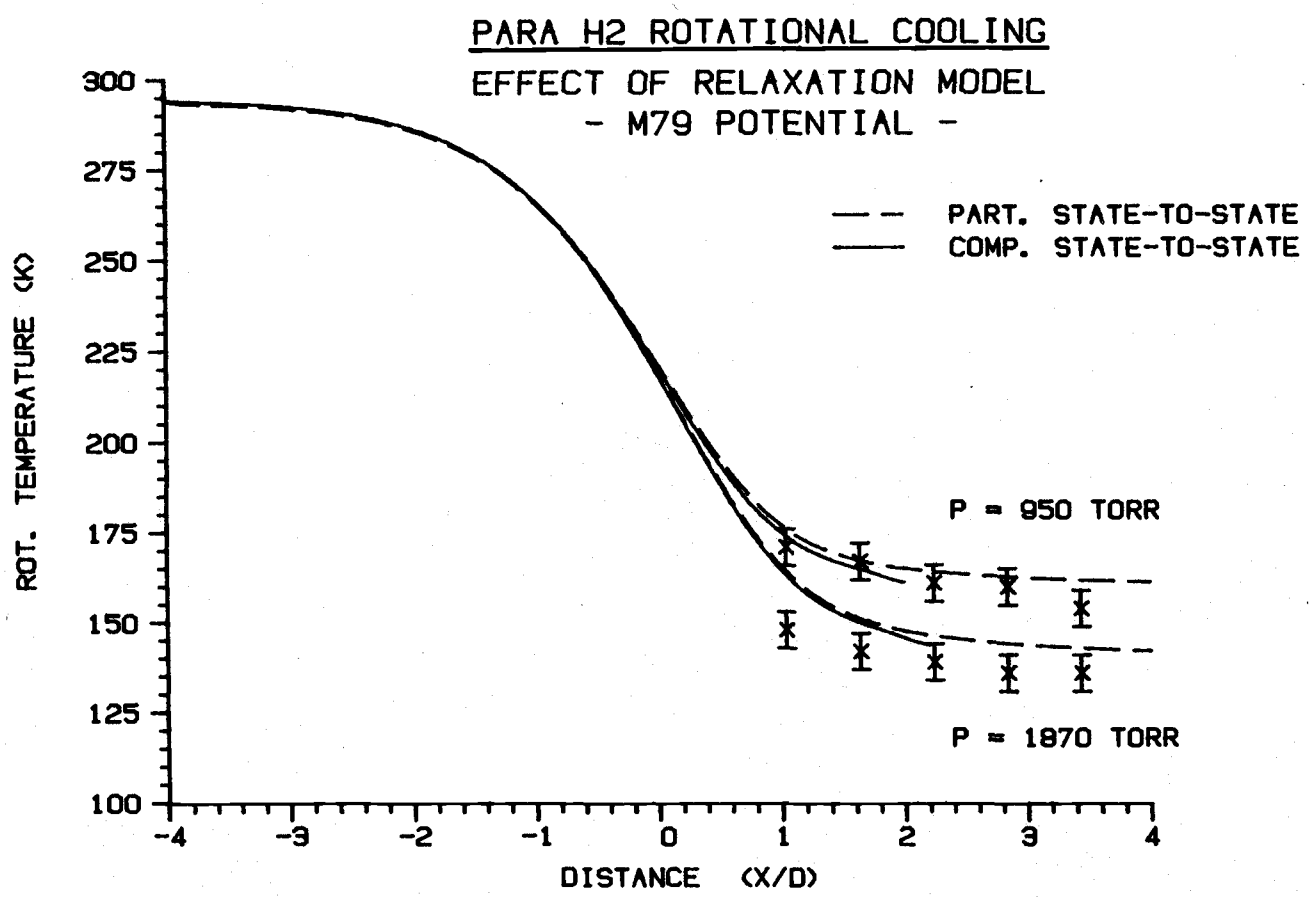

Figure 4-11 Comparison of the partial and complete state-to-state models for H_2 relaxation using the M79 potential.

partial state-to-state model and the complete state-to-state model under two expansion conditions. The rate constants calculated by Monchick and Schaefer were only tabulated down to 60 K, our calculations for the complete state-to-state model were stopped at this temperature extrapolation beyond this point led to an unrealistically large increase in the rate of change in the rotational temperature. Even down to 60 K, the complete state-to-state model gives slightly lower predicted temperatures. Most of this decrease comes from the double 22 -> 00 transition which is neglected in the partial state-to-state model. The effect is small, however, since the cross section for this transfer is about two orders of magnitude smaller than the $\sigma_{00\to02}$ and $\sigma_{02\to22}$ values.

A second complete state-to-state calculation was also done using an earlier H_2 --- H_2 potential.[68] Rabitz and Zarur have tabulated values for the rotational cross section ($\sigma_{ij\to lm}$) of H_2 as a function of total collisional energy. Following the procedure of Pollard and Lee,[58] we have fitted these cross sections to a polynomial function and have integrated them over a Maxwell-Boltzmann distribution of velocities to obtain the rate constants as a function of T_{tr} as required in equation (4.34).

The results using Rabitz and Zarur's cross sections are compared with those for the M79 potential in figure 4-12. Again, both curves reproduce the general trend of our experimental data but both are a bit high. Slightly better agreement is obtained with the M79 potential.

From all of the above calculations, several conclusions can be drawn. First, the fluid mechanical model of the expansion seems intrinsically more reasonable and for the M79 potential it models our data better than the simpler model of Anderson. Secondly, all of the cross sections for both the partial and complete state-to-state models do a fair job of fitting the experimental data but yield rotational temperatures which are a bit high. The complete state-to-state cross sections derived from the M79 potential of Kohler and Schaefer seem to give the best agreement. However, it should be said that this is a not as definitive as hoped at the outset of this work. None the less the models do permit one to adequately account for the rotational cooling that results from H_2 --- H_2 collisions and thus, it is possible to subtract this contribution in considering the added cooling when a driving gas is added.

This aspect is considered further in the final section of this chapter where we examine the H_2 --- He

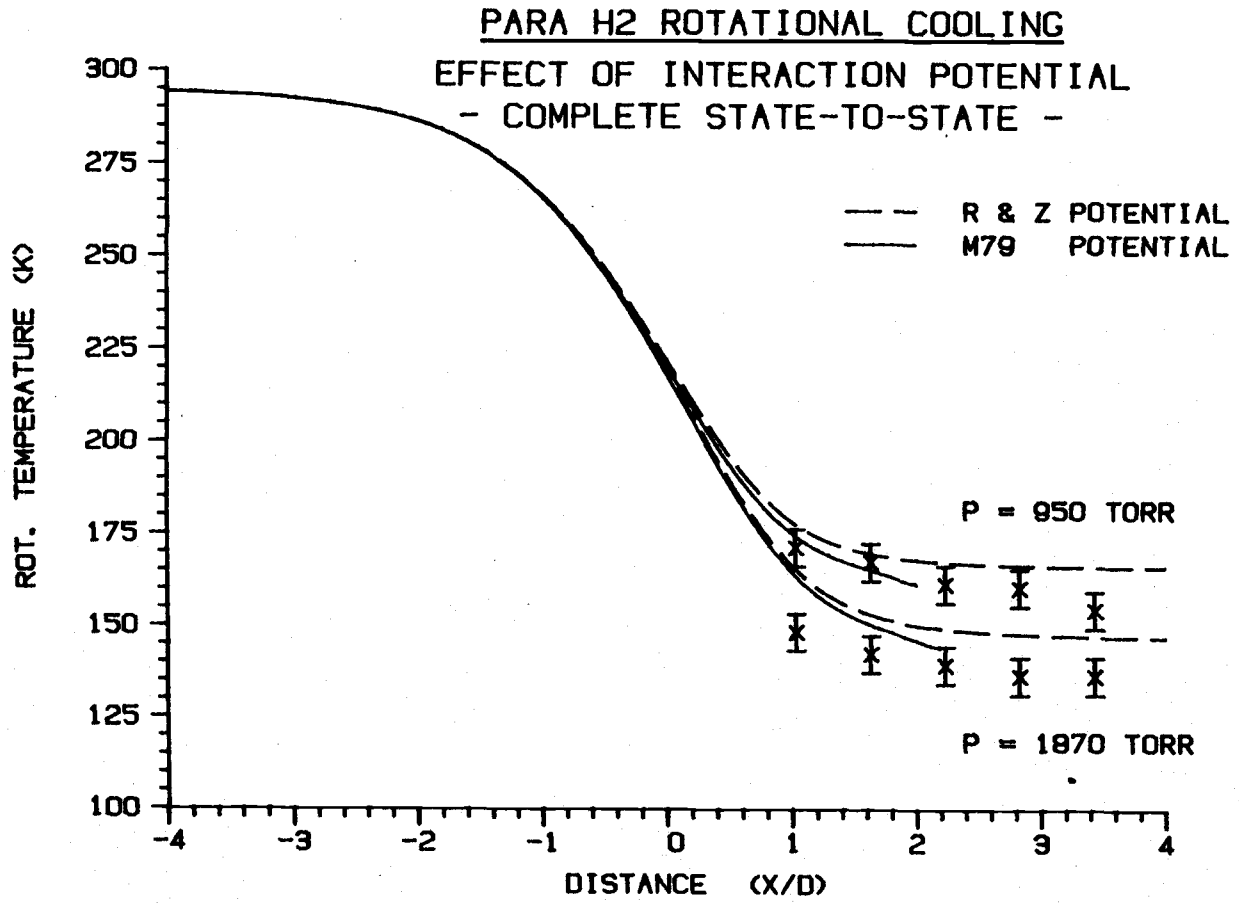

Figure 4-12 Comparison of the M79 and the Rabitz - Zarur potentials using the complete state-to-state model of H_2 relaxation.

system.

4.5.E Para H_2 --- He Relaxation Model

Since He is a monoatomic gas with no rotational states the H_2 --- He relaxation process can be treated with the partial state-to-state model. In a mixture of H_2 and He the following relaxation processes can occur

$$H_2(i) + H_2(j) \qquad H_2(l) + H_2(m) + Et$$

$$H_2(i) + He \qquad H_2(l) + He + Et$$

Therefore the total relaxation equation becomes

$$\frac{dN_2}{dx} = \frac{\rho D}{U}\left[(N_0N_0 - N_0N_2\,\frac{1}{5}\exp\{\varepsilon_2/KT_{tr}\})K_{00\to02}\right.$$

$$+2(N_0N_0 - N_2N_2\,\frac{1}{25}\exp\{2\varepsilon_2/KT_{tr}\})K_{00\to22}$$

$$+ (N_0N_2 - N_2N_2\,\frac{1}{5}\exp\{\varepsilon_2/KT_{tr}\})K_{02\to22}$$

$$\left.+\frac{8KT_{tr}}{\pi\mu_{H_2,He}}\,\sigma_{0\to2,He}\,(P_2^{o} - P_2)\right] \qquad (4.47)$$

where $\sigma_{0,1,He}$ is the rotational relaxation cross section for the H_2 and He pair, $\mu_{H_2,He}$ is the reduced mass for the pair, and U is the beam velocity for the mixture. U

is calculated using a mean mass for the mixture of

$$M_{H_2,He} = \alpha M_{He} + (1-\alpha) M_{H_2} \qquad (4.48)$$

where is the mole fraction of Helium. For further details about this calculation see the program RH2BUF in appendix B.

There have been several different calculations for the H_2 --- He cross sections and we have employed here results derived from the Secrest[86,87] and the Roberts[85,86] potentials. Using the cross sections derived from the Secrest potential[87] eq. (4.47) was numerically integrated. The resulting rotational temperatures calculated for our experimental conditions were all much higher (>15K) than those measured experimentally. Thus, the cross sections calculated using the Secrest potential appear to be much smaller then the true values. However, we should note that the Secrest cross sections used in our polynomial fit covered a significantly higher energy range then is really appropriate to our experimental temperature range. Thus, the large error in the calculated rotational temperatures may be due in part to the long extrapolation of the polynominal function.

The cross sections given for the Roberts potential

did cover the energy (and hence temperature) range of interest. These were fitted to a polynomial expression and were thermally averaged over a Maxwell-Boltzmann distribution of energies. The resulting function for the thermally averaged cross section was then used in equation (4.47) to simulate our experimental data.

Figure (4-13) shows the predicted effect of varying the ratio of helium to hydrogen in the expansion using the Rabitz - Zarur and Roberts cross sections. The conditions are: a driving pressure of 1000 torr, an initial temperature of 293 K and a nozzle diameter of 250 m. We see that the rotational temperature of H_2 drops rapidly as the ratio of He increasee. Our experimental values were taken at a He to H_2 ratio of 2:1 and a distance of 1.2 ± 0.2 X/D as the driving pressure was varied. Figure (4-14) compares these experimental results with those calculated for the Roberts potential. The agreement between the experimentally measured temperatures and the values theoretically calculated is quite good and the theoretical distance 1.0 X/D is within our measured distance of 1.2 ± 0.2 X/D. It is noteworthy that the results did not change significantly when the M79 rate constants of Monchick and Schaefer were used instead of the H_2 --- H cross sections calculated by Rabitz and

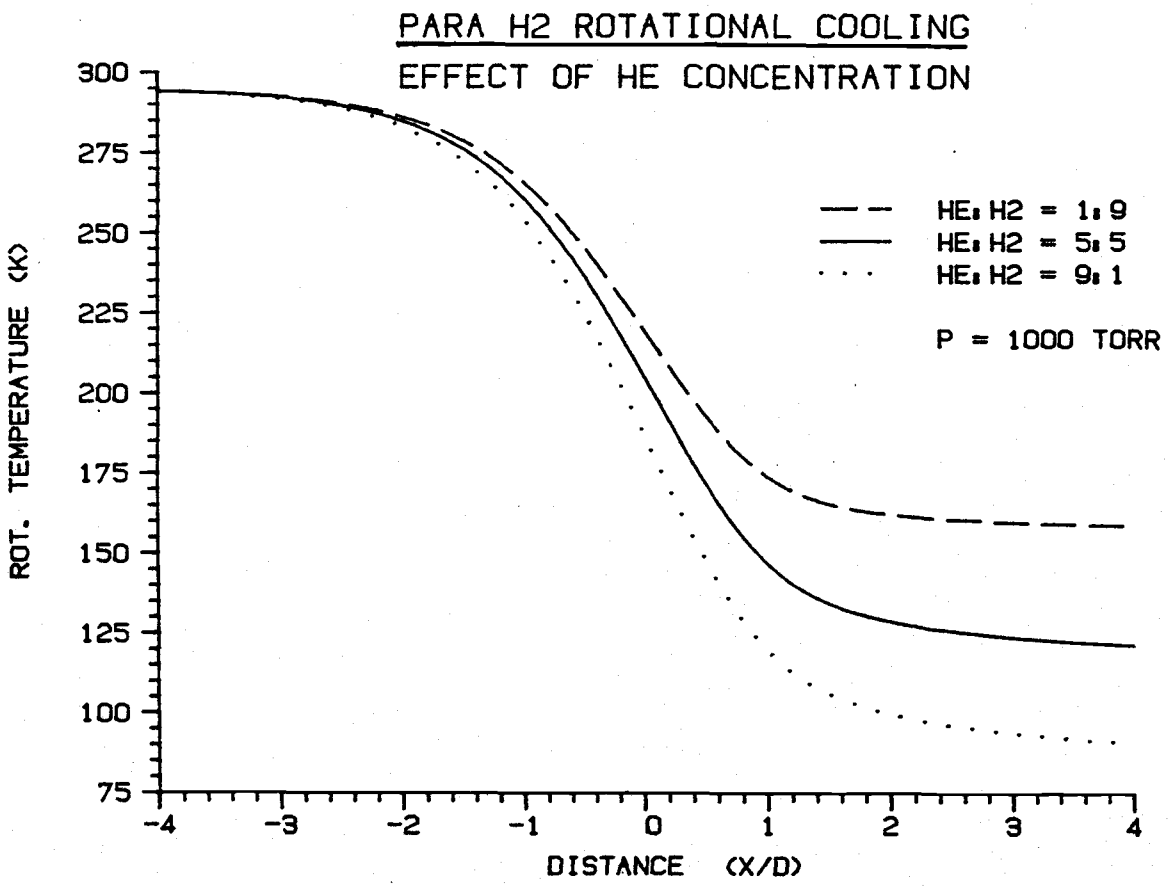

Figure 4-13 Effect of changing the He concentration on the theoretical rotational temperature of H_2.

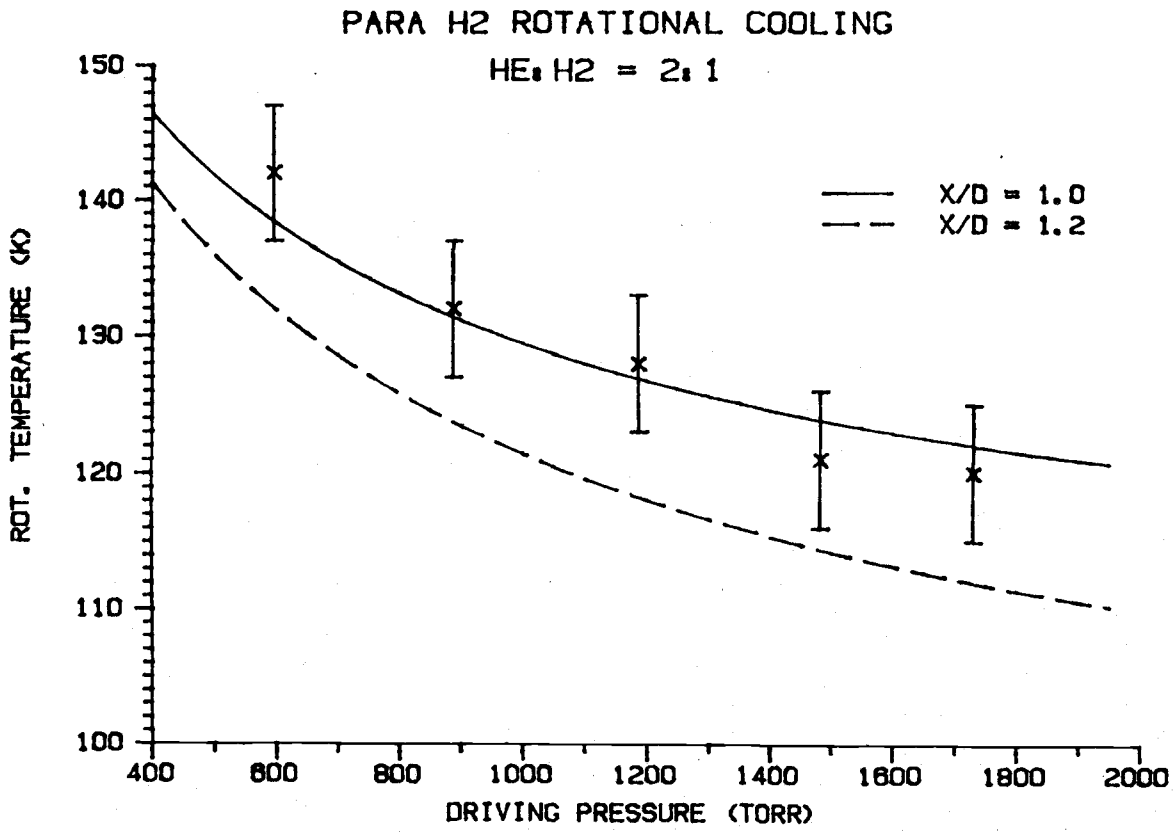

Figure 4-14 Comparison of the theoretical results for the H_2 --- He expansion using the Roberts He --- H_2 potential and the Rabitz - Zarur H_2 potential with the experimentally measured rotational temperature.

Zarur. This implies that even at this small He/H_2 ratio, relaxation by collisions with He is the dominant process.

4.6 Summary

The study of rotational relaxation processes in the gas phase is quite complicated due to the large number of states that are populated at room temperature. Hydrogen was chosen for this work because only a few rotational states are populated at room temperature and this number can be reduced further by the production of para hydrogen. For this reason a simple and efficient apparatus was constructed to produce para hydrogen by passing normal H_2 over a Fe_2O_3 catalyst cooled to 25 K by a cryogenic refrigerator. Using this method a continuous supply of pure para hydrogen was prepared for expansion measurements at pressures up to 2000 Torr. Broadband CARS spectra were recorded and analyzed to obtain rotational population distributions and temperatures for para H_2 mixtures with various driving gases.

In this chapter, we have considered three relaxation models of rotational cooling. The classical model assumes that the colliding molecules have a

continuum of rotational energy levels. The partial state-to-state model allows the relaxing H_2 to have quantized levels but quantum effects for the collision partner are averaged out. The final, complete state-to-state model permits molecules to change rotational level during a collision.

Two approaches to modeling the properties of a free jet expansion were also examined. Both are based upon the Mach number expressions of Ashkenas and Sherman. The first, the Anderson model has been widely used in studying relaxation in free jet expansions. This model gives a set of analytical equations for the ρ, T_{tr}, and U which are only dependent upon the Mach number and γ (Cp/Cv). No account is taken of the energy transfer from the internal modes in the free jet expansion. Unlike the Anderson model, the fluid mechanical model, developed by Rabitz and Lam, gives differential equations for T_{tr} and U which are directly linked to the relaxation process.

Our calculations have shown that the classical model of rotational relaxation does an inadequate job of predicting the rotational temperature profile of H_2 in a free jet expansion. No single Z^o_{rot} value could be found that fit all of our data.

Using the partial state model and the M80 cross

sections we have shown the fluid mechanical and Anderson models give comparable fits to our data. However, with the M79 cross sections, the former does a much better job of reproducing our experimental values then does the Anderson model. The Fluid mechanical approach seems inherently more reasonable and since both our data and time of flight measurements of the translational temperature[75] were consistent with it; we have used it in our subsequent analysis.

By combining the fluid mechanical description of the expansion with the M79 cross sections a test of the partial state-to-state and the complete state-to-state models for rotational relaxation was made. The results showed that both predict reasonable rotational temperatures but the complete state-to-state model gives slightly lower temperatures in better accord with our data.

Cross sections from three H_2 --- H_2 interaction potentials were tested (M79, M80 and Rabitz - Zarur). All gave adequate results in predicting the rotational temperatures in the free jet expansion. M79, with its larger cross sections, came closest to the actual experimental values. However, uncertainties and assumptions inherent in the expansion model make a difinitive statement on the three choices impossible.

Results were also obtained for the rotational temperature of H_2 in various expansion mixtures, many of which have never been studied before. This data (table 4-1, fig. 4-6) give an estimate as to the relative size of the rotational relaxation cross sections of the H_2 --- X collision, where X is the buffer gas. For the noble gas series He, Ne, and Ar we observed, as expected, that Ar has the largest cross section and He the smallest.

For the H_2 --- He system cross sections from the Roberts and Secrest potentials were tested and the Roberts potential gave results that closely matched our data. For the other buffer gases similar calculations were not possible because theoretical cross sections are not available at this time. Our experimental data could however be fitted at a later time when these theoretical cross sections become known. An alternative approach would be to assume a functional form for the H_2 --- X cross section and to use this for fitting the experimental data. Jonkman[60] has suggested that the H_2 --- X cross sections, where X is a noble gas, can be fit by the function

$$\sigma_{0\to 2,X} = b(E - \varepsilon_2)$$

where b is a fitting parameter. By integrating this

over a Maxwell-Boltzmann energy distribution the temperature dependent cross section could be deduced. This could then be used in the partial state-to-state model to test this form for the cross section and to deduce the best value of the parameter b. The program in appendix B could be modified for this purpose and this approach would be worthy of future study.

In general, we have found in doing this work that CARS is an excellent way of determining the rotational temperature profiles of free jet expansions. However, the value of this data in judging the merits of theoretical interaction potentials has not proven as great as initially hoped since the model for the beam expansion appears to be just as important as the cross sections. For this reason the results given here do not permit a definitive choice among the various available cross sections, altough a rather slight favoring of the complete state-to-state M79 potential was found.

REFERENCES

1. P. D. Marker and R. W. Terhune, Phys. Rev., 137, A801 (1965)

2. R. W. Terhune, Bull. Am. Phys. Soc., 8, 359 (1063)

3. F. Zernike and J. E. Midwinter, "Applied Nonlinear Optics", John Wiley & Sons, New York (1973)

4. S. J. Cyvin, J. E. Rauch, and J. C. Decius, J. Chem. Phys., 43, 4083 (1965)

5. C. Flytzanis, in "Quantum Electronics: A Treatise", edited by H. Tang, Vol. 1, Academic, New York (1975)

6. F. J. Woodbury and N. K. Ng, Proc. IRE, 50, 2367 (1962)

7. W. Kiefer and D. A. Long, "Nonlinear Raman Spectroscopy and Its Chemical Applications", D. Reidel, Boston (1982)

8. A. B. Harvey, "Chemical Applications of Nonlinear Raman Spectroscopy", Academic, New York (1981)

9. F. Moya, S. A. J. Druet, and J. P. E. Taran, Opt. Commun., 13, 169 (1975)

10. J. W. Nibler and G. V. Knighten, in "Topics in Current Physics", edited by A. Weber, Springer, Berlin (1979), Chap. 7 (note the expressions given here [eq. 7.61-7.64] are wrong and must be divided by 2)

11. W. J. Jones and B. P. Stoicheff, Phys. Rev. Lett., 13, 657 (1964)

12. J. J. Barrett, in "Chemical Applications of Nonlinear Raman Spectroscopy", edited by A. Harvey, Academic, New York, (1981)

13. E. J. Woodbury and N. K. Ng, Proc. IRE, 50, 2367 (1962)

14. J. J. Barrett and M. J. Berry, App. Phys. Lett., 34(2), 144 (1979)

15. G. A. West, D. A. Siebert, and J. J. Barrett, J. Appl. Phys., 51(5), 2823 (1980)

16. C. K. N. Patel and A. C. Tam, Appl. Phys. Lett., 34(11), 760 (1979)

17. J. J. Barrett and D. F. Heller, in "Nonlinear Raman Spectroscopy and Its Chemical Applications", edited by W. Kiefer and D. A. Long, D. Reidel, Boston (1982)

18. M. G. Littman and H. J. Metchalf, Appl. Opt., 17, 2224 (1978)

19. Y. Pao, "Optoacoustic Spectroscopy", Academic, New York (1977)

20. A. Rosencwaig, "Photoacoustics and Photoacoustic Spectroscopy", Wiley, New York (1980)

21. P. R. Regnier and J. P. E. Taran, in "Laser Raman Diagnostics", edited by M. Lapp and C. M. Penneys, Plenum, New York (1974)

21. D. A. Siebert, G. A. West, and J. J. Barrett, Applied Optics, 19(1), 53 (1980)

22. G. A. West and J. J. Barrett t, Optics Letters, 4(12), 395 (1979)

23. V. I. Fabelinsky, et al, Opt. Comm., 20(3), 389 (1977)

24. S. Brodersen, in "Topics in Current Physics", edited by A. Weber, Vol. 11, Springer, Berlin (1979)

25. S. A. Duret and J. E. Taran, "Prog. Quantum Electronics Vol. 7",Pregamon Press, Oxford, 1981

26. G. L. Eesley, "Coherent Raman Spectroscopy", Pergamon, Oxford (1981)

27. D. C. Hanna, M. A. Yuratich, and D. Cotter, "Nonlinear Optics of Free Atoms and Molecules", Springer, Berlin (1979)

28. W. G. Rado, Appl. Phys. Lett., 2, 123 (1967)

29. G. Hauchecourne, F. Kerherve, and G. Mayer, J. Phys. (Paris), 32, 47 (1971)

30. M. Maier, W. Kaiser, and J. A. Giordmaine, Phys. Rev, 177, 580 (1969)

31. M. Maier, Appl. Phys., 11, 209 (1976)

32. W. M. Hou and R. L. Jaffe, Phys. Rev. Lett., 47, 30 (1981)

33. D. Guthals, P. Huber-Walchli, and J. W. Nibler, Chem. Phys. Lett., 67, 233 (1979)

34. P. Huber-Walchli and J. W. Nibler, J. Chem. Phys., 76(1), 273 (1982)

35. J. F. Ward and G. H. C. New, Physics Rev., 185, 57 (1969)

36. B. J. Orr and J. F. Ward, Mol. Phys.,20, 513 (1971)

37. W. B. Roh and P. W. Schrieber, Appl. Optics, 17(9), 513 (1971)

38. H. W. Klockner and H. W. Schrotter, in "Topics in Current Physics", edited by A. Weber, Berlin (1979)

39. D. M. Golden and B. Crawford, Jr., J. Chem. Phys., 36, 1654 (1962)

40. W. F. Murphy, W. Holzer, and H. J. Berstien, Appl. Spectrosc., 23, 211 (1969)

41. A. Owyoung, Opt. Lett., 2, 91 (1978)

42. M. P. Bograad and B. J. Orr, Int. Rev. Sci. Phys. Chem. Ser. 2, 2, 149 (1975)

43. R. S. Finn and J. F. Ward, Phys. Rev. Lett., 26, 285 (1971)

44. J. F. Ward and C. K. Miller, Phys. Rev. A, 19, 826 (1979)

45. C. K. Miller and J. F. Ward, Phys. Rev. A, 16, 1179 (1977)

46. A. D. Buckingham and D. A. Dummur, Trans. Faraday Soc., 64, 1776 (1968)

47. A. D. Buckingham and B. J. Orr, Proc. R. Soc. London Ser. A, 305, 259 (1968)

48. A. D. Buckinghan, M. P. Bogaard, D. A. Dummur, C. P. Hobbs, and B. J. Orr, Trans. Faraday Soc.,66, 1548 (1970)

49. P. Sitz and R. Yaris, J. Chem. Phys., 49, 3546 (1968)

50. J. F. Ward and I. J. Bigio, Phys. Rev. A, 11, 60, (1975)

51. J. F. Ward and D. S. Elliot, J. Chem. Phys., 69, 5438 (1978)

52. A. D. Buckingham and B. J. Orr, Trans. Faraday Soc., 65, 673 (1969)

53. A. D. Buckingham, M. P. Bogaard, D. A. Dummuir, C. P. Hobbs, and J. Orr, Trans. Faraday Soc., 66, 1548 (1970)

54. K. Koura, J. Chem. Phys., 77(10), 5141 (1982)

55. H. G. Dennewitz and G. Buess, Chem. Phys., 28, 175 (1978)

56. G. M. McClelland, et al, J. Chem. Phys., 83(8), 947 (1979)

57. R. J. Gallagher and J. B. Fenn, J. Chem. Phys., 60(9), 3492 (1974)

58. J. E. Pollard, D. J. Trevor, V. T. Lee, and D. A. Shirley, J. Chem. Phys., 77(10), 4819 (1982)

59. H. P. Godfried, I. F. Silvera, and J. Van Straaten, 'Rarefied Gas Dynamics', Pt. 2, Academic, New York (1980)

60. G. J. Prangsma, et al, Physica, 61, 527 (1972)

61. R. Brout, J. Chem. Phys., 22(5), 934 (1955)

62. R. Ramaswamy and H. Rabitz, J. Chem. Phys., 66(1), 152 (1977)

R. Ramaswamy, H. Rabitz, and and S. Green, J. Chem. Phys., 66(7), 3021 (1977)
R. Ramaswamy, H. Rabitz, and and S. Green, Chem. Phys., 66(7), 3021 (1978)

63. W. E. Kohler and J. Schater, J. Chem. Phys., 78(8), 4862 (1983)

64. C. J. Sluijter, H. F. P. Knaap, and J. J. B. Beenakker, Physica, 31, 915 (1983)

65. W. E. Kohler and J. Schaefer, J. Chem. Physc., 78(1), 6602 (1983)

66. L. Monchick and J. Schaefer, J. Chem. Physc., 73(12), 6153 (1980)

67. J. Schaefer and W. Meyer, J. Chem. Physc., 70(1) 344 (1979)

68. G. Zarur and H. Rabitz, J. Chem. Phys., 60(5), 2057 (1974), (The values for the cross sections were corrected as noted in ref. 17)

69. H. Rabitz and S. H. Lam, J. Chem. Phys., 63(8), 3532 (1975)

70. W. R. Gentry and C. F. Giese, Rev. Sci. Instrum., 49, 595 (1978)

71. C. E. Otis and P. M. Johnsons, Rev. Sci. Instrum., 51, 1128 (1980)

72. J. Valentini and J. Cross, Rev. Sci. Instrum., 53(1), 38 (1982)

73. K. L. Saenger, J. Chem. Phys., 75(5), 2467 (1981)

74. M. A. Murphy, W. Holzer, and H. J. Bernstien, App. Spect., 23, 211 (1969)

75. R. J. Gallagher and J. B. Fenn, J. Chem. Phys., 60(9), 3487 (1974)

76. D. R. Miller and R. P. Anders, J. Chem. Phys., 46(9), 848 (1067)

77. T. G. Winter and R. C. Amme, J. Chem. Phys., 46(9) 848 (1967)

78. C. A. Boitnott and R. C. Warder Jr., Phys. Fluids, 14, 2313 (1971)

79. J. B. Anderson, in "Molecular Beam and Low Density Gas Dynaamics", edited by P. P. Wegener, Decker, New York (1974)

80. H. Ashkenas and F. S. Sherman, in "Rarefied Gas Dynamics, 4th Symposium", edited by J. H. deLeeuw, Academic, New York (1966)

81. W. Meyer and J. Schaefer, J. Chem. Phys.; to be published

82. B. Carnahan, H. A. Luther, J. O. Wilkes, "Applied Numerical Methods", Wiley, New York (1969)

83. G. A. Gabriel, "Introduction to Scientific Cumputing", Appleton-Century-Crofts, New York

84. J. Schaefer and B. Lui, J. Chem. Phys., to be published

85. M. D. Gordon and D. Secrest, J. Chem. Phys., 52(12), 120 (1970)
B. R. Johnson and D. Secrest, J. Chem. Phys., 48(10), 4682 (1968)
W. Eastes and D. Secrest, J. Chem. Phys., 56(1) 640 (1972)

86. G. Zarur and H. Rabitz, J. Chem. Phys., 59(2) 943 (1973)

87. C. S. Roberts, Phys. Review, 131(1), 203 (1963)

APPENDICES

Appendix A

Nonresonant Susceptibility Programs

This library contains the following program listings:

1. NRCLT.FOR
   A. COLLCT.FOR
   B. DATIN1.MAC
2. NRLINE.FOR
3. NRPLOT.FOR

These programs and subroutines were used for the collection and reduction of the spectroscopic data in the determination of the third order nonresonant susceptibilities given in chapter 3.

NRCLT.FOR

```
C*************************************************************
C*                                                           *
C* NAME    = NRCLT                                           *
C* PURPOSE = THIS PROGRAM IS USED IN THE CALCULATION         *
C*           OF THE THIRD ORDER NONRESONANT SUSCEPTI-        *
C*           BILITIES OF GASES. THE PROGRAM CALCULATES       *
C*           A NONRESONANT SIGNAL OF A GAS RELATIVE TO       *
C*           THAT OF A STANDARD GAS.  THE OUPUT IS IN        *
C*           THE FORM OF A FILE WHICH CAN BE USED WITH       *
C*           NRLINE AND NRPLT.                               *
C*                                                           *
C* THOMAS F. LUNDEEN            OREGON STATE UNIVERSITY      *
C*                                                           *
C*************************************************************

      PROGRAM NRCLT
C
      DIMENSION FILENM(4)
      INTEGER POINTS
      LOGICAL*1 BELL
      BELL =07
C
C     ACCEPT THE OUTPUT FILE NAME
C
10    TYPE 101
      ACCEPT 102,FILENM
C
C     OPEN THE OUTPUT FILE
C
      OPEN (UNIT=3,NAME=FILENM,TYPE='NEW',INITIALSIZE=40)
C
      GO TO 30
C
C     ERROR OPENING FILE, PRINT ERROR MESSAGE AND TRY AGAIN.
C
20    TYPE *,'ERROR TRY AGIAN'
      GO TO 10
C
C     GET THE NAME OF THE GAS
C
30    TYPE 103
      ACCEPT 102,FILENM
      WRITE (3,104) FILENM
C
C     FIND THE POWERS OF THE PUMP AND STOKES LASERS
C
      TYPE 120
      ACCEPT *,W1
C
      TYPE 121
```

```
      ACCEPT *,W2
C
      WRITE (3,*) W1,W2
C
C     GET THE NUMBER OF POINTS TO BE AVERAGE
C
      TYPE 105
      ACCEPT 106,POINTS
C
C     ANY TEST POINTS?
C
35    TYPE 107
      ACCEPT 106,NPNTS
C
      IF (NPNTS.EQ.0) GO TO 55
C
C     PERFORM TEST POINTS
C
      DO 1000 I=1,NPNTS
         SUM=0.0
C
         DO 2000 J=1,POINTS
C
           CALL DATIN1(ISIG)
           TYPE *,ISIG
           SIGNAL=FLOAT(ISIG)
           SUM=SUM+SIGNAL
C
2000     CONTINUE
C
         AVG=SUM/FLOAT(POINTS)
         TYPE *,'AVERAGE =',AVG
C
1000  CONTINUE
C
C     SEE IF THE USER WISHES ANY MORE TEST POINTS
C
      TYPE 108
      ACCEPT 109,IAN
C
      IF (IAN.EQ.'YE') GO TO 35
C
C     START REAL SCAN
C
55    TYPE 110
      ACCEPT *,PRES
      WRITE (3,*) PRES
C
C     ENTER THE AMPLIFICATION FACTOR
C
```

```
      TYPE 112
      ACCEPT *,AMP
C
C     COLLECT THE DATA ON SIGNAL GASES
C
      CALL COLLCT(SIGNR,POINTS,AMP)
C
C
      TYPE 123,BELL,BELL
C
C     COLLECT THE SIGNAL FOR THE STANDARD GAS
C
      PAUSE ' STANDARD'
C
C     READ THE AMPLICATION FACTOR
C
      TYPE *,'AMPLICATION OF STANDARD'
      ACCEPT *,AMP
C
C     COLLECT THE STANDARD SIGNAL
C
      CALL COLLCT(SIGSTD,POINTS,AMP)
C
C     CALCULATE THE RELATIVE SIGNAL
C
      SIGNAL=SIGNR/SIGSTD*100
C
      TYPE *,'SIGNAL RELATIVE =',SIGNAL
      WRITE (3,*) SIGNAL
C
C     QUERY FOR MORE DATA
C
      TYPE 113,BELL
      ACCEPT 109,IAN
C
      IF (IAN.EQ.'YE') GO TO 35
C
      CLOSE(UNIT=3)
C
      STOP
```

```
C
101     FORMAT(' ENTER THE FILE NAME ',$)
102     FORMAT(4A4)
103     FORMAT(' WHAT IS THE MOLECULE BEING STUDIED? ',$)
104     FORMAT(1X,4A4)
105     FORMAT (' HOW MANY POINTS DO YOU WISH TO AVERAGE? ',$)
106     FORMAT (I4)
107     FORMAT(' HOW MANY TEST POINTS DO YOU WANT? ',$)
108     FORMAT(' DO YOU WISH ANY MORE TEST POINTS? ',$)
109     FORMAT(A2)
C
110     FORMAT (' COLLECT THE SIGNAL',/,' WHAT IS THE PRESSURE? ',$)
112     FORMAT(' WHAT IS THE AMPLICATION? ',$)
113     FORMAT(' DO WANT TO TAKE ANY MORE DATA? ',A1,$)
C
120     FORMAT(' ENTER THE W1 POWER ',$)
121     FORMAT (' ENTER THE W2 POWER ',$)
123     FORMAT (1X,2A1)
C
        END
```

COLLCT.FOR

```
C*************************************************************
C*                                                           *
C* NAME    = COLLCT                                          *
C* PURPOSE = THIS SUBROUTINE USES DATAIN1 TO COLLECT         *
C*           DATA FROM CHANNEL 0 OF THE A/D CONVERTER.       *
C*           IT CALCULATES A AVERAGE VALUE FOR THE           *
C*           SIGNAL, BACKGROUND, AND BACKGROUND SUB-         *
C*           TRACTED SIGNAL.  THE PROGRAM ALSO CALC-         *
C*           ULATES THE STANDARD DEVIATION AND PERCENT       *
C*           DEVIATION OF ALL THESE VALUES. THIS             *
C*           INFORMATION IS WRITTEN ON THE FILE OPEN IN      *
C*           THE MAIN PROGRAM.                               *
C* USAGE   = CALL COLLCT(SIGNAL,POINTS,AMP)                  *
C*              SIGNAL = IS THE BACKGROUND SUBRACTED         *
C*                       SIGNA RETURN TO THE MAIN            *
C*                       PROGRAM.(REAL)                      *
C*              POINTS = THE NUMBER OF POINTS TO BE          *
C*                       AVERAGED  (INTEGER)                 *
C*              AMP    = THE AMPLICATION FACTOR OF           *
C*                       THE SIGNAL                          *
C*                       TO BE DIVIDED OUT. (REAL)           *
C*                                                           *
C* THOMAS F. LUNDEEN            OREGON STATE UNIVERSITY      *
C*                                                           *
C*************************************************************

      SUBROUTINE COLLCT(SIGNAL,POINTS,AMP)
      INTEGER POINTS
      LOGICAL*1 BELL
      BELL=7
C
C     INITIALIZE VARIABLES
C
      SUMSQ = 0.0
      SUM   = 0.0
C
C     COLLECT DATA
C
      DO 3000 I=1,POINTS
         CALL DATIN1(ISIG)
         SIGNAL = FLOAT(ISIG)/AMP
         SUM    = SUM + SIGNAL
         SUMSQ  = SUMSQ + SIGNAL*SIGNAL
3000  CONTINUE
C
C     CALCULATE THE AVERAGE, STANDARD DEVIATION, AND
C     PERCENT DEVIATION
C
      POINT = FLOAT(POINTS)
      AVG   = SUM/POINT
```

```
      STD   = SQRT((SUMSQ-POINT*AVG*AVG)/(POINT-1.0))
      PSTD  = STD/AVG*100
C
C     COLLECT BACKGROUND WITH GREEN ONLY
C
      TYPE 123, BELL,BELL
      PAUSE ' BLOCK THE RED BEAM'
C
      SIGNAL = 0.0
      SIGSQ  = 0.0
C
      DO 6000 I=1,POINTS
         CALL DATIN1(ISIG)
         SIG    = FLOAT(ISIG)/AMP
         SIGNAL = SIGNAL+SIG
         SIGSQ  = SIGSQ+SIG*SIG
6000  CONTINUE
C
C     CALCULATE THE AVERAGE, STANDARD DEVIATION, AND
C     PERCENT DEVIATION
C
      AVGB = SIGNAL/POINT
      STDB = SQRT((SIGSQ-POINT*AVGB*AVGB)/(POINT-1.0))
C
C     CALCULATE THE AVERAGE, STANDARD DEVIATION, AND
C     PERCENT DEVIATION ON THE CORRECTED SIGNAL
C

      IF (AVGB.NE.0.0) GO TO 10
      PSTDB = 0.0
      GO TO 20
C
10    PSTDB = STDB/AVGB*100
C
C     CALCULATE THE CORRECTED SIGNAL
C
20    SIGNAL = AVG - AVGB
      STDSIG = SQRT(STD*STD + STDB*STDB)
      PSTDS  = STDSIG/SIGNAL * 100.0
C
C     OUTPUT THE DATA
C
      WRITE (3,*) AVG,STD,PSTD
      WRITE (3,*) AVGB,STDB,PSTDB
      WRITE (3,*) SIGNAL,STDSIG,PSTDS
C
      RETURN
C
123   FORMAT (1X,2A1)
      END
```

DATIN1.MAC

```
;*************************************************************
;*                                                           *
;* NAME    = DATIN1                                          *
;* PURPOSE = TO COLLECT TO DO A A/D CONVERSION ON THE        *
;*           SIGNAL COMING IN CHANNEL 0.  THE A/D            *
;*           CONVERSION IS TAKEN ON THE FALLING EDGE         *
;*           OF A TRIGGER PULSE GOING IN EXT. START.         *
;* USAGE   = CALL DATIN1(ISIG)                               *
;*              ISIG = IS THE SIGNAL ON CHANNEL 0            *
;*                     (INTEGER).                            *
;*                                                           *
;* THOMAS F. LUNDEEN            OREGON STATE UNIVERSITY      *
;* DECEMBER 30, 1981                                         *
;*************************************************************

        .TITLE DATIN1.MAC
        .GLOBL DATIN1
;
; ADDRESS DEFINITIONS
;
CSR=170400
DBR=170402
CH00EX=020020
;
DATIN1: TST     (R5)+           ;NO NEED TO SAVE # OF ARGUMENTS

        MOV     #CH00EX,@#CSR   ;SAMPLE SIGNAL ON CH 00 A/D EXT
                                ;START
TTST:   TSTB    @#CSR           ;A/D DONE?
        BPL     TTST

        MOV     @#DBR,@(R5)+    ;STORE SIGNAL

        RETURN
        .END
```

NRLINE.FOR

```
C*************************************************************
C                                                            *
C NAME   = NRLINE                                            *
C PURPOSE= TO TAKE THE EXPERIMENTAL DATA COLLECTED BY        *
C*         AND PERFORM A LINEAR REGRESSION ON IT.  THE       *
C*         PROGRAM PRINTS OUT THE RESULTS ON THE LINE        *
C*         PRINTER AND CREATES A OUTPUT FILE TO BE           *
C*         USED BY NRPLT.                                    *
C                                                            *
C THOMAS F. LUNDEEN              OREGON STATE UNIVERSITY     *
C*************************************************************

      PROGRAM NRLINE
C
      LOGICAL*1 IANS
      DIMENSION XRAY(40),YRAY(40),FILENM(4)
      REAL MST,MSR,MSE
C
C     OPEN INPUT FILE
C
5     TYPE 101
      ACCEPT 102,FILENM
C

      OPEN (UNIT=3,TYPE='OLD',NAME=FILENM,READONLY)
C
C     OPEN OUTPUT FILE
C
      TYPE 103
      ACCEPT 102,FILENM
C
      OPEN (UNIT=4,TYPE='NEW',NAME=FILENM,INITIALSIZE=10)
C
C     READ THE MOLECULE NAME
C
      READ(3,102) FILENM
      READ(3,*) W1,W3
C
      ICNT=1
10    READ(3,*,END=20) PRES
      XRAY(ICNT)=PRES*PRES
C
      DO 1000 I=1,6
         READ(3,*) DATA,STD,PSTD
1000  CONTINUE
C
      READ(3,*) YRAY(ICNT)
      ICNT=ICNT+1
      GO TO 10
15    TYPE *,'ERROR'
```

```
      GO TO 25
20    CLOSE(UNIT=3,ERR=15)
25    ICNT=ICNT-1
C
C     ORDER THE DATA FROM SMALLEST X TO GREATEST
C
      DO 3000 I=1,ICNT
C
         JMAX=ICNT-I
C
         DO 2000 J=IMIN,JMAX
            IF (XRAY(J).LE.XRAY(J+1)) GO TO 2000
            TEMX=XRAY(J)
            TEMY=YRAY(J)
            XRAY(J)=XRAY(J+1)
            YRAY(J)=YRAY(J+1)
            XRAY(J+1)=TEMX
            YRAY(J+1)=TEMY
2000     CONTINUE
3000  CONTINUE
C
C     INITIALIZE VARIABLES
C
30    SST=0.0
      SSR=0.0
      MST=0.0
      MSE=0.0
      SUMX=0.0
      SUMY=0.0
      SUMXQ=0.0
      SUMYQ=0.0
      SUMXY=0.0
      XN=0.0
      N=0
C
C     OUTPUT THE VALUES
C
      TYPE *,'DO YOU WANT A PRINT OUT OF X AND Y VALUES?'
      ACCEPT 104,IANS
      IF (IANS.EQ.'N') GO TO 35
      TYPE *,'     I     X(I)           Y(I)'
C
      DO 4000 J=1,ICNT
         I=J
         TYPE *,I,XRAY(I),YRAY(I)
4000  CONTINUE
C
C     ENTER THE RANGE OF VALUES TO GET THE SLOPE FROM
C
35    TYPE *,'ENTER THE INDEX NUMBERS FOR THE MIN. AND MAX. VALUES'
```

```
      ACCEPT *,IMIN,IMAX
C
C     PERFORM THE CALCULATIONS
C
      DO 5000 I=IMIN,IMAX
          XN=XN+1.0
          N=N+1
          SUMX=SUMX+XRAY(I)
          SUMY=SUMY+YRAY(I)
          SUMXQ=SUMXQ+(XRAY(I)*XRAY(I))
          SUMYQ=SUMYQ+(YRAY(I)*YRAY(I))
          SUMXY=SUMXY+(XRAY(I) * YRAY(I))
5000  CONTINUE
C
      XMEAN=SUMX/XN
      YMEAN=SUMY/XN
      SSX=XN*SUMXQ-SUMX*SUMX
      SSY=XN*SUMYQ-SUMY*SUMY
      SP=XN * SUMXY - SUMX * SUMY
      B= SP / SSX
      A= YMEAN - B * XMEAN
      R= SP /SQRT(SSX * SSY)
      RSQ=R*R
      SESQ= (SSY - (SP * SP / SSX)) / (XN * (XN-2.))
      SB=SQRT(SESQ *XN / SSX)
      SA=SQRT(SESQ * (1./XN + SUMX * XMEAN / SSX))
      SY=SQRT(SESQ)
      IDF=N-1
      IEDF=N-2
C
      DO 6000 I=IMIN,IMAX
          SST=SST+(YRAY(I)-YMEAN)**2
          SSR=SSR+((A+B*XRAY(I)) -YMEAN)**2
6000  CONTINUE
C
      SSE=SST-SSR
      MST=SST/(XN-1.)
      MSR=SSR
      MSE=SSE/(XN-2.)
C
C        COMPUTATIONS COMPLETE - PRINT OUT RESULTS
C
      TYPE 105, A,SA,B,SB
C
C       ASK IF USER WANTS A SECOND RUN
C
      TYPE 106
      ACCEPT 104,IANS
      IF (IANS.EQ.'Y') GO TO 35
C
```

```
      PRINT 107, FILENM
      WRITE (4,108) FILENM
      WRITE (4,*) A,SA
      WRITE (4,*) B,SB
      J=0
      PRINT 109
C
      DO 7000 I=IMIN,IMAX
         J=J+1
         PRINT 110,J,XRAY(I),YRAY(I)
         WRITE (4,*) XRAY(I),YRAY(I)
7000  CONTINUE
C
      PRINT 111, A,SA,B,SB
C
      CLOSE(UNIT=4)
C
      TYPE 112
      ACCEPT 104,IANS
      IF (IANS.EQ.'Y') GO TO 5
      STOP
```

```
C
101     FORMAT (' ENTER THE DATA FILE NAME ',$)
102     FORMAT (4A4)
103     FORMAT (' ENTER OUTPUT FILE NAME ',$)
104     FORMAT(A1)
105     FORMAT ('0','REGRESSION LINE Y = A + B * X'/
        1'0',' A          =',F10.5/
        2' ','STD. ERROR OF A =',F10.5/
        3'0',' B          =',F10.5/
        4' ','STD. ERROR OF B =',F10.5)
106     FORMAT (' DO YOU WANT ANOTHER RUN? ',$)
107     FORMAT ('1',30X,4A4,//)
108     FORMAT (1X,4A4)
109     FORMAT ('0                I     X(I)          Y(I)',//)
C
110     FORMAT (10X,I7,2G15.7)
111     FORMAT ('0',10X,'REGRESSION LINE Y = A + B * X'/
        1'0',10X,' A          =',F10.5/
        2' ',10X,'STD. ERROR OF A =',F10.5/
        3'0',10X,' B          =',F10.5/
        4' ',10X,'STD. ERROR OF B =',F10.5)
112     FORMAT (' DO YOU WANT TO RUN ANOTHER DATA FILE? ',$)
C
        END
```

NRPLOT.FOR

```
C*************************************************************
C*                                                           *
C* NAME    = NRPLOT                                          *
C* PURPOSE = THIS PROGRAM TAKES THE OUTPUT FROM NRLINE       *
C*           AND PLOTS IT.                                   *
C*                                                           *
C* THOMAS F. LUNDEEN            OREGON STATE UNIVERSITY      *
C*************************************************************

      PROGRAM NRPLOT
C
      DIMENSION XRAY(20),YRAY(20),FILE(4)
      REAL*8 LB,NAME(3)
C
C     OPEN THE DATA FILE
C
      TYPE 101
      ACCEPT 102,FILE
C
      OPEN (UNIT=3,TYPE='OLD',NAME=FILE,READONLY)
C
C     READ OFF THE NAME OF THE MOLECULE
C
      READ (3,103) NAME
C
C     READ THE INTERCEPT, SLOPE, AND THEIR ERRORS
C
      READ (3,*) A,ERA
      READ (3,*) B,ERB
C
C     INPUT THE DATA
C
      ICNT=0
10    ICNT=ICNT+1
      READ (3,*,END=20) XRAY(ICNT),YRAY(ICNT)
      GO TO 10
C
C     CALCULATE THE RANGE
C
20    ICNT=ICNT-1
      XMAX=FLOAT(IFIX(XRAY(ICNT)*.1+XRAY(ICNT)))
      YMAX=FLOAT(IFIX(YRAY(ICNT)*.1+YRAY(ICNT)))
C
C     SET UP THE PLOTTER
C
      XFACT=7/XMAX
      YFACT=5/YMAX
C
      CALL SIZE(10.0,8.0)
      CALL SCALE(XFACT,YFACT,2.0,1.5,0.0,0.0)
```

```
      CALL VECTOR
C
C     DRAW THE AXIS
C
      CALL PLOT(0.0,YMAX,0,0)
      CALL PLOT(0.0,0.0,1,0)
      CALL PLOT(XMAX,0.0,1,0)
C
C     LABEL THE Y AXIS
C
      YTIC=FLOAT(IFIX(YMAX*0.20))
      XTIC=FLOAT(IFIX(XMAX*0.20))
      Y=0.0
      X=-.2/XFACT
      YP=-0.0625/YFACT
      XP=-.800/XFACT+X
C
      DO 2000 I=1,5
         Y=Y+YTIC
         YP=YP+YTIC
         CALL PLOT (X,Y,0,0)
         CALL PLOT (0.0,Y,1,0)
         ENCODE (6,104,LB) Y
         CALL SYMBOL (XP,YP,0.0,.1250,5,LB)
2000  CONTINUE
C
      LB='SIGNAL'
      XP=XP-.1250/XFACT
      YP=2.0/YFACT
      CALL SYMBOL (XP,YP,90.0,.250,6,LB)
C
C     LABEL THE X AXIS
C
      X=0.0
      Y=-.20/YFACT
      YP=-0.4/YFACT
      XP=-0.37/XFACT
C
      DO 3000 I=1,5
         X=X+XTIC
         XP=XP+XTIC
         CALL PLOT (X,Y,0,0)
         CALL PLOT (X,0.0,1,0)
         ENCODE (6,104,LB) X
         CALL SYMBOL (XP,YP,0.0,.1250,5,LB)
3000  CONTINUE
C
      LB='PRESSURE'
      YP=-1.0/YFACT
      XP=3.0/XFACT
```

```
C
      CALL SYMBOL (XP,YP,0.0,.250,8,LB)
C
      LB='2'
      YP=-0.85/YFACT
      XP=XP+2.125/XFACT
      CALL SYMBOL (XP,YP,0.0,.250,1,LB)
C
C     QUERY FOR MARK TO BE USED
C
      TYPE 105
      ACCEPT *,MARK
C
C     POINT PLOT THE DATA
C
      CALL POINTS
C
      DO 1000 I=1,ICNT
         CALL PLOT (XRAY(I),YRAY(I),1,MARK)
1000  CONTINUE
C
C     DRAW A VECTOR FOR CALCULATED FIT
C
      CALL VECTOR
      CALL PLOT (0.0,A,0,0)
      Y=B*XRAY(ICNT)+A
      CALL PLOT (XRAY(ICNT),Y,1,0)
C
C     LABEL THE PLOT
C
      YP=3.5/YFACT
      XP=1.250/XFACT
      CALL SYMBOL (XP,YP,0.0,.125,24,NAME)
C
      XP=1.5/XFACT
      YP=3.250/YFACT
      LB='SLOPE = '
C
      CALL SYMBOL (XP,YP,0.0,0.125,8,LB)
C
      XP=2.5/XFACT
      ENCODE(6,106,LB)B
      CALL SYMBOL (XP,YP,0.0,0.125,6,LB)
C
      XP=1.5/XFACT
      YP=3.0/YFACT
      LB='ERROR ='
      CALL SYMBOL (XP,YP,0.0,0.125,8,LB)
C
      XP=2.5/XFACT
```

```
      ENCODE(6,106,LB) ERB
      CALL SYMBOL (XP,YP,0.0,0.125,6,LB)
C
C     STOP PLOTTING
C
      CALL PLOTEN
C
      CLOSE(UNIT=3)
      STOP
```

```
C
101     FORMAT (' ENTER THE DATA FILE NAME ',$)
102     FORMAT (4A4)
103     FORMAT(3A8)
104     FORMAT(F6.0)
105     FORMAT (' WHAT MARK DO YOU WANT?',$)
106     FORMAT(F6.3)
C
        END
```

Appendix B

Hydrogen Relaxation Programs

This appendix contains two sample programs used to simulate para hydrogen relaxation in a free jet expasion. The first, RH2791.FOR, calculates the rotational temperature of para hydrogen in a free jet using the cross sections from the M79 potential in the partial state-to-state model and the beam expansion model of Anderson. The second program, RH2BUF, calculates the rotational temperature of para H_2 in an expansion mixture with a noble gas using the fluid mechanical description of the beam expansion. This program requires an input file consisting of expansion coefficients for each of the cross sections

$$_{ij\ lm} = A + BE_T + CE_T^2 + DE_T^3$$

followed by the initial rotational energy of the collision pair and the threshold energy of the process in Ev. A sample input file (H2HE.INP) is given for a mixture of H_2 and He using the Rabitz - Zarur cross sections for H_2--- H_2 collisions and the Roberts cross sections for the H_2 --- He collisions.

RH2791.FOR

```
C*************************************************
C*                                               *
C* Name    = RH2791                              *
C* Purpose = To calculate the rotational temper- *
C*           ature of H2 in a molecular beam     *
C*           using Anderson's model for the      *
C*           beam expansion and partial state-   *
C*           to-state model of the H2 relaxation *
C*           for the M79 potential.              *
C*                                               *
C*   Tom Lundeen              Version #4         *
C*  Oregon State University    8-19-83           *
C*                                               *
C*************************************************

        PROGRAM RH2791
C
C       SET UP THE ARRAYS USED
C
        REAL MC,K1,K2,K3,K4,MA
        LOGICAL*1 BELL
C
        DIMENSION FACTOR(3),GAMMA(2)
        1, A(2),C(2),X0(2),FILENM(4)
        2, P2TI(3)
C
        PI = 3.1416
        BELL=007
C
C       LOAD THE DATA FOR BOTH GAMMA = 1.40 AND GAMMA = 1.67
C
        DATA GAMMA /1.6667,1.40/
        DATA A     /3.26,3.65/
        DATA C     /0.31,0.20/
        DATA X0    /0.075,0.40/
C
C       OPEN THE OUTPUT FILE
C
        TYPE 101
        ACCEPT 102, FILENM
C
        OPEN (UNIT=3,NAME=FILENM,TYPE='NEW',INITIALSIZE=15)
C
C       DETERMINE WHICH SET OF DATA IS TO BE USED
C
        TYPE 103
        ACCEPT *, ID
C
C       READ IN THE MAXIUM X (XMAX)
C
```

```
      TYPE 104
      ACCEPT *, XMAX
C
C     READ IN THE MINIMUM X (XMIN)
C
      TYPE 105
      ACCEPT *, XMIN
C
C     READ IN THE DELTA X (DELTAX)
C
      TYPE 106
      ACCEPT *, DELTAX
C
C     READ IN THE STARTING TEMPERATURE (T0)
C
      TYPE 107
      ACCEPT *, T0
C
C     READ IN THE STARTING PRESSURE (PRES)
C
      TYPE 108
      ACCEPT *, PRES
C
C     READ IN THE NOZZLE DIAMETER (D)
C
      TYPE 109
      ACCEPT *, D
C
C     READ IN THE CONNECTION POINT BETWEEN
C     THE TWO MACH NUMBER EQUATIONS (XC)
C
      TYPE 110
      ACCEPT *, XC
C
C
C     QUERY FOR IF THE USER WANTS A 2 TERM PLOT OR
C     A ONE TERM PLOT
C
      TYPE 111
      ACCEPT *, IFLAG
C
C     IF A TWO TERM SET C = 0
C
      IF (IFLAG.EQ.2) C(ID) = 0.0
C
C     CALCULATE VALUES USED IN THE MACH NUMBER
C     EQUATIONS
C
      G1 = GAMMA(ID) - 1.0
      G2 = -G1
```

```
      G3 = -3.0*G1
C
      B = 0.5*(1.0/A(ID))*((GAMMA(ID)+1.0)/G1)
C
      MC = A(ID)*(XC-X0(ID))**G1 - B*(XC-X0(ID))**G2
     1    + C(ID)*(XC-X0(ID))**G3
C
      DMA = G1*A(ID)*(XC-X0(ID))**(G1-1.0)
     1    - G2*B*(XC-X0(ID))**(G2-1.0)
     2    + G3*C(ID)*(XC-X0(ID))**(G3-1.0)
C
      DMA = DMA/MC
C
C     CONVERT THE NOZZLE DIAMETER FROM MICRONS
C     TO CM
C
      D = D * 1.0E-4
C
C     CALCULATE THE STARTING NUMBER DENSITY IN
C     MOLECULES/CM3
C
C     N/V = P/R*T
C     9.65E18 = 1/R IN UNITS OF CM3*TORR/MOLECULE*K
C
      P0= (PRES * 9.65E18)/T0
C
C     SAVE THE POINTS EVERY 0.1 NOZZLE DIAMETERS
C
      ISAVE=IFIX(0.1/DELTAX)
C
      ICNT = 0
C
      TROT = T0
      X = XMIN
C
      MA = MC*EXP(DMA*(X - XC))
C
C     ISOCENTRIC TEMPERATURE (TI)
C
      TI = T0/(1.0 + 0.5*G1*MA*MA)
C
C     NUMBER DENSITY (P)
C
      P = P0*(TI/T0)**(1.0/G1)
C
C     BEAM VELOCITY (VEL)
C
      VEL = MA * SQRT (GAMMA(ID)*8.3143E07*TI/2.016)
C
C     CALCULATE SIGMA
```

```
C
      SIGMA = 5.254E-18 - 0.1755E-19*TI + 0.1875E-21*TI*TI
C
C     CALCULATE THE INITIAL PROBABILITY OF BEING IN THE
C     SECOND ROTATIONAL STATE AT TEMP. TO (P2T)
C
      P2T = 1.0/(0.2*EXP(509.74/T0) + 1.0)
C
C     CALCULATE THE INITIAL PROBABILITY OF BEING IN THE
C     SECOND ROTATIONAL STATE IF THE SYSTEM WAS AT
C     EQUALIBRIUM AT A TEMPERATURE TI (P2TI)
C

      P2TI(1) = 1.0/(0.2*EXP(509.74/TI) + 1.0)
C
C     FACTOR = (D*P/VEL)*SQRT(8*R*TI/PI*M)*SIGMA
C
      FACTOR(1) = (D*P/VEL)*SQRT(2.117E08*TI)*SIGMA
C
C     OUPUT THE INITIAL CONDITIONS
C
      TYPE *,' '
      TYPE *,' '
      TYPE 205, FILENM
      TYPE *,' '
      TYPE 201
      TYPE 202, X,P2T,TROT,TI
C
      WRITE (3,205) FILENM
      WRITE (3,*) GAMMA(ID)
      WRITE (3,*) PRES
      WRITE (3,*) IFLAG
      WRITE (3,202) X,P2T,TROT,TI
C
C     START THE CALCULATION
C
30    DO 1000 J = 2,3
C
      I=J
C
C     CALCULATE THE BEAM CONDITIONS AT X+1/2 DELTAX
C     AND AT X + DELTAX
C
      X = X + 0.5*DELTAX
C
C     MACH NUMBER
C
      IF (X.LT.XC)    MA = MC*EXP(DMA*(X - XC))
      IF (X.GE.XC)    MA = A(ID)*(X-X0(ID))**G1
     1    - B*(X-X0(ID))**G2
```

```
     2    + C(ID)*(X-X0(ID))**G3
C
C       ISOCENTRIC TEMPERATURE (TI)
C
        TI = T0/(1.0 + 0.5*G1*MA*MA)
C
C       NUMBER DENSITY (P)
C
        P  = P0*(TI/T0)**(1.0/G1)
C
C       BEAM VELOCITY (VEL)
C
        VEL = MA * SQRT (GAMMA(ID)*8.3143E07*TI/2.016)
C
C       CALCULATE THE PROBILITY OF BEING IN THE SECOND
C       ROTATIONAL STATE IF THE SYSTEM WAS AT EQUALIBRIUM
C       AT A TEMPERATURE TI (P2TI)
C
        P2TI(I) = 1.0/(0.2*EXP(509.74/TI) + 1.0)
C
C       CALCULATE SIGMA
C
        IF (TI.GT.60) SIGMA = 5.254E-18 - 0.1755E-19*TI
     1                          + 0.1875E-21*TI*TI
        IF (TI.LE.60) SIGMA = -1.069E-18 + 0.5995E-16*
     1                       (1.0/TI)**0.7238 + 0.4781E-19
     2                       *(TI)
C
C       FACTOR = (D*P/VEL)*(8*R*TI/(PI*M)*SIGMA
C
        FACTOR(I) = (D*P/VEL)*SQRT(2.117E08*TI)*SIGMA
C
1000    CONTINUE
C
C       CALCULATE THE ROTATIONAL TEMPERATURE AT
C       THE NEW X POSITION USING A FOURTH ORDER
C       RUNGE KUTTA METHOD
C
C       K1 = F(X,Y)        F(X,Y)=DY/DX
C
        P2  = P2T
C
        K1 = FACTOR(1)*(P2TI(1)-P2)
C
C       K2 = F(X+1/2DELTAX,Y+1/2*DELTAX*K1)
C
        P2 = P2T + 0.5*DELTAX*K1
C
        K2 = FACTOR(2)*(P2TI(2)-P2)
C
```

```
C       K3 = F(X+1/2DELTAX,Y+1/2*DELTAX*K2)
C
        P2 = P2T + 0.5*DELTAX*K2
C
        K3 = FACTOR(2)*(P2TI(2)-P2)
C
C       K4 = F(X+DELTAX,Y+DELTAX*K3)
C
        P2 = P2T + DELTAX*K3
C
        K4 = FACTOR(3)*(P2TI(3)-P2)
C
C       Y(I+1)=Y(I) + DELTAX/6*(K1 + 2K2 + 2K3 + K4)
C
        P2T = P2T + (DELTAX/6.0)*(K1 + 2.0*K2 + 2.0*K3 + K4)
C
C       SET THE STARTING CONDITIONS FOR THE NEXT CALCULATION
C
        FACTOR(1) = FACTOR(3)
        P2TI(1)   = P2TI(3)
C
C       CHECK IN SEE IF WE OUTPUT THIS POINT
C
        ICNT=ICNT+1
        IF (ICNT.NE.ISAVE) GO TO 40
C
        ICNT = 0
C
        TROT = 509.74/(ALOG(5.0*(1.0/P2T - 1.0)))
C
C       OUTPUT THE NEW CONDITIONS
C
        TYPE 202,X,P2T,TROT,TI
        WRITE (3,202) X,P2T,TROT,TI
C
C       CHECK FOR THE END OF CALCULATION
C
40      IF(X.LT.XMAX) GO TO 30
C
        CLOSE(UNIT=3)
        STOP
```

```
C
101     FORMAT (' ENTER IN THE NAME OF THE OUTPUT FILE'
        1,T50,'-> ',$)
102     FORMAT (4A4)
103     FORMAT (' ENTER IN 1 FOR GAMMA=1.67 AND 2 FOR GAMMA ='
        1,'1.40',T50,'-> ',$)
104     FORMAT (' ENTER IN THE MAXIUM X IN X/D UNITS',T50,'-> ',$)
105     FORMAT (' ENTER IN THE MINIMUM X IN X/D UNITS',T50,'-> ',$)
106     FORMAT (' ENTER IN DELTA X IN X/D UNITS',T50,'-> ',$)
107     FORMAT (' ENTER IN THE STARTING TEMPERATURE',T50,'-> ',$)
108     FORMAT (' ENTER IN THE STARTING PRESSURE',T50,'-> ',$)
109     FORMAT (' ENTER IN THE NOZZLE DIAMETER IN MICRONS'
        1,T50,'-> ',$)
C
110     FORMAT (' ENTER IN THE CONNECTING POINT',T50,'-> ',$)
111     FORMAT (' ENTER 2 IF YOU WANT A TWO TERM EXPANSION'
        1,T50,'-> ',$)
C
201     FORMAT ('     X/D',9X,' P2 ',11X,'TROT',10X,'TI',/)
202     FORMAT (3X,F6.2,5X,F11.7,2(5X,F7.2))
205     FORMAT (1X,4A4)
C
        END
```

RH2BUFF.FOR

```
C*****************************************************
C*                                                   *
C* Name    = RH2BUF                                  *
C* Purpose = To calculate the rotational temper-     *
C*           ature of H2 in a moleculare beam        *
C*           comprized of H2 and a monoatomic        *
C*           buffer gas.                             *
C*                                                   *
C*   Tom Lundeen              Version #1             *
C*   Oregon State University   19-NOV-83             *
C*                                                   *
C*****************************************************

      PROGRAM RH2BUF
C
C     SET UP THE ARRAYS USED
C
      REAL MC,MA,K,KT,MH2,MBUF,MASS
C
      DIMENSION FACTOR(3),FILENM(4)
     2, AR(4),AR1(4,4),DE(4)
     3, DP2(4), DT(4),DV(4)
C
C
C     DEFINE CONSTANTS
C
C     K    =  BOLTZMANN'S CONSTANT
C     UH2  =  REDUCED MASS OF H2 -- H2 COLLISION
C     MH2  =  WEIGHTED MASS OF H2 AND HE FOR A 1:2 RATIO
C     E2   =  ENERGY OF THE SECOND ROTATIONAL LEVEL
C     AN   =  AVOGADRO'S CONSTANT
C     R    =  RYDBERG'C CONSTANT
C
      K    = 1.38066E-16
      UH2  = 1.008/6.0222E23
      MH2  = 2.016
      PI   = 3.14159
      E2   = 7.0444E-14
      AN   = 6.0222E23
      R    = 8.3143E07
C
C     IN THE TEMPERATURE RANGE WE ARE CONSIDERING
C     WE CAN ASSUME THAT BOTH H2 AND THE BUFFER
C     GAS HAVE A GAMMA OF 1.6667
C
C     DEFINE THE CONSTANTS USED IN THE MACH NUMBER
C     EXPRESSION
C
      GAMMA  = 1.6667
      A      = 3.26
```

```
      C      = 0.31
      X0     = 0.075
      XC     = 1.0
C
C     READ IN THE COEFFICIENT FILE NAME
C
      TYPE 101
      ACCEPT 102, FILENM
C
      OPEN (UNIT=3,NAME=FILENM,TYPE='OLD')
C
C     READ IN THE VALUES OF THE POLYNOMIAL FIT TO
C     SIGMA
C
      DO 7000 I=1,4
C
      J=I
C
C     READ IN THE COEFFICIENTS
C
      READ (3,*) (AR(L),L=1,4)
C
C     CONVERT THEM TO CGS UNITS
C
      AR(1) = AR(1)*1.0E-16
      AR(2) = AR(2)*1.0E-16/1.6021E-12
      AR(3) = AR(3)*1.0E-16/(1.6021E-12**2)
      AR(4) = AR(4)*1.0E-16/(1.6021E-12**3)
C
C     READ IN DELTA E AND E0
C
      READ (3,*) DE(J),E0
C
C     CONVERT THE ENERGIES FROM UNITS OF EV TO ERG
C
      DE(J) = DE(J)*1.6021E-12
      E0    = E0*1.6021E-12
C
      E0 = DE(J) + E0
C
C     CALCULATE THE COEFFICIENTS USED IN THE CALCULATION
C
      AR1(J,1) = AR(1) + AR(2)*E0 + AR(3)*E0**2 + AR(4)*E0**3
      AR1(J,2) = AR(2) + 2.0*AR(3)*E0 + 3.0*AR(4)*E0*E0
      AR1(J,3) = AR(3) + 3.0*AR(4)*E0
      AR1(J,4) = AR(4)
C
7000  CONTINUE
C
C     CLOSE THE INPUT FILE
```

```
C
      CLOSE (UNIT=3)
C
C     OPEN THE OUTPUT FILE
C
      TYPE 103
      ACCEPT 102,FILENM
C
      OPEN (UNIT=3,NAME=FILENM,TYPE='NEW',INITIALSIZE=15)
C
C     READ IN THE MAXIMUM X (XMAX) IN X/D UNITS
C
      TYPE 104
      ACCEPT *, XMAX
C
C     READ IN THE MINIMUM X (XMIN) IN X/D UNITS
C
      TYPE 105
      ACCEPT *, XMIN
C
C     READ IN THE DELTA X (DELTAX) IN X/D UNITS
C
      TYPE 106
      ACCEPT *, DELTAX
C
C     READ IN THE STARTING TEMPERATURE (T0)
C
      TYPE 107
      ACCEPT *, T0
C
C     READ IN THE STARTING PRESSURE (PRES)
C
      TYPE 108
      ACCEPT *, PRES
C
C     READ IN THE M.W./MOLE OF THE DRIVING GAS (MBUF)
C
      TYPE 109
      ACCEPT *,MBUF
C
C     READ IN THE FRACTION OF DRIVING GAS (FRACB)
C
      TYPE 110
      ACCEPT *, FRACB
C
C     THE PROBABILITY OF BEING A BUFFER MOLECULE (PB)
C     IS EQUAL TO FRACTION OF BUFFER MOLECULES
C
      PB = FRACB
C
```

```
C       CALCULATE THE FRACTION H2
C
        FRACH = 1.0 - FRACB
C
C       READ IN THE NOZZLE DIAMETER (D)
C
        TYPE 111
        ACCEPT *, D
C
C       READ IN THE CONNECTION POINT BETWEEN
C       THE TWO MACH NUMBER EQUATIONS (XC)
C
        TYPE 112
        ACCEPT *,XC
C
C
C       SEE IF THE USER WANTS A 2 TERM OR
C       A THREE TERM EXPANSION
C
        TYPE 113
        ACCEPT *,IFLAG
C
C       IF A TWO TERM SET C = 0
C
        IF (IFLAG.EQ.2) C = 0.0
C
C       CALCULATE VALUES USED IN THE MACH NUMBER
C       EQUATIONS
C
        G1 = GAMMA - 1.0
        G2 = -G1
        G3 = -3.0*G1
C
C       CALC. THE SECOND TERM IN THE MACH NUMBER
C       EXPANSION
C
        B = 0.5*(1.0/A)*((GAMMA+1.0)/G1)
C
C       CALC. THE CONSTANTS FOR MACH NUMBER EXPRESSION
C       BELOW THE CONNECTION POINT
C
C       THE MACH NUMBER AT THE CONNECTION PONT (MC)
C
        MC = A*(XC-X0)**G1 - B*(XC-X0)**G2
        1     + C*(XC-X0)**G3
C
C       CALC. THE DERIVATIVE OF THE MACH NUMBER AT
C       THE CONNECTION POINT DIVIDED BY THE MACH
C       NUMBER AT THAT POINT. (DMA)
C
```

```
      DMA = G1*A*(XC-X0)**(G1-1.0)
     1      - G2*B*(XC-X0)**(G2-1.0)
     2      + G3*C*(XC-X0)**(G3-1.0)
C
      DMA = DMA/MC
C
C     CONVERT THE NOZZLE DIAMETER FROM MICRONS
C     TO CM
C
      D = D * 1.0E-4
C
C     CALCULATE THE WIEGHTED MASS (MASS)
C
      MASS = FRACB*MBUF + FRACH*MH2
C
C     CALCULATE THE REDUCED MASS OF THE
C     COLLISION H2 -- BUFF (UB)
C
      UB = MH2*MBUF/((MH2 + MBUF)*AN)
C
C     CALCULATE THE STARTING NUMBER DENSITY IN
C     MOLECULES/CM3
C
C     N/V = P/(R*T)
C     9.65E18 = 1/R  WITH R IN UNITS OF
C     CM3*TORR/MOLECULE*K
C
      D0 = (PRES * 9.65E18)/T0
C
C     SAVE THE POINTS EVERY 0.1 NOZZLE DIAMETERS
C
      ISAVE=IFIX(0.1/DELTAX)
C
      ICNT = 0
C
      TROT = T0
      X = XMIN
C
      MA = MC*EXP(DMA*(X - XC))
C
C     ISENTROPIC TEMPERATURE (TI)
C
      TI = T0
C
C     BEAM VELOCITY (VI)
C     ASSUME ANDERSON'S EQUATIONS ARE VALID FOR
C     THE INITIAL CONDITIONS
C
      VI = MA * SQRT (GAMMA*R*TI/MASS)
C
```

```
C       NUMBER DENSITY (DI)
C
        DI = DO*(1.0 + 0.5*G1*MA*MA)**(1.0/G2)
C
C       CALCULATE THE DERIVATIVE OF THE NUMBER
C       DENSITY AT X
C
        DD = - MA*DO*(1.0 + 0.5*G1*MA*MA)**(1.0/G2 - 1.0)
        1     *DMA*MC*EXP(DMA*(X-XC))
C
C       CALCULATE THE INITIAL NUMBER DENSITY IN THE 2ND
C       ROTATIONAL STATE (P2I)
C
        P2I = FRACH/(0.2*EXP(509.74/TO) + 1.0)
C
C       OUTPUT THE INITIAL CONDITIONS
C
        TYPE *,' '
        TYPE *,' '
        TYPE 205, FILENM
        TYPE *,' '
        TYPE 201
        TYPE 202, X,P2I,TROT,TI
C
        WRITE (3,205) FILENM
        WRITE (3,*) GAMMA
        WRITE (3,*) PRES
        WRITE (3,*) IFLAG
        WRITE (3,202) X,P2I,TROT,TI
C
C       START THE CALCULATION
C
C       FIRST APPROXIMATION
C
30      KT = K*TI
C
C       CALCULATE R1 K 00 -> 02
C
        C1 = EXP(-DE(1)/KT)*SQRT(8.0/(PI*UH2))
C
        R1 = C1*((KT)**(-0.5)*AR1(1,1)*DE(1)
        1     + (KT)**(0.5)*(AR1(1,1) + AR1(1,2)*DE(1))
        2     + (KT)**(1.5)*2.0*(AR1(1,2) + AR1(1,3)*DE(1))
        3     + (KT)**(2.5)*6.0*(AR1(1,3) + AR1(1,4)*DE(1))
        4     + (KT)**(3.5)*24.0*AR1(1,4))
C
C       CALCULATE R2 K 00 -> 22
C
        C1 = EXP(-DE(2)/KT)*SQRT(8.0/(PI*UH2))
C
```

```
      R2 = C1*((KT)**(-0.5)*AR1(2,1)*DE(2)
     1    + (KT)**(0.5)*(AR1(2,1) + AR1(2,2)*DE(2))
     2    + (KT)**(1.5)*2.0*(AR1(2,2) + AR1(2,3)*DE(2))
     3    + (KT)**(2.5)*6.0*(AR1(2,3) + AR1(2,4)*DE(2))
     4    + (KT)**(3.5)*24.0*AR1(2,4))
C
C     CALCULATE R3 K 02 -> 22
C
      C1 = EXP(-DE(3)/KT)*SQRT(8.0/(PI*UH2))
C
      R3 = C1*((KT)**(-0.5)*AR1(3,1)*DE(3)
     1    + (KT)**(0.5)*(AR1(3,1) + AR1(3,2)*DE(3))
     2    + (KT)**(1.5)*2.0*(AR1(3,2) + AR1(3,3)*DE(3))
     3    + (KT)**(2.5)*6.0*(AR1(3,3) + AR1(3,4)*DE(3))
     4    + (KT)**(3.5)*24.0*AR1(3,4))
C
C     CALCULATE R4 K 0 -> 2 FOR H2 TO BUFFER
C
      C1 = EXP(-DE(4)/KT)*SQRT(8.0/(PI*UB))
C
      R4 = C1*((KT)**(-0.5)*AR1(4,1)*DE(4)
     1    + (KT)**(0.5)*(AR1(4,1) + AR1(4,2)*DE(4))
     2    + (KT)**(1.5)*2.0*(AR1(4,2) + AR1(4,3)*DE(4))
     3    + (KT)**(2.5)*6.0*(AR1(4,3) + AR1(4,4)*DE(4))
     4    + (KT)**(3.5)*24.0*AR1(4,4))
C
      TEXP = 0.20*EXP(509.74/TI)
C
      P2 = P2I
      P0 = FRACH - P2I
C
C     CALCULATE THE RATE OF CHANGE IN P2
C     (DP2)
C
      D1 = P0*P0 - P0*P2*TEXP
      D2 = P0*P0 - P2*P2*TEXP*TEXP
      D3 = P2*P0 - P2*P2*TEXP
      D4 = P0*PB - P2*PB*TEXP
C
      DP2(1) = (D*DI/VI)*(D1*R1 + 2.0*D2*R2 + D3*R3
     1          + D4*R4)
C
C     CALCULATE THE DERIVATIVE OF THE TEMPERATURE
C     AT X (DT)
C
      DT(1) = 0.6667*TI*(DD/DI - E2*DP2(1)/KT)
C
C     CALCULATE THE DERIVATIVE OF THE VELOCITY AT
C     X (DV)
C
```

```
      DV(1) = -(AN/(V1*MASS))*(2.5*K*DT(1) + E2*DP2(1))
C
C     CALCULATE THE FIRST APPROXIMATE POSITION
C
      P2 = P21 + 0.5*DELTAX*DP2(1)
      T  = T1  + 0.5*DELTAX*DT(1)
      V  = V1  + 0.5*DELTAX*DV(1)
C
C     SECOND APPROXIMATION
C
      X = X + 0.5*DELTAX
C
C     MACH NUMBER
C
      IF (X.LT.XC)    MA = MC*EXP(DMA*(X - XC))
      IF (X.GE.XC)    MA = A*(X-X0)**G1
     1    - B*(X-X0)**G2
     2    + C*(X-X0)**G3
C
C     NUMBER DENSITY (D1)
C
      D1 = D0*(1.0 + 0.5*G1*MA*MA)**(1.0/G2)
C
C     CALCULATE THE DERIVATIVE OF THE MACH NUMBER
C     AT X (DMAX)
C
      IF (X.LT.XC) DMAX = DMA*MC*EXP(DMA*(X-XC))
C
      IF (X.GE.XC) DMAX  = G1*A*(X-X0)**(G1-1.0)
     1     - G2*B*(X-X0)**(G2-1.0)
     2     + G3*C*(X-X0)**(G3-1.0)
C
C     CALCULATE THE DERIVATIVE OF THE NUMBER
C     DENSITY AT X
C
      DD = - MA*D0*(1.0 + 0.5*G1*MA*MA)**(1.0/G2 - 1.0)
     1    *DMAX
C
      KT = K*T
C
C     CALCULATE R1 K 00 -> 02
C
      C1 = EXP(-DE(1)/KT)*SQRT(8.0/(PI*UH2))
C
      R1 = C1*((KT)**(-0.5)*AR1(1,1)*DE(1)
     1    + (KT)**(0.5)*(AR1(1,1) + AR1(1,2)*DE(1))
     2    + (KT)**(1.5)*2.0*(AR1(1,2) + AR1(1,3)*DE(1))
     3    + (KT)**(2.5)*6.0*(AR1(1,3) + AR1(1,4)*DE(1))
     4    + (KT)**(3.5)*24.0*AR1(1,4))
C
```

```
C       CALCULATE R2 K 00 -> 22
C
        C1 = EXP(-DE(2)/KT)*SQRT(8.0/(PI*UH2))
C
        R2 = C1*((KT)**(-0.5)*AR1(2,1)*DE(2)
        1    + (KT)**(0.5)*(AR1(2,1) + AR1(2,2)*DE(2))
        2    + (KT)**(1.5)*2.0*(AR1(2,2) + AR1(2,3)*DE(2))
        3    + (KT)**(2.5)*6.0*(AR1(2,3) + AR1(2,4)*DE(2))
        4    + (KT)**(3.5)*24.0*AR1(2,4))
C
C       CALCULATE R3 K 02 -> 22
C
        C1 = EXP(-DE(3)/KT)*SQRT(8.0/(PI*UH2))
C
        R3 = C1*((KT)**(-0.5)*AR1(3,1)*DE(3)
        1    + (KT)**(0.5)*(AR1(3,1) + AR1(3,2)*DE(3))
        2    + (KT)**(1.5)*2.0*(AR1(3,2) + AR1(3,3)*DE(3))
        3    + (KT)**(2.5)*6.0*(AR1(3,3) + AR1(3,4)*DE(3))
        4    + (KT)**(3.5)*24.0*AR1(3,4))
C
C       CALCULATE R4 K 0 -) 2 FOR H2 TO BUFFER
C
        C1 = EXP(-DE(4)/KT)*SQRT(8.0/(PI*UB))
C
        R4 = C1*((KT)**(-0.5)*AR1(4,1)*DE(4)
        1    + (KT)**(0.5)*(AR1(4,1) + AR1(4,2)*DE(4))
        2    + (KT)**(1.5)*2.0*(AR1(4,2) + AR1(4,3)*DE(4))
        3    + (KT)**(2.5)*6.0*(AR1(4,3) + AR1(4,4)*DE(4))
        4    + (KT)**(3.5)*24.0*AR1(4,4))
C
        TEXP = 0.20*EXP(509.74/T)
C
        P0 = FRACH - P2
C
C       CALCULATE THE RATE OF CHANGE IN P2
C       (DP2)
C
        D1 = P0*P0 - P0*P2*TEXP
        D2 = P0*P0 - P2*P2*TEXP*TEXP
        D3 = P2*P0 - P2*P2*TEXP
        D4 = P0*PB - P2*PB*TEXP
C
        DP2(2) = (D*D1/V)*(D1*R1 + 2.0*D2*R2 + D3*R3
        1          + D4*R4)
C
C       CALCULATE THE DERIVATIVE OF THE TEMPERATURE
C       AT X (DT)
C
        DT(2) = 0.6667*T*(DD/D1 - E2*DP2(2)/KT)
C
```

```
C       CALCULATE THE DERIVATIVE OF THE VELOCITY AT
C       X (DV)
C
        DV(2) = -(AN/(V*MASS))*(2.5*K*DT(2) + E2*DP2(2))
C
C       CALCULATE THE SECOND APPROXIMATE POSITION
C
        P2 = P2I + 0.5*DELTAX*DP2(2)
        T  = TI  + 0.5*DELTAX*DT(2)
        V  = VI  + 0.5*DELTAX*DV(2)
C
C       THIRD APPROXIMATION
C
        KT = K*T
C
C       CALCULATE R1 K 00 -> 02
C
        C1 = EXP(-DE(1)/KT)*SQRT(8.0/(PI*UH2))
C
        R1 = C1*((KT)**(-0.5)*AR1(1,1)*DE(1)
     1     + (KT)**(0.5)*(AR1(1,1) + AR1(1,2)*DE(1))
     2     + (KT)**(1.5)*2.0*(AR1(1,2) + AR1(1,3)*DE(1))
     3     + (KT)**(2.5)*6.0*(AR1(1,3) + AR1(1,4)*DE(1))
     4     + (KT)**(3.5)*24.0*AR1(1,4))
C
C       CALCULATE R2 K 00 -> 22
C
        C1 = EXP(-DE(2)/KT)*SQRT(8.0/(PI*UH2))
C
        R2 = C1*((KT)**(-0.5)*AR1(2,1)*DE(2)
     1     + (KT)**(0.5)*(AR1(2,1) + AR1(2,2)*DE(2))
     2     + (KT)**(1.5)*2.0*(AR1(2,2) + AR1(2,3)*DE(2))
     3     + (KT)**(2.5)*6.0*(AR1(2,3) + AR1(2,4)*DE(2))
     4     + (KT)**(3.5)*24.0*AR1(2,4))
C
C       CALCULATE R3 K 02 -> 22
C
        C1 = EXP(-DE(3)/KT)*SQRT(8.0/(PI*UH2))
C
        R3 = C1*((KT)**(-0.5)*AR1(3,1)*DE(3)
     1     + (KT)**(0.5)*(AR1(3,1) + AR1(3,2)*DE(3))
     2     + (KT)**(1.5)*2.0*(AR1(3,2) + AR1(3,3)*DE(3))
     3     + (KT)**(2.5)*6.0*(AR1(3,3) + AR1(3,4)*DE(3))
     4     + (KT)**(3.5)*24.0*AR1(3,4))
C
C       CALCULATE R4 K 0 -> 2 FOR H2 TO BUFFER
C
        C1 = EXP(-DE(4)/KT)*SQRT(8.0/(PI*UB))
C
        R4 = C1*((KT)**(-0.5)*AR1(4,1)*DE(4)
```

```
     1    + (KT)**(0.5)*(AR1(4,1) + AR1(4,2)*DE(4))
     2    + (KT)**(1.5)*2.0*(AR1(4,2) + AR1(4,3)*DE(4))
     3    + (KT)**(2.5)*6.0*(AR1(4,3) + AR1(4,4)*DE(4))
     4    + (KT)**(3.5)*24.0*AR1(4,4))
C
      TEXP = 0.20*EXP(509.74/T)
C
      P0 = FRACH - P2
C
C     CALCULATE THE RATE OF CHANGE IN P2
C     (DP2)
C
      D1 = P0*P0 - P0*P2*TEXP
      D2 = P0*P0 - P2*P2*TEXP*TEXP
      D3 = P2*P0 - P2*P2*TEXP
      D4 = P0*PB - P2*PB*TEXP
C
      DP2(3) = (D*D1/V)*(D1*R1 + 2.0*D2*R2 + D3*R3
     1         + D4*R4)
C
C     CALCULATE THE DERIVATIVE OF THE TEMPERATURE
C     AT X (DT)
C
      DT(3) = 0.6667*T*(DD/D1 - E2*DP2(3)/KT)
C
C     CALCULATE THE DERIVATIVE OF THE VELOCITY AT
C     X (DV)
C
      DV(3) = -(AN/(V*MASS))*(2.5*K*DT(3) + E2*DP2(3))
C
C     CALCULATE THE THIRD APPROXIMATE POSITION
C
      P2 = P2I + 0.5*DELTAX*DP2(3)
      T  = TI  + 0.5*DELTAX*DT(3)
      V  = VI  + 0.5*DELTAX*DV(3)
C
C     FORTH APPROXIMATION
C
      X = X + 0.5*DELTAX
C
C     MACH NUMBER
C
      IF (X.LT.XC)    MA = MC*EXP(DMA*(X - XC))
      IF (X.GE.XC)    MA = A*(X-X0)**G1
     1    - B*(X-X0)**G2
     2    + C*(X-X0)**G3
C
C     NUMBER DENSITY (D1)
C
      D1 = D0*(1.0 + 0.5*G1*MA*MA)**(1.0/G2)
```

```
C
C       CALCULATE THE DERIVATIVE OF THE MACH NUMBER
C       AT X (DMAX)
C
        IF (X.LT.XC) DMAX = DMA*MC*EXP(DMA*(X-XC))
C
        IF (X.GE.XC) DMAX = G1*A*(X-X0)**(G1-1.0)
        1      - G2*B*(X-X0)**(G2-1.0)
        2      + G3*C*(X-X0)**(G3-1.0)
C
C       CALCULATE THE DERIVATIVE OF THE NUMBER
C       DENSITY AT X
C
        DD = - MA*D0*(1.0 + 0.5*G1*MA*MA)**(1.0/G2 - 1.0)
        1    *DMAX
C
        KT = K*T
C
C       CALCULATE R1 K 00 -> 02
C
        C1 = EXP(-DE(1)/KT)*SQRT(8.0/(PI*UH2))
C
        R1 = C1*((KT)**(-0.5)*AR1(1,1)*DE(1)
        1    + (KT)**(0.5)*(AR1(1,1) + AR1(1,2)*DE(1))
        2    + (KT)**(1.5)*2.0*(AR1(1,2) + AR1(1,3)*DE(1))
        3    + (KT)**(2.5)*6.0*(AR1(1,3) + AR1(1,4)*DE(1))
        4    + (KT)**(3.5)*24.0*AR1(1,4))
C
C       CALCULATE R2 K 00 -> 22
C
        C1 = EXP(-DE(2)/KT)*SQRT(8.0/(PI*UH2))
C
        R2 = C1*((KT)**(-0.5)*AR1(2,1)*DE(2)
        1    + (KT)**(0.5)*(AR1(2,1) + AR1(2,2)*DE(2))
        2    + (KT)**(1.5)*2.0*(AR1(2,2) + AR1(2,3)*DE(2))
        3    + (KT)**(2.5)*6.0*(AR1(2,3) + AR1(2,4)*DE(2))
        4    + (KT)**(3.5)*24.0*AR1(2,4))
C
C       CALCULATE R3 K 02 -> 22
C
        C1 = EXP(-DE(3)/KT)*SQRT(8.0/(PI*UH2))
C
        R3 = C1*((KT)**(-0.5)*AR1(3,1)*DE(3)
        1    + (KT)**(0.5)*(AR1(3,1) + AR1(3,2)*DE(3))
        2    + (KT)**(1.5)*2.0*(AR1(3,2) + AR1(3,3)*DE(3))
        3    + (KT)**(2.5)*6.0*(AR1(3,3) + AR1(3,4)*DE(3))
        4    + (KT)**(3.5)*24.0*AR1(3,4))
C
C       CALCULATE R4 K 0 -> 2 FOR H2 TO BUFFER
C
```

```
      C1 = EXP(-DE(4)/KT)*SQRT(8.0/(PI*UB))
C
      R4 = C1*((KT)**(-0.5)*AR1(4,1)*DE(4)
     1    + (KT)**(0.5)*(AR1(4,1) + AR1(4,2)*DE(4))
     2    + (KT)**(1.5)*2.0*(AR1(4,2) + AR1(4,3)*DE(4))
     3    + (KT)**(2.5)*6.0*(AR1(4,3) + AR1(4,4)*DE(4))
     4    + (KT)**(3.5)*24.0*AR1(4,4))
C
      TEXP = 0.20*EXP(509.74/T)
C
      P0 = FRACH - P2
C
C     CALCULATE THE RATE OF CHANGE IN P2
C     (DP2)
C
      D1 = P0*P0 - P0*P2*TEXP
      D2 = P0*P0 - P2*P2*TEXP*TEXP
      D3 = P2*P0 - P2*P2*TEXP
      D4 = P0*PB - P2*PB*TEXP
C
      DP2(4) = (D*D1/V)*(D1*R1 + 2.0*D2*R2 + D3*R3
     1         + D4*R4)
C
C     CALCULATE THE DERIVATIVE OF THE TEMPERATURE
C     AT X (DT)
C
      DT(4) = 0.6667*T*(DD/D1 - E2*DP2(4)/KT)
C
C     CALCULATE THE DERIVATIVE OF THE VELOCITY AT
C     X (DV)
C
      DV(4) = -(AN/(V*MASS))*(2.5*K*DT(4) + E2*DP2(4))
C
C     CALCULATE THE NEW PROBABILTIY OF BEING IN THE
C     2ND ROTATIONAL LEVEL
C
      P2I = P2I + (DELTAX/6.0)*(DP2(1) + 2.0*DP2(2)
     1     + 2.0*DP2(3) + DP2(4))
C
C     CALCULATE THE NEW ISENTROPIC TEMPERATURE
C
      TI = TI + (DELTAX/6.0)*(DT(1) + 2.0*DT(2)
     1     + 2.0*DT(3) + DT(4))
C
C     CALCULATE THE NEW BEAM VELOCITY
C
      VI = VI + (DELTAX/6.0)*(DV(1) + 2.0*DV(2)
     1     + 2.0*DV(3) + DV(4))
C
C     SEE IF WE STORE THIS POINT
```

```
C
      ICNT = ICNT + 1
      IF(ICNT.NE.ISAVE) GO TO 40
C
      ICNT = 0
C
      TROT = 509.74/(ALOG(5.0*(FRACH/P2I -1.0)))
C
C     OUTPUT THE NEW CONDITIONS
C
      TYPE 202, X,P2I,TROT,TI
      WRITE (3,202) X,P2I,TROT,TI
C
C     CHECK FOR THE END OF CALCULATION
C
40    IF (X.LT.XMAX) GO TO 30
C
      STOP
```

```
C
101     FORMAT (' ENTER IN THE NAME OF COEFFICIENT FILE'
        1,T50,'-> ',$)
102     FORMAT (4A4)
103     FORMAT (' ENTER IN THE NAME OF THE OUTPUT FILE'
        1,T50,'-> ',$)
104     FORMAT (' ENTER IN THE MAXIMUM X IN X/D UNITS',T50,'-> ',$)
105     FORMAT (' ENTER IN THE MINIMUM X IN X/D UNITS',T50,'-> ',$)
106     FORMAT (' ENTER IN DELTA X IN X/D UNITS',T50,'-> ',$)
107     FORMAT (' ENTER IN THE STARTING TEMPERATURE',T50,'-> ',$)
108     FORMAT (' ENTER IN THE STARTING PRESSURE',T50,'-> ',$)
109     FORMAT (' ENTER THE M.W. OF THE DRIVING GAS',T50,'-> ',$)
110     FORMAT (' ENTER THE FRACTION OF DRIVING GAS',T50,'-> ',$)
C
111     FORMAT (' ENTER IN THE NOZZLE DIAMETER IN MICRONS'
        1,T50,'-> ',$)
112     FORMAT (' ENTER IN THE CONNECTING POINT',T50,'-> ',$)
113     FORMAT (' ENTER 2 IF YOU WANT A TWO TERM EXPANSION'
        1,T50,'-> ',$)
C
201     FORMAT ('     X/D',9X,' P2 ',11X,'TROT',10X,'TI',/)
202     FORMAT (3X,F6.2,5X,F11.7,2(5X,F7.2))
205     FORMAT (1X,4A4)
C
        END
```

H2HE.INP

```
-0.2021 4.057 8.571 -15.50
0.04397 0.0
-0.02291 0.2137 0.3547 -0.3960
0.08784 0.0
-0.3076 3.480 -0.9555 -1.496
0.04397 0.04397
0.8885 -0.4396E02 0.6238E03 -0.1672E04
0.04397 0.0
```

Appendix C

Expansion Coefficients Used in the Hydrogen Relaxation Programs

This appendix contains tables of the expansion coefficients used in the relaxation programs, for the various cross sections and rate constants.

σ_{rot} for the M79 Potential

$$\sigma_{rot} = A(1) + A(2)(T)^{A(3)} + A(4) \quad ;\text{For } T_{tr} < 60 \text{ K}$$

$A(1) = -1.069$
$A(2) = 0.5995E02$
$A(3) = -0.7238$
$A(4) = 0.4781E-01$

$$\sigma_{rot} = A(1) + A(2)T + A(3)T^2 \quad ;\text{For } T_{tr} > 60 \text{ K}$$

$A(1) = 5.254$
$A(2) = -0.1755E-01$
$A(3) = 0.1875E-02$

T_{tr} (K)	σ_{rot} (thoer.) $\AA^2 X10^2$	σ_{rot} (calc.) $\AA^2 X10^2$
10	10.80	10.7
20	6.606	6.74
30	5.474	5.48
40	5.046	5.00
50	4.889	4.85
60	4.867	4.90
70	4.923	4.94
80	5.030	5.05
90	5.178	5.19
100	5.363	5.37
110	5.586	5.59
120	5.846	5.85
130	6.145	6.14
140	6.480	6.47
150	6.853	6.84
160	7.261	7.25
170	7.702	7.68
180	8.178	8.17
190	8.682	8.68
200	9.215	9.24

σ_{rot} for the M80 Potential

$$\sigma_{rot} = A(1) + A(2)(T)^{A(3)} + A(4) \quad ;\text{For } T_{tr} < 60 \text{ K}$$

A(1) = 0.2973E-02
A(2) = 0.5369
A(3) = -0.8630
A(4) = 0.2830E-03

$$\sigma_{rot} = A(1) + A(2)T + A(3)T^2 \quad ;\text{For } T_{tr} > 60 \text{ K}$$

A(1) = 4.4320
A(2) = -0.3061E-01
A(3) = 0.2637E-03

T_{tr} (K)	σ_{rot} (thoer.) $Å^2X10^2$	σ_{rot} (calc.) $Å^2X10^2$
10	7.961	7.94
20	4.852	4.91
30	4.008	4.00
40	3.684	3.65
50	3.562	3.55
60	3.541	3.56
70	3.585	3.58
80	3.678	3.67
90	3.820	3.81
100	4.010	4.01
110	4.253	4.26
120	4.550	4.56
130	4.902	4.91
140	5.309	5.32
150	5.771	5.77
160	6.287	6.28
170	6.885	6.85
180	7.472	7.47
190	8.137	8.14
200	8.847	8.86

State-to-State Cross Sections for the M79 Potential

$$k_{ij \to lm} = A(1) + A(2)T + A(3)T^2 + A(4)T^3$$

$k_{00 \to 02}$

A(1) =	0.1418E-12
A(2) =	-0.3902E-14
A(3) =	0.2690E-16
A(4) =	0.0

T_{tr}	$k_{00 \to 02}$ (thoer.)	$k_{00 \to 02}$ (calc.)
60	0.517E-15	0.447E-14
70	0.189E-14	0.409E-15
80	0.511E-14	0.173E-14
90	0.112E-13	0.843E-14
100	0.214E-13	0.205E-13
110	0.367E-13	0.380E-13
120	0.579E-13	0.608E-13
130	0.860E-13	0.890E-13
140	0.122E-12	0.123E-12
150	0.165E-12	0.162E-12

$k_{00\rightarrow22}$

A(1)	=	-0.1954E+05
A(2)	=	0.7203E+03
A(3)	=	-0.8639E+01
A(4)	=	0.3400E-01

T_{tr}	$k_{00\rightarrow22}$ (thoer.)	$k_{00\rightarrow22}$ (calc.)
60	0.130E-19	
70	0.166E-18	0.217E-16
80	0.115E-17	0.208E-16
90	0.528E-16	0.103E-16
100	0.183E-16	0.107E-16
110	0.514E-16	0.423E-16
120	0.123E-15	0.126E-15
130	0.262E-15	0.281E-15
140	0.504E-15	0.529E-15
150	0.898E-15	0.889E-15

$k_{02\rightarrow22}$

A(1)	=	-0.1476E-13
A(2)	=	0.1413E-14
A(3)	=	-0.3400E-16
A(4)	=	0.2502E-18

T_{tr}	$k_{02\rightarrow22}$ (thoer.)	$k_{02\rightarrow22}$ (calc.)
60	0.870E-15	0.168E-14
70	0.318E-14	0.339E-14
80	0.859E-14	0.882E-14
90	0.189E-13	0.195E-13
100	0.359E-13	0.368E-13
110	0.615E-13	0.624E-13
120	0.971E-13	0.976E-13
130	0.144E-12	0.144E-12
140	0.203E-12	0.203E-12
150	0.276E-12	0.277E-12

Rabitz-Zarur State-to-State Cross Sections

$$\sigma_{ij\to lm} = A(1) + A(2)E_T + A(3)E_T^2 + A(4)E_T^3$$

$\sigma_{00\to02}$

A(1) =	-0.2021E+00
A(2) =	0.4057E+01
A(3) =	0.8571E+01
A(4) =	-0.1550E+02

E_T	$\sigma_{00\to02}$ (thoer.)	$\sigma_{00\to02}$ (calc.)
0.05	0.222E-01	0.203E-01
0.10	0.268E+00	0.274E+00
0.15	0.551E+00	0.547E+00
0.20	0.832E+00	0.828E+00
0.25	0.110E+01	0.111E+01
0.30	0.137E+01	0.137E+01

$\sigma_{00\to22}$

A(1) =	-0.2292E-01
A(2) =	0.2137E+00
A(3) =	0.3547E+00
A(4) =	-0.3960E+00

E_T	$\sigma_{00\to22}$ (thoer.)	$\sigma_{00\to22}$ (calc.)
0.10	0.170E-02	0.160E-02
0.15	0.155E-01	0.158E-01
0.20	0.312E-01	0.308E-01
0.25	0.462E-01	0.465E-01
0.30	0.625E-01	0.624E-01

$\sigma_{02\to22}$

A(1) =	-0.3076E+00
A(2) =	0.3480E+01
A(3) =	-0.9555E+00
A(4) =	-0.1496E+01

E_T	$\sigma_{02\to22}$ (thoer.)	$\sigma_{02\to22}$ (calc.)
0.10	0.298E-01	0.294E-01
0.15	0.188E+00	0.188E+00
0.20	0.339E+00	0.338E+00
0.25	0.480E+00	0.479E+00
0.30	0.611E+00	0.610E+00

Roberts Cross sections for H_2 --- He

$$\sigma_{0\to1,He} = A(1) + A(2)E_T + A(3)E_T^2 + A(4)E_T^3$$

$\sigma_{0\to2,He}$

A(1) =	0.9813E+00
A(2) =	-0.4920E+02
A(3) =	0.7037E+03
A(4) =	-0.2148E+04

E_T	$\sigma_{0\to2,He}$ (thoer.)	$\sigma_{0\to2,He}$ (calc.)
0.30	0.625E-01	0.624E-01
0.05	0.148E-01	0.121E-01
0.06	0.101E+00	0.988E-01
0.07	0.274E+00	0.271E+00
0.08	0.452E+00	0.450E+00
0.09	0.689E+00	0.688E+00
0.01	0.953E+00	0.951E+00

Secrest Cross sections for H_2 --- He

$$\sigma_{0\to1,He} = A(1) + A(2)E_T + A(3)E_T^2 + A(4)E_T^3$$

$\sigma_{0\to2,He}$

A(1) =	0.4590E-01
A(2) =	-0.6079E+01
A(3) =	0.1184E+03
A(4) =	-0.2831E+03

E_T	$\sigma_{0\to2,He}$ (thoer.)	$\sigma_{0\to2,He}$ (calc.)
0.054	0.188E-01	0.176E-01
0.081	0.175E+00	0.178E+00
0.107	0.414E+00	0.409E+00
0.134	0.679E+00	0.681E+00
0.188	0.121E+01	0.121E+01